

Tectonic evolution and deep mantle structure of the eastern Tethys since the latest Jurassic

Authors

Sabin Zahirovic^{a,*}, Kara J Matthews^{a,#}, Nicolas Flament^a, R Dietmar Müller^a, Kevin C Hill^b, Maria Seton^a and Michael Gurnis^c

^a EarthByte Group, School of Geosciences, The University of Sydney, NSW 2006, Australia

^b Oil Search Limited, Sydney, NSW 2000, Australia

^c Seismological Laboratory, California Institute of Technology, Pasadena, California 91125, USA

* Corresponding author at: EarthByte Group, School of Geosciences, The University of Sydney, NSW 2006, Australia. E-mail address: sabin.zahirovic@sydney.edu.au (S. Zahirovic)

Present address: Department of Earth Sciences, University of Oxford, South Parks Road, Oxford OX1 3AN, UK

Invited review submitted to *Earth-Science Reviews*

21	1 Introduction	5
22	1.1 Plate tectonic models of the eastern Tethys	12
23	1.2 Seismic tomography constraints	18
24	1.3 Numerical modelling of Tethyan geodynamics	22
25	1.3.1 Numerical models of India-Eurasia convergence.....	23
26	1.3.2 Numerical modelling of Southeast Asia and New Guinea geodynamics.....	27
27	2 Methods	28
28	2.1 Plate tectonic reconstructions.....	28
29	2.2 Insights from seismic tomography.....	36
30	2.3 Coupled plate reconstructions and mantle convection numerical models.....	38
31	3 Regional tectonic evolution	43
32	3.1 Late Jurassic plate boundary configuration and rifting mechanism along northern	
33	Gondwana.....	43
34	3.2 Active margin evolution in the Lhasa segment	51
35	3.3 Convergence along the West Burma and Sumatra margin segment.....	56
36	3.3.1 Development of the Woyla intra-oceanic arc.....	57
37	3.3.2 Subduction of the Woyla back-arc basin	58
38	3.4 Accretionary history of the Java and Borneo margin segment.....	64
39	3.4.1 Subduction and accretion history of southern Sundaland	64
40	3.4.2 Northern Sundaland collisions.....	70
41	3.4.3 Sundaland oroclinal bending.....	73
42	3.5 New Guinea and the Philippines	75
43	3.5.1 Origin and evolution of the Philippine Archipelago	75
44	3.5.2 Nature of the New Guinea margin since the Late Jurassic.....	76
45	4 Insights from age-coded slabs in seismic tomography.....	81
46	5 Numerical modelling results	87
47	5.1 Large-scale post-Jurassic mantle evolution of the Tethyan tectonic domain.....	87
48	5.2 Regional interpretations of mantle evolution.....	91
49	5.2.1 India-Eurasia convergence.....	91
50	5.2.2 Woyla and Sumatra active margin evolution	95
51	5.2.3 Java and Borneo subduction history.....	98
52	5.2.4 New Guinea margin evolution	101
53	6 Discussion	106
54	6.1 Intra-oceanic subduction in the Meso- and Neo-Tethys	106
55	6.2 Southeast Asia and New Guinea	108
56	6.3 Relevance to global plate reconstructions and geodynamics.....	111
57	7 Conclusions	111
58		

60 **Abstract**

61 The breakup of Pangea in the Jurassic saw the opening of major ocean basins at the expense
62 of older Tethyan and Pacific oceanic plates. Although the Tethyan seafloor spreading history has
63 been lost to subduction, proxy indicators from multiple generations of Tethyan ribbon terranes and
64 the active margin geological histories of volcanism and ophiolite obduction events can be used to
65 reconstruct these ancient oceanic plates. The resulting plate reconstructions reconcile observations
66 from ocean basins and the onshore geological record to provide a regional synthesis, embedded in a
67 global plate motion model, of the India-Eurasia convergence history, the accretionary growth of
68 Southeast Asia and the Tethyan-Pacific tectonic link through the New Guinea margin.

69 The global plate motion model captures the time-dependent evolution of plates and their
70 tectonic boundaries since 160 Ma, which are assimilated as surface boundary conditions for
71 numerical experiments of mantle convection. We evaluate subducted slab locations and geometries
72 predicted by forward mantle flow models against P- and S-wave seismic tomography. This
73 approach harnesses modern plate reconstruction techniques, mantle convection models with
74 imposed one-sided subduction, and constraints from the surface geology to address a number of
75 unresolved Tethyan geodynamic controversies.

76 Our synthesis reveals that north-dipping subduction beneath Eurasia in the latest Jurassic
77 consumed the Meso-Tethys, and suggests that northward slab pull opened the younger Neo-Tethyan
78 ocean basin from ~155 Ma. We model the rifting of ‘Argoland’, representing the East Java and
79 West Sulawesi continental fragments, which were transferred northward in latest Jurassic times
80 from the northwest Australian shelf – likely colliding first with parts of the Woyla intra-oceanic arc
81 in the mid-Cretaceous, and accreting to the Borneo (Sundaland) core by ~80 Ma. The Neo-Tethyan
82 ridge was likely consumed along an intra-oceanic subduction zone south of Eurasia from ~105 Ma,
83 leading to a major change in the motion of the Indian Plate by ~100 Ma, as observed in the Wharton
84 Basin fracture zone bends.

85 We investigate the geodynamic consequences of long-lived intra-oceanic subduction within
86 the Neo-Tethys, requiring a two-stage India-Eurasia collision involving first contact between
87 Greater India and the Kohistan-Ladakh Arc sometime between ~60 and 50 Ma, followed by
88 continent-continent collision from ~47 Ma. Our models suggest the Sunda slab kink beneath
89 northwest Sumatra in the mantle transition zone results from the rotation and extrusion of Indochina
90 from ~30 Ma. Our results are also the first to reproduce the enigmatic Proto South China Sea slab
91 beneath northern Borneo, as well as the Tethyan/Woyla slab that is predicted at mid-mantle depths
92 south of Sumatra. Further east, our revised reconstructions of the New Guinea margin, notably the
93 evolution of the Sepik composite terrane and the Maramuni subduction zone, produce a better
94 match with seismic tomography than previous reconstructions, and account for a slab at ~30°S
95 beneath Lake Eyre that has been overridden by the northward advancing Australian continent. Our
96 plate reconstructions provide a framework to study changing patterns of oceanic circulation, long-
97 term sea level driven by changes in ocean basin volume, as well as major biogeographic dispersal
98 pathways that have resulted from Gondwana fragmentation and accretion of Tethyan terranes to
99 south- and southeast-Eurasia.

100

101

102 Keywords:

103 Tethys, Pangea, tectonics, geodynamics, Sundaland, Southeast Asia

104

105

106 **1 Introduction**

107

108 Southern Eurasia, Southeast Asia and New Guinea represent a unique example of long-term
109 tectonic convergence between multiple tectonic domains that has resulted in a complex assemblage
110 of continental fragments, intra-oceanic arcs, ophiolite belts and marginal basins (Figs. 1 and 2). The
111 Southeast Asian continental promontory, known as Sundaland, has grown through successive
112 accretionary episodes resulting from the breakup of Pangea (Acharyya, 1998; Audley-Charles,
113 1988; Metcalfe, 1994), and subsequent northward transfer of Gondwana-derived continental ribbon
114 terranes and microcontinents on the Tethyan oceanic “conveyors” towards Eurasia. Importantly, the
115 region records a complex interaction between the Tethyan and (proto-) Pacific tectonic domains,
116 which has opened and consumed successive oceanic basins and gateways (Metcalfe, 1999), and has
117 had major consequences for biogeographic dispersal pathways such as the origin of the Wallace
118 Line (Burrett et al., 1991; de Bruyn et al., 2014; Lohman et al., 2011), oceanic circulation (Gaina
119 and Müller, 2007; Gurlan et al., 2008; Heine et al., 2004), global climate and sea level (Morley,
120 2012b; Wang, 2004; Xu et al., 2012), and the development of economic resources (Goldfarb et al.,
121 2014; Zaw et al., 2014).

122 Plate tectonic reconstructions play a pivotal role in unravelling the complexity of this region
123 and provide a platform to address long-standing geological questions in a geodynamic context. We
124 apply a modern approach of modelling entire plates, their evolving plate boundaries and the terranes
125 they carry. This study aims to synthesise previously published onshore and offshore geological
126 constraints, as well as incorporate decades of developments in plate tectonic reconstructions, into a
127 modern plate motion model to document the post-Pangea geodynamic evolution of southern
128 Eurasia, Southeast Asia and New Guinea since the Late Jurassic in a regional and global context.
129 Despite significant technological and methodological advancements in plate reconstruction

130 approaches, very few reconstructions of the eastern Tethys exist in an open-access digital form that
131 can be tested and expanded by the scientific community.

132 As part of this work, we release detailed plate reconstructions for the eastern Tethys (from
133 the India-Eurasia collision zone eastward to Papua New Guinea, Figs. 1-3) that are embedded in a
134 self-consistent global plate motion model, as a collection of digital geometry files and rotation
135 parameters compatible with the open-source and cross-platform plate reconstruction tool, GPlates
136 (www.gplates.org). We provide a brief background to previous regional tectonic reconstructions in
137 Section 1.1, as well as tomographic and numerical modelling approaches in Sections 1.2-1.3 that
138 have been used to gain insight into the tectonic and geodynamic processes controlling the regional
139 evolution. In Sections 2 to 4, we outline our approach of building modern plate reconstructions for
140 the three key regions that comprise the eastern Tethys, including i) the India-Eurasia convergence
141 zone, ii) Southeast Asia, and iii) the New Guinea margin, and compare our approach and findings
142 with previous work. In Section 5, we show how modern plate reconstructions that incorporate
143 evolving plate boundaries can be used with numerical models of mantle flow to predict mantle
144 structure, study the distribution of ancient slabs, and test alternative plate motion scenarios where
145 geological constraints are vague or interpretation is ambiguous. In Sections 6 and 7 we highlight the
146 implications of our work in a regional and global context, and provide some key findings from our
147 modelling of the tectonic and geodynamic evolution of the entire eastern Tethyan domain.

148 The coupled global plate reconstructions and mantle flow models provide a context for
149 better understanding the latest Jurassic rifting events from northern Gondwana (Metcalf, 1994;
150 Pigram and Panggabean, 1984), which opened the Neo-Tethys at the expense of the Meso-Tethys
151 ocean basin (Fig. 4a). This rifting episode transferred the ‘Argoland’ ribbon continent, which
152 included East Java, West Sulawesi and Mangkalihat (Hall, 2012; Zahirovic et al., 2014), north
153 towards Eurasia, while also marking the onset of major intra-oceanic subduction systems along
154 southern Eurasia and northern New Guinea. In the absence of preserved seafloor spreading histories
155 for Neo-Tethyan evolution, we test alternative scenarios of subduction using geodynamic models of

156 mantle flow that are compared with the present-day mantle structure interpreted from seismic
157 tomography.

158 The improvement in the methods applied to plate reconstructions and increasing levels of
159 detail in complex regions have implications for linking plate tectonic evolution with the deep
160 mantle and other Earth systems, and have been extensively used to better understand biogeographic
161 dispersal and evolutionary pathways (Monod and Prendini, 2015; Rolland et al., 2015), long-term
162 climate and sea level change (Herold et al., 2014; Huber and Goldner, 2012; Lee et al., 2013;
163 Müller et al., 2008; Scotese et al., 1999; Spasojevic and Gurnis, 2012; van der Meer et al., 2014),
164 and paleo-bathymetry and oceanic gateway evolution (Gaina and Müller, 2007). Improved plate
165 tectonic reconstruction techniques have enabled the quantification of time-dependent convergence
166 rates (Lee and Lawver, 1995; Sdrolias and Müller, 2006; Whittaker et al., 2007), and inferences on
167 regional and global plate re-organization events (Matthews et al., 2011; Matthews et al., 2012), as
168 well as providing insight into the size distribution of tectonic plates (Morra et al., 2013) and factors
169 controlling the speed of tectonic plates (Zahirovic et al., 2015). The plate reconstructions presented
170 in this work have important implications for our understanding of the mid-Cretaceous seafloor
171 spreading pulse (Seton et al., 2009) that may have led to higher eustatic sea levels (Müller et al.,
172 2008), the proposed major regional and global plate reorganization at ~105-100 Ma (Matthews et
173 al., 2012) that may be linked to the subduction of the Neo-Tethyan mid oceanic ridge. In addition,
174 plate reconstructions of the Tethyan domain have consequences for understanding the atmospheric
175 carbon budget resulting from the initiation and abandonment of major Andean-style and intra-
176 oceanic Tethyan subduction zones (Jagoutz et al., 2016; van der Meer et al., 2014).

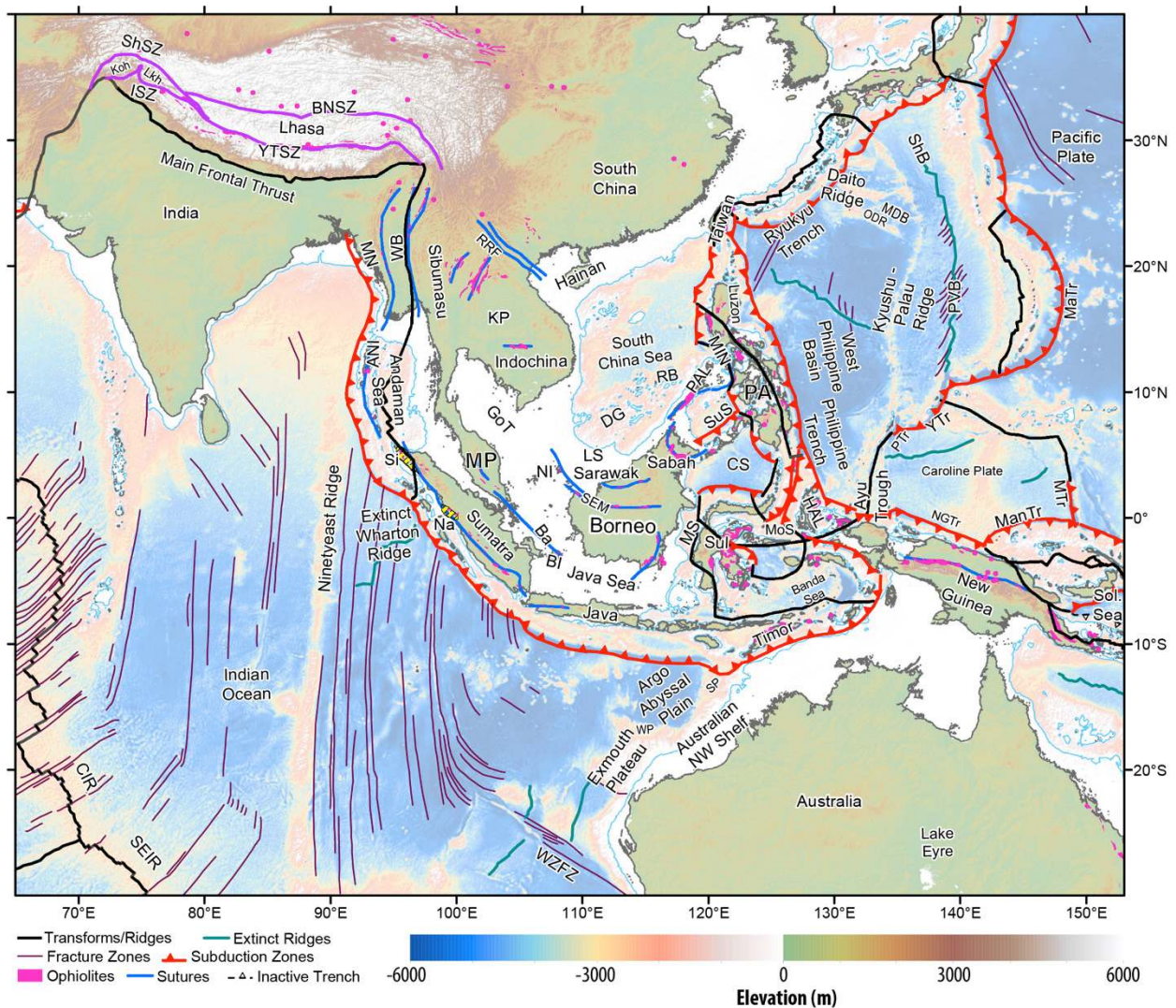
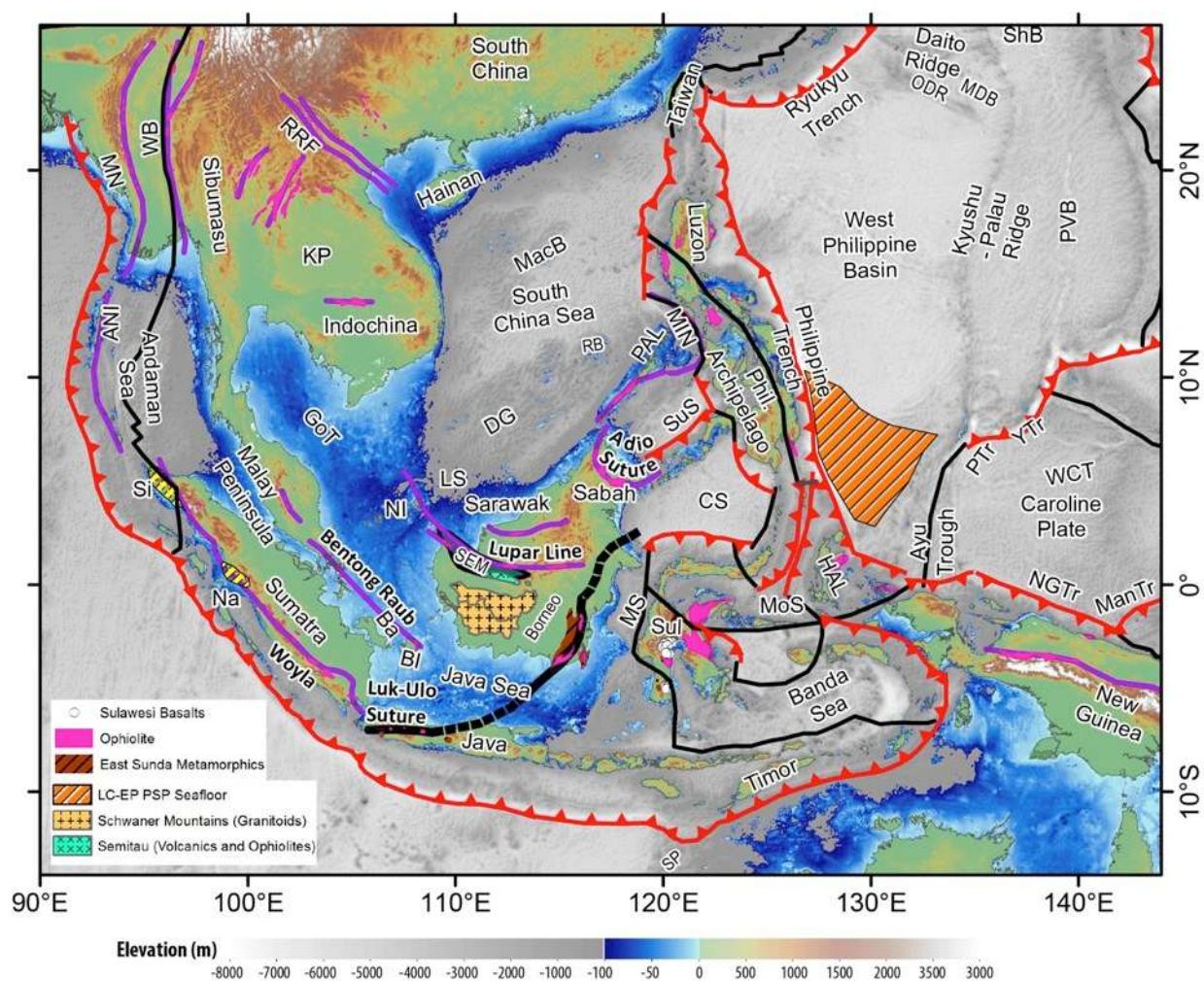


Fig. 1. Regional tectonic setting of southern Eurasia, Southeast Asia and New Guinea. The plate boundaries are modified from Bird (2003), the topography is from Amante et al. (2009), and the seafloor fabric is from Matthews et al. (2011). Southeast Asian sutures (blue) and ophiolites are modified from Hutchison (1975), with additional ophiolites for New Guinea from Baldwin et al. (2012), and for Southeast Asia from Pubellier et al. (2004). The Tethyan sutures in the Indian segment of the margin (violet lines) are from Yin and Harrison (2000). ANI – Andaman-Nicobar Islands, Ba – Bangka Island, BI – Billiton Island, BNSZ – Bangong-Nujiang Suture Zone, CIR – Central Indian Ridge, CS – Celebes Sea, DG – Dangerous Grounds, GoT – Gulf of Thailand, HAL – Halmahera, ISZ – Indus Suture Zone, Koh-Lkh – Kohistan-Ladakh, KP – Khorat Plateau, LS – Luconia Shoals, ManTr – Manus Trench, MaTr – Izu-Bonin-Mariana Trench, MDB – Minami Daito Basin, MIN – Mindoro, MN – Mawgyi Nappe, MoS – Molucca Sea, MP – Malay Peninsula,

189 MS – Makassar Straits, MTr – Mussau Trench, Na – Natal, NGTr – New Guinea Trench, NI –
 190 Natuna Island, ODR – Oki Daito Ridge, PA – Philippine Arc, PAL – Palawan, PTr – Palau Trench,
 191 PVB – Parece Vela Basin, RB – Reed Bank, RRF – Red River Fault, SEIR – Southeast Indian
 192 Ridge, ShB – Shikoku Basin, ShSZ – Shyok Suture Zone, Si – Sikuleh, SP – Scott Plateau, Sul –
 193 Sulawesi, SuS – Sulu Sea, WB – West Burma, WP – Wombat Plateau, WZFZ – Wallaby Zenith
 194 Fracture Zone, YTr – Yap Trench, YTSZ – Yarlung-Tsangpo Suture Zone.
 195



196
 197 **Fig. 2.** Regional tectonic framework of Southeast Asia and New Guinea, with high-resolution
 198 Global Multi-Resolution Topography of depths shallower than 100 m from Ryan et al. (2009). The
 199 Cretaceous Luk Ulo-Meratus sutures are depicted as the thick black line through Java and Borneo.
 200 Abbreviations follow those used in Fig. 1. LC-EP PSP – Late Cretaceous(?)–early Paleogene
 201 Philippine Sea Plate seafloor crust, WCT – West Caroline Trough.

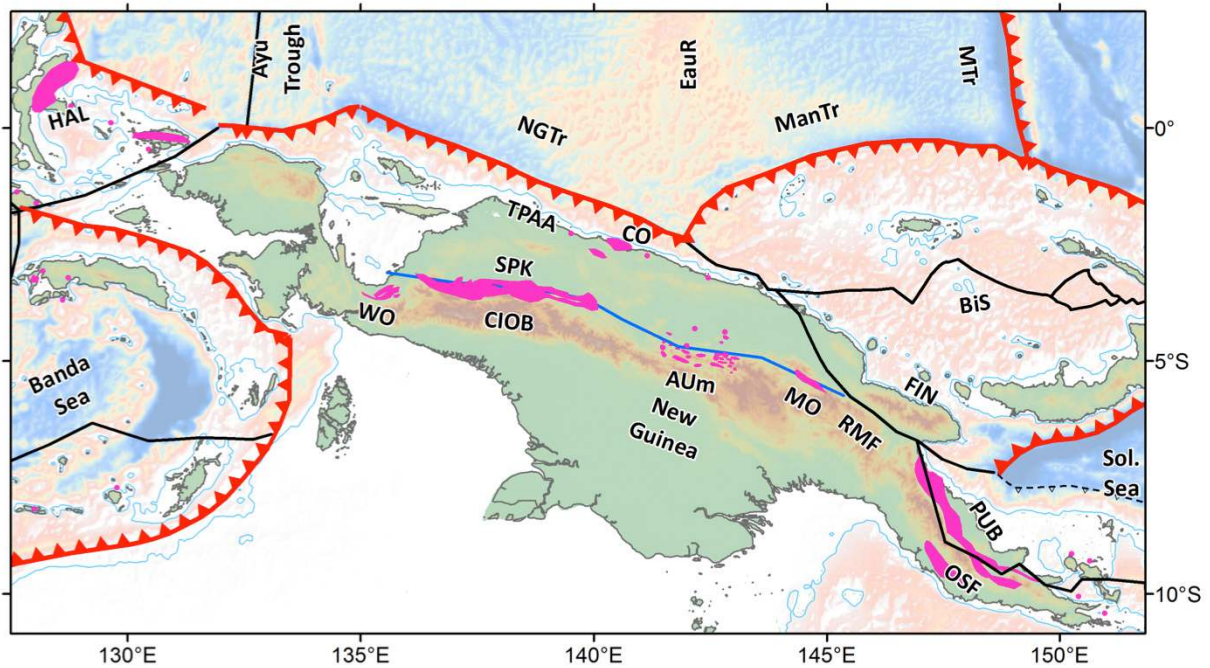


Fig. 3. Tectonic framework and topography of New Guinea. AUm – April Ultramafics, BiS – Bismarck Sea, CIOB – Central Irian Ophiolite Belt, CO – Cyclops Ophiolite, EauR – Eauripik Rise, FIN – Finisterre Terrane, MO – Marum Ophiolite, OSF – Owen Stanley Fault, PUB – Papuan Ultramafic Belt, SPK – Sepik Terrane, Sol. Sea – Solomon Sea, TPAA – Torricelli-Prince Alexander Arc, WO – Weyland Overthrust. Other abbreviations follow Fig. 1.

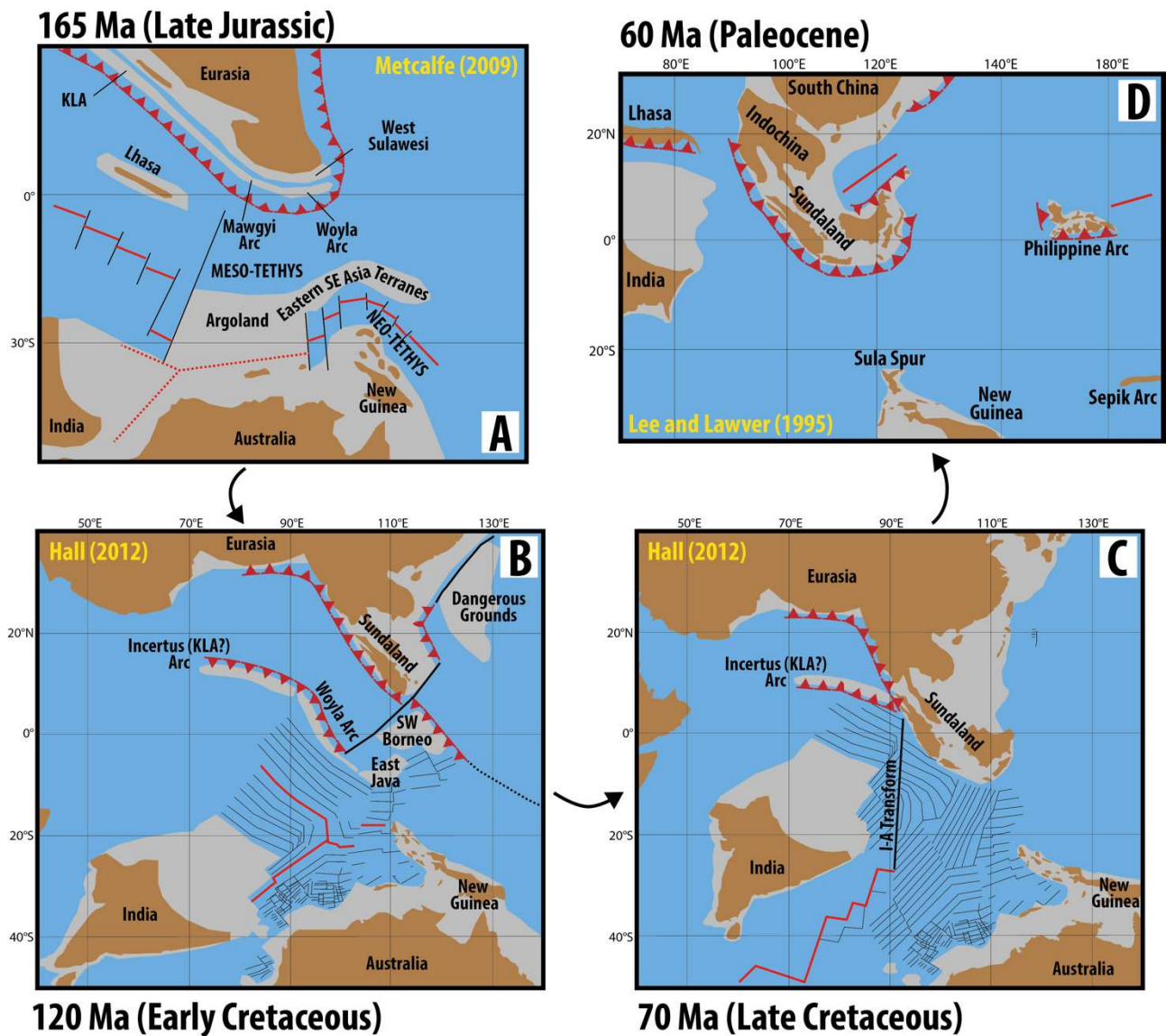


Fig. 4. A wide range of tectonic reconstructions have been proposed for the eastern Tethys between the India-Eurasia convergence zone and New Guinea. A) The Late Jurassic rifting event along northern Gondwana has been modelled as a westward propagating rift from New Guinea towards Argoland, and joining up as a triple junction in between India and Australia in the model of Metcalfe (2009). The rifting mechanism is implied as northward slab pull from Tethyan subduction along southern Eurasia. B) The model of Hall (2012) instead invokes a south-dipping subduction zone along northern Gondwana in the latest Jurassic, leading to the opening of the Neo-Tethys as a large back-arc basin. The related Incertus Arc likely represents the Kohistan-Ladakh (KLA) and Woyla arc systems in the Neo-Tethys. C) By the Late Cretaceous, subduction polarity reverses across the Incertus Arc to produce northward slab pull along a north-dipping intra-oceanic

subduction zone. The Hall (2012) model imposes a subduction hiatus along southern Sundaland between 90 and 45 Ma, which requires the segmentation of the Neo-Tethys across a transform that cross-cuts Tethyan seafloor fabric at ~90°E (I-A Transform). D) The model of Lee and Lawver (1995) presents eastern Tethyan plate reconstructions since 60 Ma in a South China fixed reference frame. The size of Greater India is similar as proposed in Hall (2012), but is about twice the northward extent presented in this study, largely to accommodate an India-Eurasia continent-continent collision at ~55 Ma. The Lee and Lawver (1995) model also presents all plate rotation parameters, which enables the reproducibility and testability of this model. A common feature between the models (A-D) is relatively less detail for the New Guinea region, which has been difficult to reconstruct due to the lack of data and the dominance of complex interactions between Asian and Pacific subduction systems.

233

234 **1.1 Plate tectonic models of the eastern Tethys**

235

As many generations of plate reconstructions have been proposed for the eastern Tethyan tectonic domain, it is useful to understand the historical context and help categorize successive generations of models that have been proposed. Even before the acceptance of plate tectonic principles, Southeast Asian geology was of great interest due to significant hydrocarbon (Halbouty et al., 1970; Wennekers, 1958) and metallogenic (Brown, 1951; Leith, 1926; Matthews, 1990; Penrose, 1903) discoveries. Early attempts to explain the geology of Southeast Asia led to a large number of competing hypotheses. Fairbridge (1963) explained the geological affinities between Southeast Asia and Gondwana by invoking a range of mechanisms from now-abandoned ideas of mantle contraction, mantle expansion, rising and sinking land bridges, galactic expansion, to then emerging ideas of continental drift. A few years on, Audley-Charles (1966) provided the first synthesis of stratigraphic evidence to describe the region's Mesozoic paleogeographic evolution in

247 the context of continental drift, with special reference to paleo-latitude indicators from paleo-
248 climatic and paleo-magnetic data.

249 It was only in the 1970s that plate tectonic principles of subduction, seafloor spreading and
250 transform tectonic boundaries (Forsyth and Uyeda, 1975; Le Pichon, 1968; McKenzie, 1969;
251 McKenzie and Parker, 1967) were invoked in first-generation continental reconstructions (Table 1)
252 to explain the present-day tectonic complexity of the eastern Tethys (Fitch, 1972; Hamilton, 1979;
253 Katili, 1971). These models were subsequently used to create the first schematic “plate
254 reconstructions” (Katili, 1975) that largely focused on the dominance of active volcanic arcs and
255 associated subduction zones in controlling the tectonic complexity of the region. Importantly, the
256 work of Katili (1975) identified a number of parallel and arcuate paleo-arc systems, which recorded
257 post-Permian subduction of Tethyan oceanic crust. Pioneering work in the 1970s and 1980s applied
258 paleomagnetic techniques to infer that parts of Southeast Asia originated from the northern
259 Gondwana margin (McElhinny et al., 1981), and more specifically somewhere between north
260 Africa and Greater India (the portion of India currently under-thrust beneath Eurasia) (Stauffer,
261 1983). Although the origin of Southeast Asian continental fragments from Arabia or Africa in the
262 Paleozoic have since been discounted (see Metcalfe, 1988; Metcalfe, 1994; Metcalfe, 1999;
263 Veevers, 2004), these early works established the wider notion of Southeast Asian crustal accretion
264 via the northward transfer of continental fragments originating from the northern Gondwana
265 margins (Fig. 4A).

266 Pioneering reconstructions of Gondwana breakup, and the northward transfer of crustal
267 fragments towards Asia, were largely presented as schematic scenarios portraying the drift of
268 continents with consideration of some major regional plate boundaries. Pigram and Panggabean
269 (1984) and Audley-Charles (1988) combined regional stratigraphic composite wells to identify a
270 major Late Jurassic breakup unconformity across the NW Australian margin, which suggested that
271 a number of continental fragments had detached to form the north Gondwana passive margin and
272 open the “Mesozoic Tethys” ocean basin. Based on the interpretation of rift-drift sedimentary

273 sequences, including the timing of the post-breakup unconformity, Pigram and Panggabean (1984)
274 provided schematic reconstructions of the Late Jurassic drifting episode and concluded that seafloor
275 spreading initiated sometime in the Early Jurassic along New Guinea and Middle Jurassic along the
276 NW Australian shelf. The generally northward transfer of Gondwana terranes opened successive
277 Tethyan ocean basins including the rifting of a ribbon continent comprising Iran, North Tibet
278 (Qiangtang) and Indochina to open “Tethys II” in the late Permian (Audley-Charles, 1988). A
279 subsequent major rifting phase in the Late Jurassic opened the “Tethys III”, detaching fragments
280 including South Tibet (Lhasa), West Burma, Malaya, Borneo, Sulawesi, Sumatra and a number of
281 Banda allochthons (Audley-Charles, 1988). Importantly, the work of Audley-Charles (1988) and
282 Audley-Charles et al. (1988) introduced a paleogeographic reconstruction framework using the
283 computerised University of Cambridge Atlas plotting workflow, which we classify as a second
284 generation reconstruction methodology (Table 1). This early generation of reconstructions assessed
285 the prior continental affinities and inferred major rifting phases using biostratigraphic constraints, as
286 well as made use of paleomagnetic syntheses and structural interpretations from seismic sections to
287 infer rift and drift histories.

288 The third generation of plate reconstructions, largely developed in the late 1980s and
289 throughout the 1990s (e.g., Besse and Courtillot, 1988; Daly et al., 1991; Jolivet et al., 1989; Lee
290 and Lawver, 1994; Lee and Lawver, 1995), made use of extensive identifications of marine
291 magnetic anomalies from the Indian Ocean and West Pacific calibrated to a geological timescale
292 (e.g., Taylor and Hayes, 1980; Taylor and Hayes, 1983). The seafloor spreading histories,
293 supplemented with paleomagnetic data from the continental blocks (e.g., Haile et al., 1977), were
294 applied to make plate reconstructions using rigid body motions on the surface of a sphere (i.e.,
295 Euler rotations). The Jurassic to recent plate reconstructions of Besse and Courtillot (1988) and
296 Scotese et al. (1988) were an important benchmark for subsequent plate motion models, as the work
297 synthesised marine magnetic anomalies and continental paleomagnetism, yet also took into account

298 the plate boundary evolution. Pertinent to this study, the work of Besse and Courtillot (1988) and
299 Scotese et al. (1988) enabled reproducibility by providing finite rotation parameters.

300 Although the plate reconstructions of Lee and Lawver (1994) and Lee and Lawver (1995)
301 covered only the Cenozoic evolution of Southeast Asia (Fig. 4d), these were the first detailed
302 regional reconstruction that published testable and reproducible finite rotation parameters that
303 quantitatively described the motion of Southeast Asian crustal elements, building on the more
304 regional approach presented in Jolivet et al. (1989). The relative plate motions, provided as finite
305 rotations, were linked into a plate motion hierarchy that tied back to the South China block, and
306 thus only provide a regional perspective (Lee and Lawver, 1994; Lee and Lawver, 1995). However,
307 the provision of Euler rotations significantly increased their utility even over more recent models as
308 they allow for reproducibility and refinement by subsequent researchers.

309 A major improvement in regional plate reconstructions was presented in Hall (1996), and
310 subsequent works by the same author (Hall, 2002; Hall, 2012) (Fig. 4B-C), where the regional plate
311 reconstructions were embedded in a global plate circuit – that links Australia and India back to
312 Africa, and Asian fragments through Eurasia, North America and Africa. Using a global plate
313 circuit combines relative plate motions with a frame of reference with respect to the mantle using a
314 hotspot frame (e.g., Müller et al., 1993), which enables linkages between the plate-mantle system.
315 In the absence of hotspot tracks (i.e., before ~120 Ma), plate reconstructions make use of
316 paleomagnetic reference frames (e.g., Hall and Spakman, 2015), which enable the reconstruction of
317 paleo-latitudes of climate-sensitive data, and can be corrected for True Polar Wander to create more
318 explicit links between the plate-mantle system in deep time. The reconstructions presented in Hall
319 (1996) and Hall (2002) provide a regional post-Jurassic evolution of the India-Eurasia convergence
320 zone, Southeast Asia and New Guinea embedded in a detailed synthesis of relevant data, and are
321 presented in 1 Myr interval snapshots. Such high temporal resolution is important for capturing
322 major plate boundary reconfigurations and resulting changes in plate motion magnitudes and
323 directions, such as the change in India's plate motions and northward advance from ~100 Ma

(Gibbons et al., 2015; Matthews et al., 2012; van Hinsbergen et al., 2011). Although the reconstructions are presented in 1 Myr intervals, no relative or absolute plate rotation parameters have been provided, which limits the testability of such models.

These first- to fourth-generation plate reconstructions provide considerable detail and insight into the tectonic evolution of the eastern Tethys, but cannot be easily linked to methods that take into account the geodynamic evolution of the plate-mantle system. Schematic reconstructions cannot be linked to numerical models of convection as they usually lack the continuous network of plate boundaries through time that enables the use of plate velocities as surface boundary conditions. As plate motions are inextricably linked to mantle convection (Hager and O'Connell, 1981; Turcotte and Oxburgh, 1972), and since much of the Tethyan seafloor spreading history has since been subducted (Hutchison, 1975; Şengör et al., 1988), some authors have inferred plate motion histories from high velocity seismic anomalies as given by mantle tomography models (Hall and Spakman, 2003; Hall and Spakman, 2015; Replumaz et al., 2004; van der Voo et al., 1999b; Wu et al., 2016). We expand on these approaches and make use of our most recent plate reconstructions coupled to numerical models of mantle convection that are validated using seismic tomographic images and a suite of onshore and offshore geological constraints.

340

Table 1. Generations of continental and plate reconstructions depicting the kinematic and geodynamic evolution of Southeast Asia.

Generation of reconstruction	Description	Examples
First	Schematic reconstructions of continental motions.	Pigram and Panggabean (1984) Metcalf (1988)
Second	Continental reconstructions are made using digital approaches, with schematic paleo- plate boundaries.	Audley-Charles et al. (1988) Rangin et al. (1990)
Third	Additionally provide regional reconstructions using seafloor spreading histories, constraints from onshore geology	Besse and Courtillot (1988) Scotese et al. (1988)

	(paleomagnetism, stratigraphy, seismic, structural, biogeography, etc.) and an incomplete network of plate boundaries. Although these models are classified as 3 rd generation reconstructions, they have a significant advantage over any other reconstructions that do not provide Euler rotation parameters that are provided in 5 th generation models. These models are important examples of reproducible and testable plate reconstructions of Southeast Asia.	Jolivet et al. (1989) Lee and Lawver (1994) Lee and Lawver (1995)
Fourth	Regional reconstructions embedded in a global rotation hierarchy, constraining relative plate motions using seafloor spreading histories that are tied to an absolute hotspot or paleomagnetic reference frame. Synthetic seafloor spreading histories are generated in regions and times where seafloor has been subducted.	Hall (1996) Hall (2002) Hall (2012) Stampfli and Borel (2002) [#]
Fifth	A continuous global network of evolving plate boundaries is modelled, with complete model rotation parameters and digital geometry files released for testability and reproducibility. Such models can be linked to regional and global geodynamic numerical calculations that link plate tectonics with underlying mantle convection. Some of these models incorporate regional refinements that include retro-deformation of continental crust to provide better full-fit reconstructions of Pangea.	Gurnis et al. (2012) Seton et al. (2012) Zahirovic et al. (2012) Zahirovic et al. (2014) Domeier and Torsvik (2014) [^] Gibbons et al. (2015) This study
Future	Build on previous approaches with stronger emphasis on quantifying uncertainties, and using ensemble computer modelling that incorporates all constraints (offshore and onshore) simultaneously and all relevant uncertainties to derive a quantitative “best-fit” plate reconstruction that is fully consistent with plate boundary forces and mantle convection models. Global plate reconstructions incorporate all major regions of deformation to provide better full-fit reconstructions and address the oversimplification of plate rigidity assumptions.	Such models are not yet available, and represent an aspirational goal to produce better plate tectonic reconstructions.

343 ^ The Domeier and Torsvik (2014) reconstructions cover the Late Paleozoic global plate motion history, and include
344 major blocks of Southeast Asia.

The model of Stampfli and Borel (2002) has linked plate boundaries and synthetic seafloor spreading histories, which are important components of 5th-generation models, but only provides snapshots without rotation parameters or (evolving plate boundary) geometries.

1.2 Seismic tomography constraints

Seismic tomographic techniques have provided an important link between the present-day arrangement of plate boundaries and deep mantle structure around Southeast Asia resulting from long-term subduction of Tethyan and Pacific lithosphere. High-resolution P-wave seismic tomographic models have demonstrated that the Sunda slab from the subduction of the Indo-Australian oceanic plate penetrates to depths of ~1500 km (Li et al., 2008; Widiyantoro and van der Hilst, 1996), and that it is distinct from the older and deeper Tethyan slabs (Widiyantoro and van der Hilst, 1996). Due to the complexity of Tethyan convergence, and the lack of preserved seafloor spreading histories, interpretations of mantle structure provide an important additional insight into the past geometry and evolution of active margins in the region. For example, Hall and Spakman (2002) and Hall and Spakman (2003) used a P-wave seismic tomographic model to infer Cenozoic subduction histories in the vicinity of the northern Australian margin. Hall and Spakman (2003) interpreted the Bijwaard and Spakman (2000) P-wave seismic tomographic model to suggest north-dipping subduction north of Australia along the Philippine Archipelago occurred between 45 and 25 Ma, and inferred that little subduction occurred north of Australia since 25 Ma due to the likelihood of a margin dominated by strike-slip motion rather than convergence. Hall and Spakman (2015) recently attributed the 1600 km deep Sunda slab to subduction since 45 Ma, but discounted the possibility that the Proto South China Sea slab is in the upper mantle, and concluded that it is instead likely in the lower mantle at ~1200 km depth. Further south, a large east-west slab beneath Australia (including Lake Eyre) at ~800-1200 km depths has been interpreted to be the result of north-dipping subduction that ceased following accretion of the Sepik Terrane along New Guinea at ~50 Ma (Schellart and Spakman, 2015).

372 The India-Eurasia Tethyan mantle structure was interpreted in van der Voo et al. (1999b)
373 where a global P-wave seismic tomographic model (Bijwaard et al., 1998) was used to infer the
374 subduction history related to post-Jurassic subduction (Fig. 5). The large slabs, with a generally
375 northwest-southeast trend and largely at mid-mantle depths, were interpreted to be the result of two
376 simultaneous north-dipping subduction zones in the Neo-Tethys (van der Voo et al., 1999b), a
377 scenario which requires a two-stage India-Eurasia collision. Hafkenscheid et al. (2006) elaborated
378 on this approach by quantifying Tethyan slab volumes and inferring average slab sinking rates in
379 the mantle. Hafkenscheid et al. (2006) tested end-member scenarios of convergence, including
380 long-lived Andean-style subduction following Norton (1999) and Şengör and Natal'in (1996).
381 Instead, the analysis by Hafkenscheid et al. (2006) suggested that an additional intra-oceanic
382 subduction zone, following Stampfli and Borel (2002), could better reproduce the volume and
383 distributions of slabs interpreted from 3D seismic tomography. The preferred scenario in
384 Hafkenscheid et al. (2006) invoked an arc-continent collision between Greater India and the Spong
385 Arc, likely contemporaneous with the Kohistan-Ladakh Arc (McDermid et al., 2002), at ~65-
386 60 Ma, with continent-continent collision occurring at ~48 Ma, and infer a “free sinking rate” (i.e.,
387 when not attached to a subducting plate) of 3 and 2 cm/yr in the upper and lower mantle,
388 respectively.
389

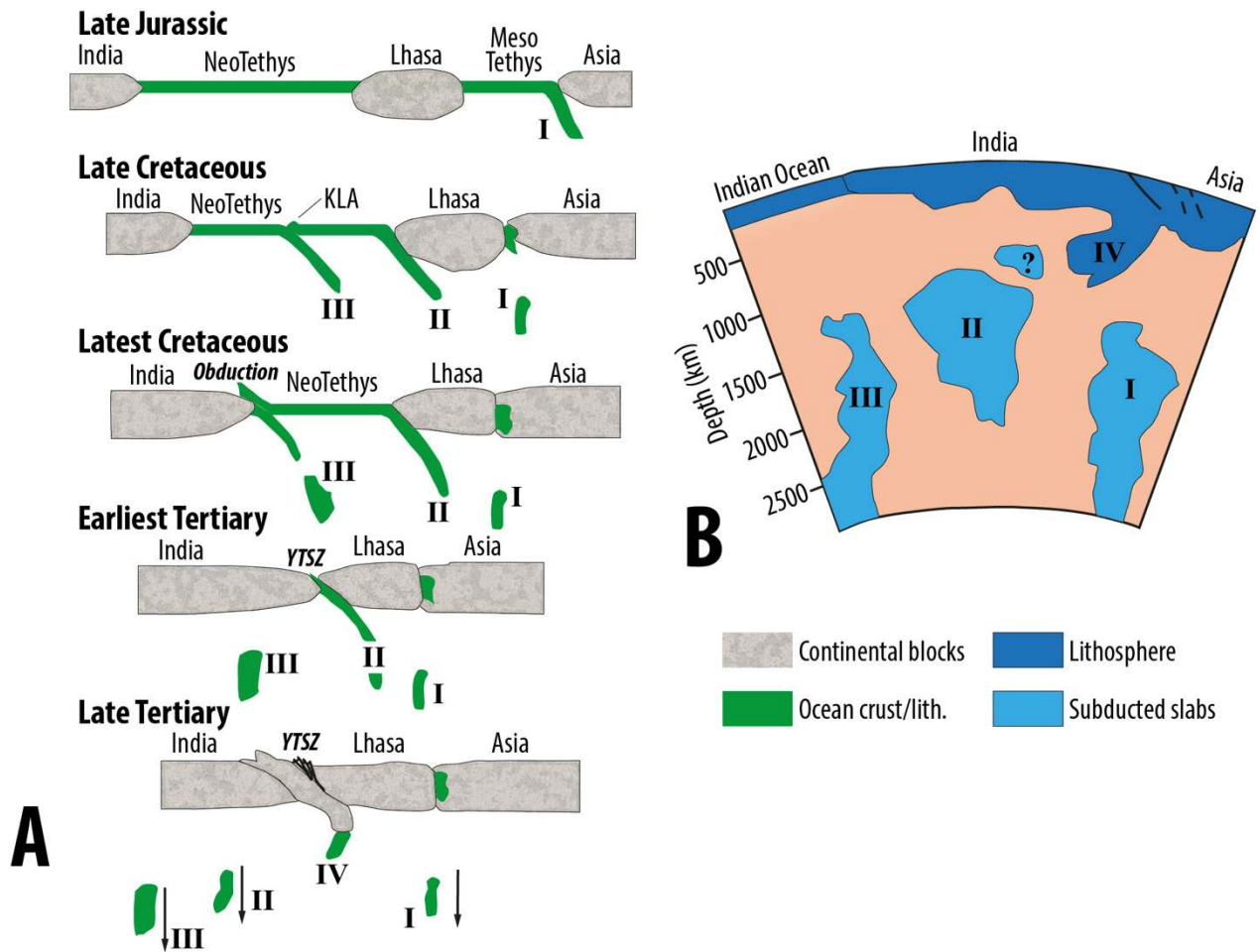


Fig. 5. A) Schematic synthesis of Tethyan subduction history accommodating India-Eurasia convergence, as interpreted from P-wave seismic tomography by van der Voo et al. (1999b). B) The three slab volumes in the lower mantle are interpreted as representing intra-oceanic subduction and a two-stage India-Eurasia collision. Figure adapted from van der Voo et al. (1999b). Note that the Tethyan ocean basin nomenclature in van der Voo et al. (1999b) differs slightly from the terminology used in this study. KLA – Kohistan-Ladakh Arc, YTSZ – Yarlung Tsangpo Suture Zone.

Incorporating 3D seismic tomographic interpretations, Replumaz et al. (2004) combined an assumption of vertical slab sinking with a tectonic reconstruction of Southeast Asia in a Siberia reference frame, and interpreted the pre-collision geometry of the southern Eurasian active margin using tomographic depth slices. The analysis of tomography linked to a “retro-deformation” model

403 of block motions in Southeast Asia (using available fault offsets and slip rates) for Cenozoic times
404 suggests that the India-Eurasia continental collision occurred sometime between 55 and 40 Ma,
405 based on changes in slab morphology, and suggests a sinking rate of 5 cm/yr in the upper mantle
406 and 2 cm/yr in the lower mantle. The resulting upper mantle sinking rates are slightly higher than
407 the values suggested by Hafkenscheid et al. (2006). A similar approach of age-coding slabs in P-
408 and S-wave seismic tomographic depth slices, assuming constant and vertical slab sinking was used
409 in Zahirovic et al. (2012) and Zahirovic et al. (2014) as a general estimate of the location of
410 Tethyan subduction zones that were then implemented into a global plate motion model. One
411 important distinction was the use of multiple P- and S-wave seismic tomographic models, which is
412 an important consideration in determining the distribution of Tethyan slabs. To supplement the
413 assumption of vertical slab sinking, Zahirovic et al. (2012) used numerical mantle convection
414 models kinematically driven by time-dependent plate reconstructions, and found that an intra-
415 oceanic subduction scenario, as suggested by van der Voo et al. (1999b), Hafkenscheid et al. (2006)
416 and Aitchison et al. (2007), better reproduced the Tethyan mantle structure than Andean-style
417 subduction alone.

418 More generally, the approach of age-coding slabs in seismic tomographic depth slices has
419 been applied globally to derive average slab sinking rates (Butterworth et al., 2014; van der Meer et
420 al., 2010), and to propose a subduction reference frame using the assumption of vertical sinking and
421 constant sinking rates (van der Meer et al., 2010). The cataloguing of global slab volumes by van
422 der Meer et al. (2010) suggests that a ~ 15 to 20° longitudinal global shift of all continents is
423 required to account for the observed distribution of post-Jurassic slabs in the mantle. Such an
424 observation is an important first-order constraint of paleo-longitude in the absence of preserved
425 hotspot tracks during the Late Jurassic and Early Cretaceous, and provides an estimated average
426 global slab-sinking rate of 1.2 ± 0.3 cm/yr. A similar synthesis of slabs interpreted from seismic
427 tomography in Butterworth et al. (2014) suggests a comparable average sinking rate of $1.3 \pm$
428 0.3 cm/yr for the whole mantle. However, such an approach does not take into account the

429 contrasting viscosities of the upper and lower mantle, or the effects of slab stagnation and lateral
430 slab advection from mantle flow, which may be an important factor contributing to Tethyan mantle
431 structure (Becker and Faccenna, 2011; Zahirovic et al., 2012). To address this, Butterworth et al.
432 (2014) made use of global numerical modelling of mantle flow to test competing absolute reference
433 frames against present-day seismic tomographic constraints, and suggest that the longitudinal
434 correction argued in van der Meer et al. (2010) is likely too large. The numerical modelling
435 approach in Butterworth et al. (2014) highlighted the need to account for variable slab sinking rates
436 resulting from factors such as oblique convergence, diachronous collisions and suturing, as well as
437 two orders of magnitude increase in viscosity between the upper and lower mantle. The slab sinking
438 rates from numerical mantle convection models in Butterworth et al. (2014) suggests a global
439 mantle sinking rate of 1.5 to 2.0 cm/yr, which is also consistent with the 2.0 ± 0.8 cm/yr mantle
440 sinking rate inferred from mantle flow modelling (Steinberger et al., 2012). However, other work
441 applying mantle flow modelling highlights the time-varying nature of slab sinking rates, which is an
442 important consideration when interpreting slabs from the present-day snapshot in seismic
443 tomography (Bower et al., 2013).

444

445 **1.3 Numerical modelling of Tethyan geodynamics**

446

447 The evolution of the Tethyan realm has been the focus of decades of research, to better
448 understand the India-Eurasia collision and the complex tectonics of Southeast Asia and New
449 Guinea. A wide range of physical (analogue) and numerical experiments at crustal, lithosphere and
450 mantle scales have revealed important aspects of the plate-mantle system that are responsible for
451 the geodynamics of the Tethyan, Eurasian and Pacific tectonic domains. Since our approach
452 requires modelling in a spherical domain with assimilation of plate reconstructions, only numerical
453 methods are appropriate to study the long-term eastern Tethyan subduction history in a regional and
454 global framework.

455 Wide ranges of numerical approaches exist to model mantle behaviour – including forward
456 or backward advection models (including inverse and adjoint approaches), forward models with
457 data assimilation, and fully geodynamic models that do not have imposed boundary conditions.
458 Forward models assume that the plate motion histories are a reasonably good recorder of plate-
459 mantle evolution, and use the plate motions as a surface kinematic boundary condition to predict
460 mantle structure that can be compared to seismic tomography. Backward advection models use
461 seismic tomography (as a present-day snapshot of the mantle) as an input where the seismic
462 velocity anomalies are converted to density perturbations, assuming that the bulk of the anomaly
463 has a thermal source, and the sign of gravity and time reversed to compute the past position of the
464 mantle material (Glišović and Forte, 2014; Liu and Gurnis, 2008; Steinberger and O'Connell, 1998).
465 The backward advection models take into account the complex present-day mantle structure, but
466 can only be successfully used for times since ~70 Ma due to the inherent issues of irreversible
467 thermal diffusion and the interaction of the boundary layers with internal flow (Bunge et al., 2003;
468 Conrad and Gurnis, 2003; Steinberger and O'Connell, 1998). More advanced approaches using
469 adjoint models overcome the limitations of irreversible backward advection (Liu and Gurnis, 2008;
470 Spasojevic et al., 2009), but have yet to be applied to the Tethyan domain. Since our region of
471 interest requires deeper time considerations, we use forward geodynamic flow experiments that are
472 tested against mantle tomography.

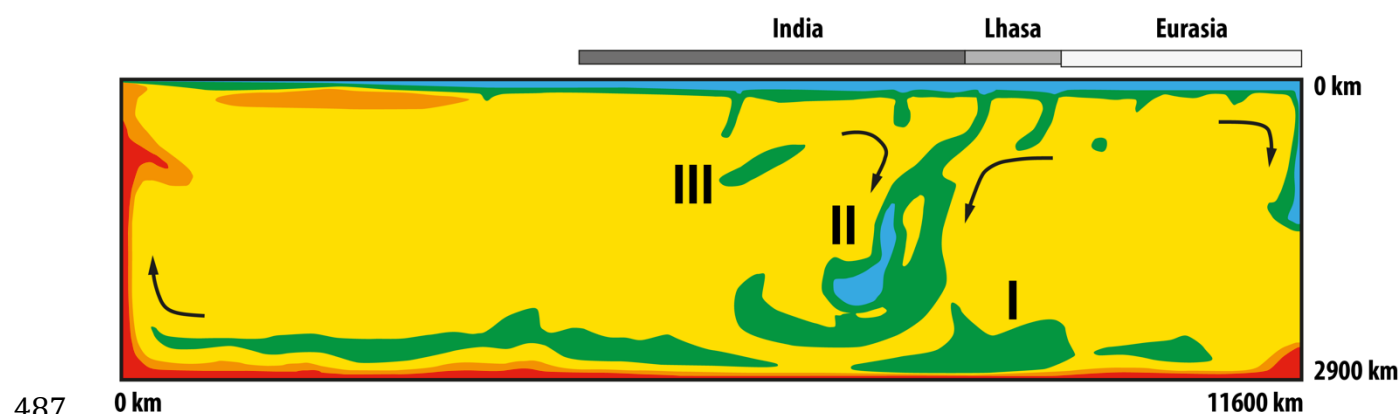
473

474 ***1.3.1 Numerical models of India-Eurasia convergence***

475

476 Following the interpretation of discrete Tethyan slab volumes at mid-mantle depths beneath
477 India in P-wave seismic tomographic models by van der Voo et al. (1999b), a numerical approach
478 using a 2D box (with 16.5 km mesh resolution) was used by Jarvis and Lowman (2005) to interpret
479 the inferred Tethyan mantle structure (Fig. 6). A number of experiments were conducted,
480 specifically varying the poorly-constrained viscosity contrast between the upper and lower mantle,

481 with the results requiring a lower mantle that was at least 30 times more viscous than the upper
 482 mantle to maintain Tethyan slabs at mid-mantle depths (Jarvis and Lowman, 2005). The resulting
 483 upper and lower mantle viscosity contrast from Jarvis and Lowman (2005) was also consistent with
 484 earlier estimates of a 10 to 30 times more viscous lower mantle from global models fitting geoid
 485 anomalies over slabs (Hager, 1984).
 486



487 **Fig. 6.** Numerical 2D box model of India-Eurasia convergence, adapted from Jarvis and Lowman
 488 (2005), provided an important benchmark for quantifying and testing tectonic reconstruction
 489 scenarios of India-Eurasia convergence and Tethyan geodynamics.
 490

491
 492 Due to the limitation of a 2D box set-up, the India-Eurasia convergence modelled by Jarvis
 493 and Lowman (2005) required a simplified convergence history along a single transect despite a
 494 complex active margin with periods of oblique convergence. The applied velocity boundary
 495 condition led to symmetric downwellings rather than one-sided subduction. However, the work of
 496 Jarvis and Lowman (2005) highlighted the need for quantitative approaches to test plate
 497 reconstructions, while suggesting a lower limit on the viscosity contrast between the upper and
 498 lower mantle. The approach utilised simple kinematic boundary conditions for the convergence
 499 velocities, which were assumed to be ~17 and 6 cm/yr (Besse and Courtillot, 1988) before and after
 500 the India-Eurasia collision, respectively, at 42 Ma. Their subsequent numerical approach made use
 501 of a simple sinking slab in a 2D and 3D Cartesian box (Jarvis and Lowman, 2007), which suggested

502 a viscosity contrast of a factor of 100 to 300 between the upper and lower mantle to maintain
503 Tethyan slabs in the mid-mantle. These results suggested that Jurassic slabs likely retain a thermally
504 anomalous signature with respect to the ambient mantle, enabling their detection by seismic
505 tomographic techniques.

506 Becker and Faccenna (2011) used a 3D global approach to investigate the plate driving
507 forces acting on the circum-Tethyan regions, and converted P- and S-wave seismic tomographic
508 models to density anomalies driving instantaneous mantle flow models. They found that there was a
509 dominant first-order mantle conveyor belt with northward velocities in the shallow mantle beneath
510 India, sinking of mantle material near the suture zone, and accompanying southward flow that is
511 interrupted by mantle upwelling in the region of the Carlsberg and Central Indian ridges. The work
512 highlights the power of global models in capturing the complexity of slab interactions from circum-
513 Tethyan subduction, with results suggesting that large-scale mantle flow and an associated Tethyan
514 conveyor supports ongoing indentation by India. Similarly, a 3D global spherical approach using
515 CitcomS (Zhong et al., 2000) was applied in Zahirovic et al. (2012), where plate kinematic
516 boundary conditions were applied from 140 Ma to test end-member subduction scenarios
517 accommodating India-Eurasia convergence. The forward numerical model predictions were
518 compared to slabs interpreted from seismic tomography (Zahirovic et al., 2012), and showed that
519 the mantle structure could be better reproduced when taking into account intra-oceanic subduction
520 and a two-stage India-Eurasia collision (Aitchison et al., 2007; Hafkenscheid et al., 2006; van der
521 Voo et al., 1999b). This earlier work highlights the need to test end-member plate reconstruction
522 scenarios using mantle flow models, and comparisons to mantle structure from seismic tomography
523 as an additional criterion for reconciling surface geology.

524 More recently, a 3D approach was also employed in Yoshida and Hamano (2015), who ran a
525 forward convection model from Pangea times, but without applying a kinematic boundary condition
526 or being able to incorporate one-sided subduction. Although many of the experiments failed to
527 reproduce present-day arrangements of continents (such as predicting a problematic fit of

528 Antarctica with South America), one aspect of the models reproduced the approximate present
529 position of India and highlights the requirement of long-lived subduction along southern Eurasia
530 since Pangea breakup (Yoshida and Hamano, 2015). When considering the motion of India towards
531 Eurasia, the anomalously high velocities (more than 14 cm/yr) of India between ~80 and 65 Ma can
532 be modelled numerically through a viscous coupling mechanism between two simultaneous north-
533 dipping subduction zones in the Neo-Tethys prior to India-Eurasia collision (Jagoutz et al., 2015).
534 This modelling approach suggests that two subduction zones in the Neo-Tethys are required to
535 account for the high convergence rates as long-lived (~20 Myr) accelerations cannot be explained
536 by plume influences, which are likely to diminish over a shorter timeframe of several millions of
537 years (van Hinsbergen et al., 2011).

538 When considering the mantle-surface interaction from Tethyan tectonics,, the work of Pusok
539 and Kaus (2015) used a 3D numerical box model that captured both subduction processes and the
540 resulting topographic response to the India-Eurasia collision, providing insight on the formation of
541 oroclinal in the eastern and western syntaxes of the convergence zone, as well as the uplift of the
542 Tibetan Plateau and lateral expulsion of continental material. Major advances are also being made
543 in reducing the uncertainties in the rheology of the mantle and lithosphere in such numerical
544 models, with the recent work (Baumann and Kaus, 2015) highlighting a new, and currently
545 computationally-intensive, approach of parallel inversion of observables including the gravity field,
546 topography and GPS velocities to better model the lithospheric and crustal rheology. Other
547 advances in inverse methods have the potential to fully incorporate the details of slabs and their
548 coupling to lithospheric plates with fault-zones between plates with fully non-linear rheologies,
549 which remains one of the largest uncertainties in mantle convection modelling (Ratnaswamy et al.,
550 2015; Worthen et al., 2014). Such approaches provide a framework for geodynamic computations
551 that capture realistic non-linear rheologies, including strain rate weakening and yielding, to better
552 account for plate velocity observations, complex slab-trench interactions, and intra-plate

553 deformation that goes beyond the simplifying assumption of plate rigidity (Alisic et al., 2012; Alisic
554 et al., 2010).

555

556 ***1.3.2 Numerical modelling of Southeast Asia and New Guinea geodynamics***

557

558 Few geodynamic models of mantle-, lithospheric- and crustal-scale evolution exist for the
559 tectonically complex and less constrained Sundaland and New Guinea regions than for other parts
560 of the Tethyan tectonic domain. For example, the synthesis by van Ufford and Cloos (2005) of at
561 least six competing proposed scenarios for the Cenozoic evolution of New Guinea highlights the
562 uncertain chronology of major tectonic events, as well as poorly-constrained subduction polarities.
563 As a result, much of the numerical modelling has been restricted to understanding the present-day
564 geodynamic character of the region. Ghose et al. (1990) used focal mechanism solutions to build a
565 3D finite element numerical experiment of subducted slabs and generalised mantle structure in the
566 Sundaland region to compute the flow and stress field acting on the overriding continental
567 promontory. The results indicate significantly higher plate coupling across the Sumatra segment of
568 the Sunda Trench, resulting in a higher seismogenic potential than the Java region. This may be due
569 to lower coupling assumed to be due to the lubricating effect of soft sediments in the trench (e.g.,
570 Clements and Hall, 2011), as well as the subduction of older Indian Ocean crust than along the
571 Sumatra segment (Ghose et al., 1990).

572 North of New Guinea, the geodynamic significance of the Philippine Sea Plate has been the
573 subject of a number of studies that employ numerical modelling to quantify the effects of Izu-
574 Bonin-Mariana subduction initiation (Gurnis et al., 2004; Hall et al., 2003; Leng and Gurnis, 2015)
575 on the Pacific Plate boundary forces, and its contribution to a change in Pacific Plate motion
576 between ~50 and 40 Ma based on force balance calculations (Faccenna et al., 2012). Temporally
577 linked to the inception of (proto-) Izu-Bonin-Mariana subduction, major changes in subduction
578 along New Guinea in the Eocene have been invoked to explain the acceleration of Australia's

579 northward motion (Schellart and Spakman, 2015; Zahirovic et al., 2014) from ~43 Ma (Williams et
580 al., 2011). Schellart and Spakman (2015) identified a subducted slab at depths between ~800 and
581 1200 km beneath Lake Eyre in eastern Australia, and argued based on a simple Stokes flow model
582 that the topographic depression is caused by dynamic subsidence induced by the sinking of a slab
583 that detached along New Guinea at ~55-45 Ma. However, the complex interaction of slabs from
584 regional subduction zones plays an important role that can only be tested in regional and global
585 geodynamic numerical simulations that capture the time-dependent evolution of Southeast Asian
586 plate boundaries.

587

588 **2 Methods**

589

590 **2.1 Plate tectonic reconstructions**

591

592 Reconstructions of the Tethyan domain have taken many forms over decades of research (see
593 Section 1.1, Table 1, Fig. 4), with the post-Pangea plate reconstruction timeframe (since ~200 Ma)
594 generally associated with lower uncertainties than earlier times due to greater preservation of
595 oceanic crust (Zahirovic et al., 2015). Due to the ambiguity in reconstructing regions with no
596 preserved seafloor spreading records and/or poor geological constraints, testing alternative
597 scenarios becomes an avenue to evaluate the uncertainty inherent in plate reconstructions. In this
598 study we present a new post-Jurassic plate motion model spanning the Tethyan region from the
599 westernmost India-Eurasia convergence segment, in the vicinity of Kohistan-Ladakh, eastward to
600 Southeast Asia (including Sundaland and the proto-South China Sea) and Papua New Guinea. The
601 model is also compared to the previous synthesis of the region presented in Zahirovic et al. (2014)
602 for Southeast Asia and New Guinea, and in Gibbons et al. (2015) for the India-Eurasia convergence
603 zone, highlighting the alternative kinematic scenarios that can account for the constraints from

604 marine and onshore data (Supplementary Animation 1). The refinements presented in this study
605 focus on an alternative model for the Neo-Tethys, transferring the East Java-West Sulawesi blocks
606 from the Argo Abyssal Plain on the NW Australian shelf towards Sundaland, as well as refinements
607 to the evolution of the Kohistan-Ladakh, Woyla, and Philippine intra-oceanic arcs, in the context of
608 the evolving Sundaland and New Guinea continental margins (see Section 3).

609 Relative plate motions are derived from preserved seafloor spreading histories (as in third and
610 fourth generation reconstructions from Table 2), where seafloor magnetic anomalies are identified
611 and combined with directional constraints from fracture zones to compute the Euler rotation that
612 defines the relative rigid body motions on the surface of a sphere. We use the Global Seafloor and
613 Magnetic Lineation Database of previously-published magnetic anomaly picks (Seton et al., 2014)
614 and fracture zone geometries (Matthews et al., 2011), which were combined to compute relative
615 plate motion parameters in previous studies (see discussion and references in Seton et al., 2012),
616 preferably using the least-squares best-fit statistical method following Hellinger (1981) and Royer
617 and Chang (1991). The rotation parameters are calibrated to the geomagnetic polarity reversal
618 timescale of Gee and Kent (2007), which is an updated timescale compared to the one used in our
619 previous plate reconstruction of the Tethyan region in Zahirovic et al. (2014) and Gibbons et al.
620 (2015). In the absence of preserved seafloor spreading histories, we use onshore geological
621 constraints to estimate the pre-rift position of continental fragments, the timing and trajectory of
622 rifting, as well as the age and location of the accretion events (Tables 2-3). We construct synthetic
623 oceanic plates that are consistent with plate tectonic driving mechanisms and reasonable relative
624 plate motions across plate boundaries (e.g., convergence across subduction zones, divergence across
625 mid-oceanic ridges, strike-slip motion along transform faults).

626 The relative plate motions form a chain that is hierarchical and typically ties all plate motions
627 back to Africa, largely due to the central position of Africa within Pangea and relative stability
628 because it is surrounded by mid-oceanic ridges (Torsvik et al., 2008). The motion of Africa is
629 expressed with respect to the underlying mantle, using Indo-Atlantic or global hotspot tracks since

630 ~100 Ma to derive a frame of reference for the global plate motion model. For earlier times when
631 no hotspot tracks are available, the True Polar Wander- (TPW) corrected paleomagnetic reference
632 frame of Steinberger and Torsvik (2008) is used. Due to the lack of paleo-longitudinal constraints in
633 a paleomagnetic reference frame resulting from the radial symmetry of the Earth’s magnetic dipole,
634 we apply a 10° longitudinal shift gradually between 70 and 105 Ma to the TPW-corrected reference
635 frame, following Butterworth et al. (2014) and van der Meer et al. (2010) to provide a better paleo-
636 longitudinal link between subduction zones and Jurassic and Cretaceous subducted slabs interpreted
637 from seismic tomography.

638 The combination of relative plate motions with an absolute reference frame enables the
639 computation of absolute plate motions through time, modelled using the GPlates software (Boyden
640 et al., 2011). Evolving plate boundaries are constructed using continuously-closing plate polygon
641 algorithm (Gurnis et al., 2012), which provides global coverage of plates through time in 1 Myr
642 intervals. The Tethyan plate motions are embedded in a global model, which is based on the
643 synthesis in Seton et al. (2012) with regional refinements that are documented in Müller et al.
644 (2016). The time-dependent plate boundaries, seafloor age-grids and plate velocities are assimilated
645 into the numerical models of mantle convection, described in Section 2.3. By considering the
646 evolution of the entire plate (Gurnis et al., 2012; Stampfli and Borel, 2002) rather than only
647 focusing on continental blocks, plate reconstructions can be linked to geodynamic models (Conrad
648 and Lithgow - Bertelloni, 2004; Lithgow - Bertelloni and Richards, 1998). The coupling of plate
649 kinematics to geodynamic models provides the opportunity to reproduce the mantle structure
650 interpreted from seismic tomography as well as reconstruct past mantle flow using the present-day
651 surface geology and tectonics as constraints.

652

653 Table 3. Constraints used to construct plate motion model.

Region	Event	Timing	Dating method/ interpretation	Interpretations based on data and
--------	-------	--------	----------------------------------	--------------------------------------

				models
Australian NW Shelf	Onset of rifting	Sometime in Late Jurassic	Stratigraphic rift-drift sequences	Pigram and Panggabean (1984)
	Triple junction mid-oceanic ridge configuration	Latest Jurassic	Geometrical requirement, and evidence of possible plume influence	Audley-Charles (1988), Audley-Charles et al. (1988), Gibbons et al. (2012), Rohrman (2015)
	Onset of seafloor spreading	155 ± 3.4 Ma	K-Ar of basaltic basement	Gradstein and Ludden (1992)
West Sulawesi, East Java, Mangkalihat and easternmost Borneo	Onset of rifting	Late Jurassic	Biostratigraphic constraints in Paremba Sandstone and shallow marine sandstones in Bantimala Complex	Sukamoto and Westermann (1992), Wakita (2000)
	Onset of seafloor spreading	~158-155 Ma	K–Ar of diorite, microgabbro and basaltic dyke	Polvé et al. (1997)
	Oldest seafloor spreading magnetic anomalies	M25A M26 (~153-155 Ma)	Magnetic anomaly identifications from shiptracks	Heine and Müller (2005) Gibbons et al. (2012)
	Youngest preserved seafloor spreading magnetic anomaly in the Argo Abyssal Plain region	M10Ny, 128.9 Ma	Magnetic anomaly identifications from shiptracks	Gibbons et al. (2012)
	Suturing of ‘Argoland’ to	~80 Ma	Stratigraphy, K–Ar and U–Pb of	Wakita (2000) Clements and Hall

	southwest Borneo core		metamorphics, synthesis of previous studies	(2011)
New Guinea	Rifting on northern New Guinea (opening of Sepik ocean basin)	Late Jurassic 172 Ma ~157 ± 16 Ma	Jurassic granite in Bena Bena Terrane SSZ ophiolites in Central Ophiolite Belt	Davies (2012) Permana (1998)
	Subduction influence on eastern New Guinea	Early Cretaceous	Kondaku Tuffs	Dow (1977), Rickwood (1954)
	Onset of Sepik ocean basin subduction	Maastrichtian (~71 to 66 Ma)	Stratigraphic correlation and dating using foraminifera	Worthing and Crawford (1996)
		68 Ma	High-temperature metabasites on West Papuan Ophiolite	Davies (2012)
	Sepik Terrane docking with New Guinea	35-31 Ma	Ar-Ar age of Emo metamorphics	Worthing and Crawford (1996)
		~30 Ma	Cooling histories from exhumation	Crowhurst et al. (1996)
	South-dipping subduction	~18-8 Ma	Maramuni Arc volcanics	Hill and Hall (2003), Page (1976)
	Halmahera Arc collision	~14 Ma	Compression in PNG Mobile Belt, apatite fission track geochronology	Hill and Raza, (1999), Kendrick (2000)
Lhasa	Onset of Neo-Tethyan subduction	~170 Ma (to 137 Ma)	Calc-alkaline granites and granitoids	Zhang et al. (2012)

	Onset of intra-oceanic subduction along Kohistan-Ladakh Arc	~154 Ma	Matum Das tonalite	Schaltegger et al. (2003)
	Subduction along Zedong Terrane	161.0 ± 2.3 Ma, ~156 Ma, 152.2 ± 3.3 Ma	Dacite breccia, Andesite dyke/breccia, Quartz diorite, Andesitic dyke	McDermid et al. (2002)
	Magmatic hiatus on Lhasa	~137 to 109 Ma, ~75 to 60 Ma	Magmatic gap in Gangdese Batholith	Ji et al. (2009), Wen et al. (2008), Chung et al. (2005)
	Initiation of Kohistan-Ladakh back-arc basin subduction along Lhasa	~109 Ma	Resumption of arc volcanism in Gangdese Batholith	Ji et al. (2009), Wen et al. (2008)
	Maximum southward position of Kohistan-Ladakh Arc	~100 Ma	Equatorial paleo-latitudes from mid- to Late Cretaceous red beds	Zaman and Torii (1999)
	Kohistan-Ladakh collision with Greater India	~60 to 50 Ma	Cessation of calc-alkaline magmatism, stratigraphic constraints of collision, slowdown in Indian Ocean seafloor spreading at ~52 Ma, change in arc magma chemistry by ~50 Ma	Khan et al. (2009) Hu et al. (2015) Cande et al. (2010) Bouilhol et al. (2013)

	Kohistan-Ladakh collision with Eurasia	~47 to 40 Ma	Slowdown in India-Africa seafloor spreading, Indian Ocean microplate formation, completion of Andean-style subduction (Linzizong), change in arc magma chemistry by ~40 Ma	Cande and Patriat (2015) Matthews et al. (2016) Chung et al. (2005) Bouilhol et al. (2013)
West Burma	Onset of Neo-Tethyan subduction	~163-152 Ma	Jadeite geochronology	Shi et al. (2008, 2014)
	Onset of Neo-Tethyan intra-oceanic subduction	~156-150 Ma	Biostratigraphic ages of cherts constraining age of Naga Ophiolite formation	Baxter et al. (2011)
	Subduction of Woyla back-arc basin	~113-110 Ma (Albian) ~105-90 Ma 95 ± 2 Ma	Albian unconformity on West Burma Wuntho-Popa Arc SSZ formation of Andaman Ophiolite	Morley (2012a) Mitchell et al. (2012) Pedersen et al. (2010)
Sumatra	Onset of Neo-Tethyan subduction	~170 Ma ~165-140 Ma (?)	Onset of arc volcanism in Sumatra segment Minor UHP/VHP metamorphism	McCourt et al. (1996) Parkinson et al. (1998)
	Subduction of Woyla back-arc basin	From ~115 Ma	Peak in UHP/VHP metamorphism in	Parkinson et al. (1998)

		~105-75 Ma	Meratus and Luk Ulo sutures Wuntho-Popa Arc volcanism to the west, and Woyla intrusions	Mitchell et al. (2012), McCourt et al. (1996), Wajzer et al. (1991)
	Woyla Arc accretion	~75-62 Ma	Magmatic gap of arc volcanics on Sumatra	McCourt et al. (1996)
	Onset of Sunda subduction	62 Ma	Arc volcanism on Sumatra	McCourt et al. (1996)
West Java/ East Borneo	Onset of NeoTethyan subduction	~180-165 Ma	Schist in Meratus Complex	Wakita et al. (1998)
		~170 Ma (Bajocian)	Radiolarians	Wakita et al. (1998)
		~160 Ma	Zircon age spectra	Clements and Hall (2007)
	Late stage of Woyla/Barito back-arc basin subduction along Sunda continental margin	~100 Ma	Peak in zircon age spectra	Clements and Hall (2007)
		~100-93 Ma	Cenomanian/Turonian Meratus Ophiolite obduction	Pubellier et al. (2004), Yuwono et al. (1988)
	Suturing of East Java	~80 Ma	Stratigraphy, K–Ar and U–Pb of metamorphics, synthesis of previous studies	Wakita (2000) Clements and Hall (2011)
	Onset of Sunda	65 Ma	Subduction-related	Guntoro (1999), van

	subduction		rocks on Sulawesi	Leeuwen (1981)
Philippine Arc	Onset of south-dipping subduction along New Guinea (Sepik)	156.3 ± 2.0 Ma and 150.9 ± 3.3 Ma 142 ± 4 Ma	SSZ ophiolitic crust from the Lagonoy Ophiolite Ophiolite crystallisation from Gag Island, Halmahera	Encarnación (2004)
	Continued arc volcanism	126 ± 3 Ma and 119 ± 2 Ma 99.9 ± 7.0 Ma 100 ± 4 Ma	SSZ volcanics from Cebu Island Ar-Ar age of the Calaguas Ophiolite Arc rocks reported from Obi Island on Halmahera	Deng et al. (2015) Geary et al. (1988), Geary and Kay (1989) Hall et al. (1995b)

2.2 Insights from seismic tomography

The distribution of ophiolites, intra-oceanic arc fragments and a complex network of sutures within southern Eurasia (Figs. 1-3), Southeast Asia and New Guinea preserve the remnants of oceanic basins that have been lost to subduction. Although the consumption of oceanic basins leaves physical evidence in the form of arc volcanics, accreted seamounts and ocean floor sediments, and ophiolites, the present-day mantle structure illuminated using seismic tomographic methods holds additional clues to the geodynamic evolution of these regions (Hafkenscheid et al., 2006; Replumaz et al., 2004; van der Voo et al., 1999a; van der Voo et al., 1999b).

As an estimate of the location of subduction through time, depth slices of fast seismic velocity anomalies are age-coded according to an assumption of vertical slab sinking with an average

sinking rate. In this study we compare our revised plate reconstructions with the publicly-available P-wave seismic tomography depth slices from Li et al. (2008), assuming a sinking rate of 3 and 2 cm/yr in the upper and lower mantle, respectively, following Hafkenscheid et al. (2006). Hafkenscheid et al. (2006) also noted that the upper mantle sinking rates are likely to be similar to the convergence rate at the trenches, which may suggest even higher sinking rates for the circum-Tethyan region in the context of Australia's 6-8 cm/yr, the Pacific's ~8 cm/yr, and India's ~5 cm/yr root mean square velocities since ~40 Ma (Zahirovic et al., 2015). To investigate, we test a higher end-member sinking rate of 8 cm/yr in the upper mantle, which is likely only meaningful for the Cenozoic as constrained by seafloor spreading histories and detailed hotspot tracks for the Pacific. The sinking rates applied in this study are significantly higher than the ~1.2-1.3 cm/yr whole-mantle average global slab sinking rates (Butterworth et al., 2014; van der Meer et al., 2010), with a similar slower and constant sinking rate scenario applied to age-coding of slabs in P- and S-wave seismic tomography in Zahirovic et al. (2014). However, a faster sinking rate, with differential rates in the upper and lower mantle, was found to better reproduce the evolution of major Tethyan and Southeast Asian subduction zones (Zahirovic et al., 2014). Importantly, we note that the assumption of vertical and temporally constant sinking rates along a single subduction zone, not to mention across a range of subduction zones in a region, is likely an oversimplification and requires testing using numerical simulations of mantle flow, as was carried out in Butterworth et al. (2014).

We compare our numerical mantle flow predictions to a number of P- and S-wave seismic tomography models, because tomographic models are typically constructed using a variety of methods, which incorporate different seismic phases and parameterisations (Grand, 2002; Romanowicz, 2008). P-wave models tend to have higher resolutions than S-wave models, due to the limited number of S-wave phases that can be used in seismic tomographic inversions (Widiyantoro et al., 1998). Beyond the inherent higher resolution of P-wave models in well-sampled continental regions, the Li et al. (2008) global seismic tomography model has additional coverage by

691 incorporating coverage using the Chinese Seismographic Network, leading to a better sampling of
692 the Tethyan and Asian mantle.

693 The limitation of P-wave models is that they tend to bias their sampling of the mantle beneath
694 continental crust, leading to lower seismic velocity anomaly amplitudes in oceanic regions. For
695 example, a subducted slab that may straddle oceanic and continental regions (such as the Tethyan
696 slabs) may appear “faded” beneath the oceanic regions. Although S-wave models tend to have
697 lower resolution, they offer more equal sampling of the mantle beneath oceans and continents
698 (Grand, 2002). Due to the lack of permanent seismic stations in the oceans (except for some stations
699 located on islands) and over Antarctica, the coverage and sampling for both P- and S-wave seismic
700 tomography models is poorer for the southern hemisphere and all oceanic regions (Romanowicz,
701 2008). As regional tomographic models can have edge artefacts (Foulger et al., 2013), and typically
702 are not represented as seismic velocity anomalies with respect to the global mantle, we focus on
703 using only global tomographic models in our comparisons.

704

705 **2.3 Coupled plate reconstructions and mantle convection numerical models**

706

707 To better understand the geodynamic implications of the plate reconstructions, and go beyond
708 the assumption of constant and vertical slab sinking used in simple interpretations of mantle
709 structure, we couple the plate kinematics to computations of mantle flow. We use the mantle
710 convection modelling code CitcomS (Zhong et al., 2000)
711 (<https://geodynamics.org/cig/software/citcoms/>), modified to progressively assimilate surface plate
712 velocities, the thermal structure of the lithosphere and the shallow thermal structure of subducting
713 slabs (Bower et al., 2015) from our plate motion model (Fig. 7a). The temperature and thickness of
714 the lithosphere is derived using a half-space cooling model and the synthetic age of the ocean floor.
715 Slabs are assimilated into the mantle to a depth of 350 km but convection is entirely dynamic away
716 from slabs and below the lithosphere. We computed numerical models from 230 Ma to the present

717 to capture the post-Pangea mantle evolution, with global plate reconstructions of the pre-Late
718 Jurassic described in Müller et al. (2016). However, we analyse the mantle evolution since the latest
719 Jurassic (~160 Ma) for which time the plate reconstructions are regionally refined, and the mantle
720 flow models have reached a dynamic equilibrium from the synthetic initial condition (Flament et
721 al., 2014). Initially at 230 Ma, slabs are inserted down to 1400 km depth, with a 45° dip down to
722 425 km and 90° below 425 km. In the initial conditions, slabs are twice as thick in the lower mantle
723 than in the upper mantle to account for advective thickening observed in tests in which slabs are
724 only initially inserted in the upper mantle. The initial condition includes a basal thermochemical
725 layer 113 km thick just above the core–mantle boundary (CMB) that consists of material 3.6%
726 denser than ambient mantle. This condition suppresses the formation of plumes, but does not
727 impede the formation of large-scale mantle upwellings. The surface and CMB are isothermal at
728 273 K and 3100 K, respectively (Fig. 7b). Subduction zones that appear (initiate) during the model
729 run are progressively inserted as slabs in the uppermost mantle (Bower et al., 2015). The kinematic
730 boundary conditions, generated in GPlates, and the thermal volume conditions for the lithosphere
731 and shallow subduction, are assimilated in 1 Myr intervals, as described in Bower et al. (2015). The
732 average model resolution, obtained with $\sim 13 \times 10^6$ nodes and radial mesh refinement, is
733 $\sim 50 \times 50 \times 15$ km at the surface, $\sim 28 \times 28 \times 27$ km at the core–mantle boundary (CMB), and $\sim 40 \times$
734 40×100 km in the mid-mantle.

735

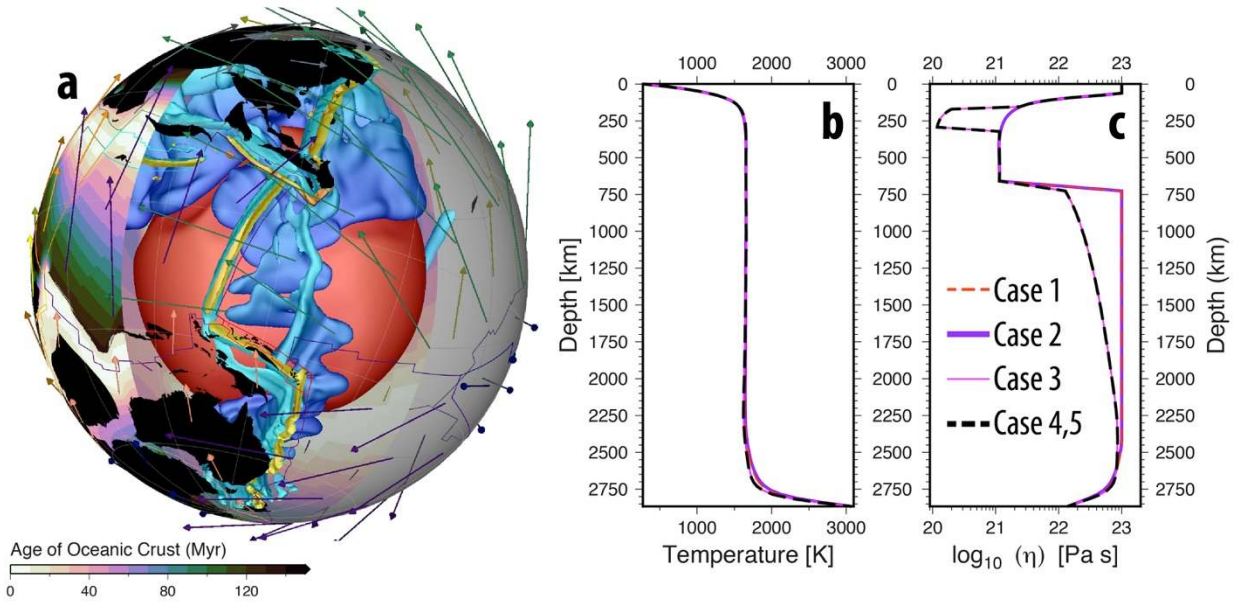


Fig. 7. a) Assimilation of plate velocities (arrows), subduction zones (yellow) and thermal lithospheric thickness based on the age of the seafloor from plate reconstructions in GPlates, with 3D volume contours of dynamic cold slabs (blue) and hotter upwellings (red) predicted by the mantle convection code CitcomS (here using Case 5, see Section 2.3 and Table 5). Reconstructed present-day coastlines (black) are provided as a reference. Slab colouring is a function of depth from light blue (shallow mantle) to darker blue (deep mantle). Seafloor age-grid is applied globally, but is cut out in this schematic to highlight the internal mantle structure. b) Horizontally-averaged present-day mantle temperature, and c) present-day average viscosity in the five numerical cases (see Section 2.3, and Table 5).

The vigour of mantle convection is defined by the Rayleigh number, Ra , where:

$$Ra = \frac{\alpha_0 \rho_0 g_0 \Delta T h_M^3}{\kappa_0 \eta_0},$$

in which α is the coefficient of thermal expansion, ρ the density, g the acceleration of gravity, ΔT the temperature difference between surface and CMB, h_M the thickness of the mantle, κ the thermal diffusivity, and η the viscosity; the subscript “0” indicates reference values (see Table 4). The viscosity of the slabs and mantle are stress- and temperature-dependent, following

$$\eta = \eta_0(r) \exp \left(\frac{E_\eta}{R(T + T_\eta)} - \frac{E_\eta}{R(T_b + T_\eta)} \right)$$

753 where $\eta_0(r)$ is a depth-dependent pre-factor defined with respect to the reference viscosity, η_0 , E_η is
 754 the dimensional activation energy (E_{UM} in the upper mantle and E_{LM} in the lower mantle), R is the
 755 universal gas constant, T is the temperature, T_η is a temperature offset, and T_b is the ambient mantle
 756 temperature outside the thermal lithosphere, slabs or the basal thermal boundary layer (see Table 4).
 757 Although the viscosity of the upper mantle can be estimated in studies of post-glacial rebound
 758 (Fjeldskaar et al., 2000; Gasperini and Sabadini, 1989; Lambeck et al., 1998), the viscosity of the
 759 lower mantle is less well constrained, which has resulted in a wide range of proposed viscosity
 760 profiles. Previous approaches have argued for a factor of 10 increase in viscosity between the upper
 761 and lower mantle (Paulson et al., 2007), while others have argued for a factor of 30 (Hager, 1984)
 762 or 100 (Forte and Mitrovica, 1996; Steinberger and Calderwood, 2006). We vary the viscosity
 763 profile (Fig. 7c, Table 5) with cases 1 to 4 based on the plate reconstructions from Zahirovic et al.
 764 (2014) and Gibbons et al. (2015), and a fifth case based on the refined plate reconstructions
 765 presented in this study. The viscosity of the lower mantle in each cases is either 100 times more
 766 viscous than the upper mantle, or increases gradually with depth from a factor of 10 at the base of
 767 the transition zone (660 km) to a maximum of 100 in the lowermost mantle (Steinberger and
 768 Calderwood, 2006). Cases 3, 4 and 5 also incorporate a low-viscosity asthenosphere, which has
 769 been suggested to be an important decoupling layer that enables the elevated velocities of typically
 770 oceanic plates (Becker, 2006; Debayle and Ricard, 2013). Since paleo-longitudes are less well
 771 constrained earlier than ~ 100 Ma, we incorporate the van der Meer et al. (2010) subduction
 772 reference frame and their time-dependent longitudinal shift into Case 3. By using a variety of radial
 773 viscosity profiles, different absolute reference frames, and plate reconstructions between the five
 774 cases, allows us to capture some of the uncertainties involved in our approach of modelling deep-
 775 time plate reconstructions and mantle convection, and help test end-member plate reconstructions of
 776 the Tethyan region.

777 The time-dependent mantle structure is presented in 3D visualisations made with GPlates
 778 and as a series of vertical cross-sections that are reconstructed with the overriding plate to capture

779 the evolution of subduction, plotted using Generic Mapping Tools (Wessel et al., 2013). The
780 predicted present-day mantle structure is qualitatively compared to equivalent slices of P- and S-
781 wave seismic tomography models, where fast seismic velocity anomalies are compared to slab
782 contours (10% colder than ambient mantle, representing temperatures colder than $\sim 1270^{\circ}\text{C}$) from
783 the mantle convection models.

784

785 **Table 4.** Parameters common to all model cases. Subscript “0” denotes reference values.

Parameter	Symbol	Value	Units
Rayleigh Number	Ra	7.84×10^7	
Thermal expansion coefficient	α_0	3×10^{-5}	K^{-1}
Density	ρ_0	4000	kg m^{-3}
Gravity acceleration	g_0	9.81	m s^{-2}
Temperature change	ΔT	2825	K
Temperature offset	T_η	452	K
Background mantle temperature	T_b	1685	K
Mantle thickness	h_M	2867	km
Thermal diffusivity	κ_0	1×10^{-6}	$\text{m}^2 \text{s}^{-1}$
Reference viscosity	η_0	1×10^{21}	Pa s
Activation energy (upper mantle)	E_{UM}	100	kJ mol^{-1}
Activation energy (lower mantle)	E_{LM}	33	kJ mol^{-1}
Activation temperature	T_η	452	K
Universal gas constant	R	8.31	$\text{J mol}^{-1} \text{K}^{-1}$

Radius of the Earth	R_0	6371	km
---------------------	-------	------	----

786

787 **Table 5.** Model set-up for Case 1 – 5. Also refer to Fig. 7b-c.

	Case 1	Case 2	Case 3	Case 4	Case 5
Mesh nodes	$129 \times 129 \times 12$ (nodes on the surface) $\times 65$ (depth levels)				
Viscosity relative to Reference Viscosity (Lithosphere 0-160 km depth, Asthenosphere 160- 310 km depth, Upper mantle 310-660 km depth, Lower Mantle > 660 km depth)	1,0.1,1,100	1,1,1,100	$1,0.1,1,10 \rightarrow 100$ linear increase of viscosity from 10 to 100 with depth in the lower mantle to approximate the viscosity profile of Steinberger and Calderwood (2006)		
Plate reconstructions for the eastern Tethys	Zahirovic et al. (2014)		Slab-calibrated longitudinal positions from Zahirovic et al. (2014)	Zahirovic et al. (2014)	This Study

788

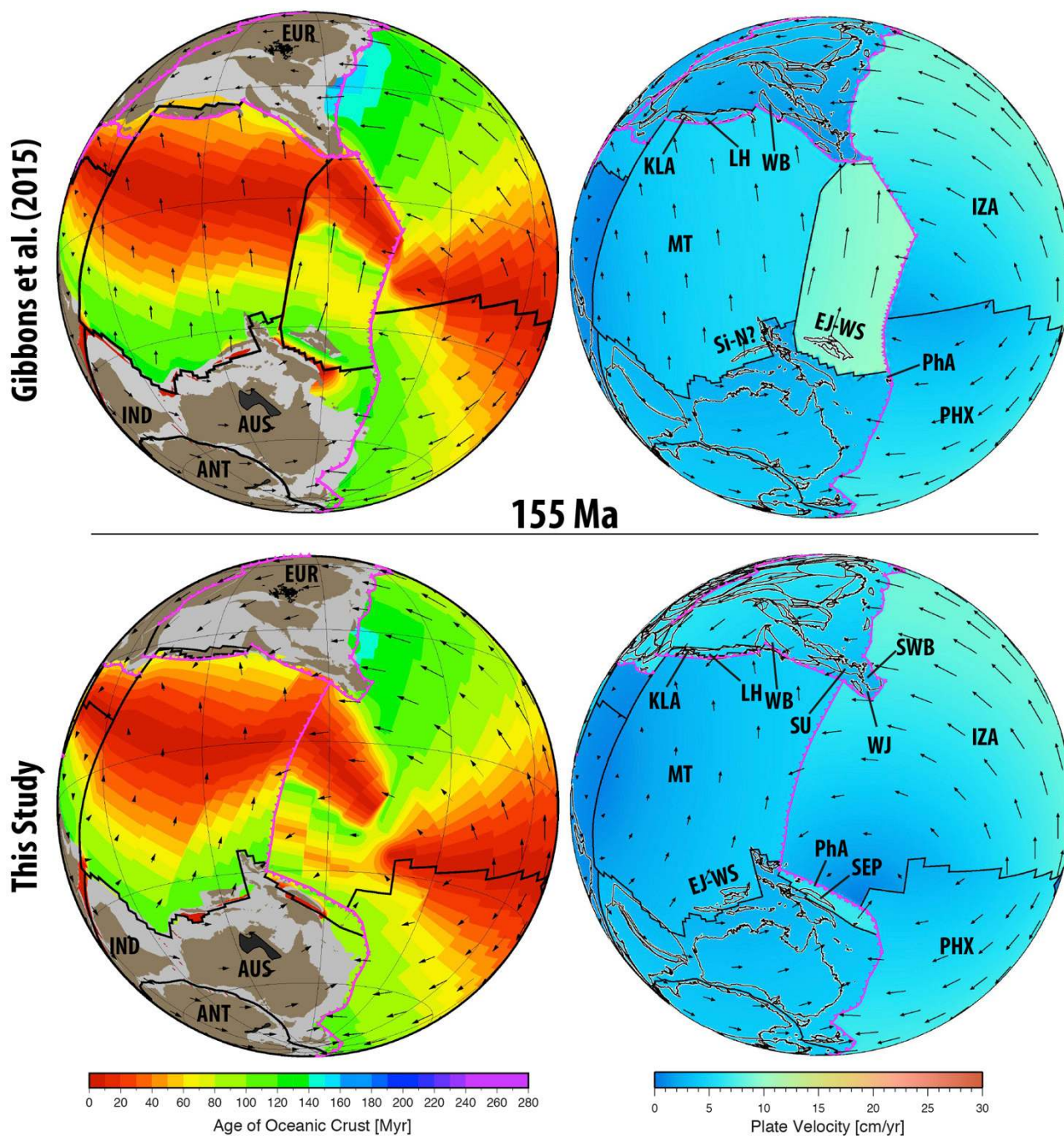
789 **3 Regional tectonic evolution**790 **3.1 Late Jurassic plate boundary configuration and rifting mechanism along northern**791 **Gondwana**

792

793 The Late Jurassic is marked by a major rifting event along northern Gondwana (Pigram and
794 Panggabean, 1984) (Figs. 4a and 8), which transferred a number of continental blocks (including
795 East Java, West Sulawesi, Mangkalihat and east Borneo) northward towards Eurasia (Hall, 2012;

796 Zahirovic et al., 2014), with the only portions of the seafloor spreading system preserved in the
797 Argo Abyssal Plain on the NW Australian shelf (Gibbons et al., 2013). Beyond the oldest preserved
798 oceanic crust, the plate configuration can only be inferred from proxy indicators found on
799 continents. One pertinent argument is that Audley-Charles (1988) and Audley-Charles et al. (1988)
800 required a triple junction plate boundary configuration in the Late Jurassic and Early Cretaceous in
801 the vicinity of the NW Australian shelf where northward slab pull from subduction along southern
802 Eurasia was the driving mechanism for detaching the Neo-Tethyan ribbon terrane (also in Fig. 4a).
803 This northward slab pull detached the continental fragments forming passive margins along the
804 northern and southern boundaries of the ribbon terrane, the preferred scenario presented here. An
805 alternative scenario has south-dipping subduction along northern Gondwana in the Late Jurassic,
806 leading to the opening of the Neo-Tethys and transfer of continental fragments northward through
807 slab rollback (Hall, 2012) (Fig. 4b). Both mechanisms are thought to be capable of detaching
808 continental fragments (see Stampfli and Borel, 2002), but, the south-dipping subduction end-
809 member requires continuous arc volcanism, some of which ought to be preserved on the drifting
810 ribbon terranes.

811



812

813 **Fig. 8.** Reconstruction of Neo-Tethyan ocean basin opening along northern Gondwana in the latest
814 Jurassic. Both the Zahirovic et al. (2014) and Gibbons et al. (2015) models (top) invoke East Java
815 and West Sulawesi rifting from New Guinea, as the simplest tectonic scenario to transfer the blocks
816 northwards toward Southeast Asia, and a possible origin of the Sikuleh and Natal (Si-N) fragments
817 from the Argo Abyssal Plain. Southwest Borneo (SWB), West Java (WJ), Sumatra (SU), West
818 Burma (WB) and Lhasa (LH) form the active Eurasian continental margin. Seafloor spreading in
819 the Neo-Tethys is driven by north-dipping subduction along southern Eurasia (EUR), consuming

820 the Meso-Tethyan (MT) oceanic crust and resulting in the incipient formation of the Kohistan-
821 Ladakh Arc (KLA). In the revised reconstructions, East Java and West Sulawesi (EJ-WS) are the
822 'Argoland' continental fragment originating in the Argo Abyssal Plain on the NW Australian shelf.
823 South-dipping subduction along New Guinea is modelled to detach the Sepik Terrane (SEP) from
824 the New Guinea margin through slab rollback, generating the embryonic components of the
825 Philippine Archipelago (PhA). The scale bars are relevant to all plate reconstruction figures. Grey
826 regions represent the extent of continental crust, dark grey represents large igneous provinces and
827 other plume products, and thin brown lines represent reconstructed fracture zones. ANT –
828 Antarctica, AUS – Australia, IND – India, IZA – Izanagi Plate, PHX – Phoenix Plate. Orthographic
829 reconstructions are centred on 115°E, 15°S. See Supplementary Animation 2, 3 and 4.

830

831 The NW Australian shelf, the putative source of the Argoland ribbon terrane records some
832 Late Jurassic and Early Cretaceous volcanic plateaus (e.g., Scott and Wombat plateaus, Joey Rise,
833 etc. – see Fig. 1), rift-related volcanics and seaward dipping reflectors (Heine and Müller, 2005;
834 Rohrman, 2015; von Rad et al., 1992). An earlier phase of rhyolitic volcanism between ~213 and
835 190 Ma erupted on the Wombat Plateau (von Rad and Exon, 1983; von Rad et al., 1992), but cannot
836 be temporally linked to the latest Jurassic (~155 Ma) rifting and seafloor spreading phase recorded
837 on the NW Australian shelf. Although the latest Jurassic NW Australian margin was volcanic, little
838 evidence exists that it was dominated by an Andean-style active margin (von Rad and Exon, 1983;
839 von Rad et al., 1992). Although the seismic interpretations by Hopper et al. (1992) of the margin's
840 volcanic history do not indicate widespread plume activity, the recent work of Rohrman (2015)
841 suggests a plume origin for the large volume of underplated material and widespread sills
842 interpreted from seismic sections in the Exmouth Plateau region (Fig. 1). One critical aspect of the
843 latest Jurassic event is that the onset of seafloor spreading is well-constrained by a 155 ± 3.4 Ma K-
844 Ar age of the oldest seafloor in the Argo Abyssal Plain (Gradstein and Ludden, 1992), consistent
845 with rapid tectonic subsidence in the latest Jurassic on the NW Australian shelf (Heine and Müller,

846 2005; Rohrman, 2015; Tovaglieri and George, 2014), and the identification of M25A (Heine and
847 Müller, 2005) or M26 (Gibbons et al., 2012) as the oldest magnetic anomalies (~153-155 Ma) in the
848 seafloor spreading record.

849 Due to the lack of latest Jurassic arc volcanics on the NW Australian Shelf, together with
850 strong indicators of north-dipping subduction initiation along southern Eurasia (see following
851 sections), we prefer northward slab pull as the driving mechanism for rifting and seafloor spreading
852 to open the Neo-Tethys from ~155 Ma. Although more work is required to test whether a plume
853 model can explain the volcanism on the NW Australian shelf in the latest Jurassic (Rohrman, 2015),
854 such a scenario would be consistent with the triple junction scenario invoked for this region
855 (Audley-Charles, 1988; Audley-Charles et al., 1988; Gibbons et al., 2015; Gibbons et al., 2012;
856 Zahirovic et al., 2014), and the similarity to the East African rift-plume interaction (Burke and
857 Dewey, 1973; Montelli et al., 2006; Yirgu et al., 2006). Since the Neo-Tethyan seafloor spreading
858 history is incomplete, it remains difficult to ascertain which continental blocks rifted from the Argo
859 segment of the Australian margin (Table 2). Rifting of East Java and West Sulawesi from New
860 Guinea was invoked as a preferred scenario in our base models in the Late Jurassic (Gibbons et al.,
861 2015; Zahirovic et al., 2014), with the possibility that micro-continental fragments along Sumatra
862 (such as the now-disputed Natal and Sikuleh fragments, Fig. 2) had an origin in the Argo Abyssal
863 Plain, following Audley-Charles et al. (1988), Metcalfe (1994) and Heine and Müller (2005).
864 However, recent zircon age spectra analyses from East Java suggesting strong affinities with the
865 NW Australian Shelf (Sevastjanova et al., 2015; Smyth et al., 2007), led Hall (2012) to argue that
866 East Java was the enigmatic “Argoland” fragment (Table 2). We present both a NW Australian
867 shelf and a New Guinea origin for Argoland in our alternative plate reconstruction scenarios, and
868 evaluate their plate kinematic and geodynamic consequences on the Neo-Tethyan tectonic
869 evolution.

870

871 Table 2. Previously-interpreted continental fragments originating from northern Gondwana in the eastern Tethys in the
872 Late Jurassic.

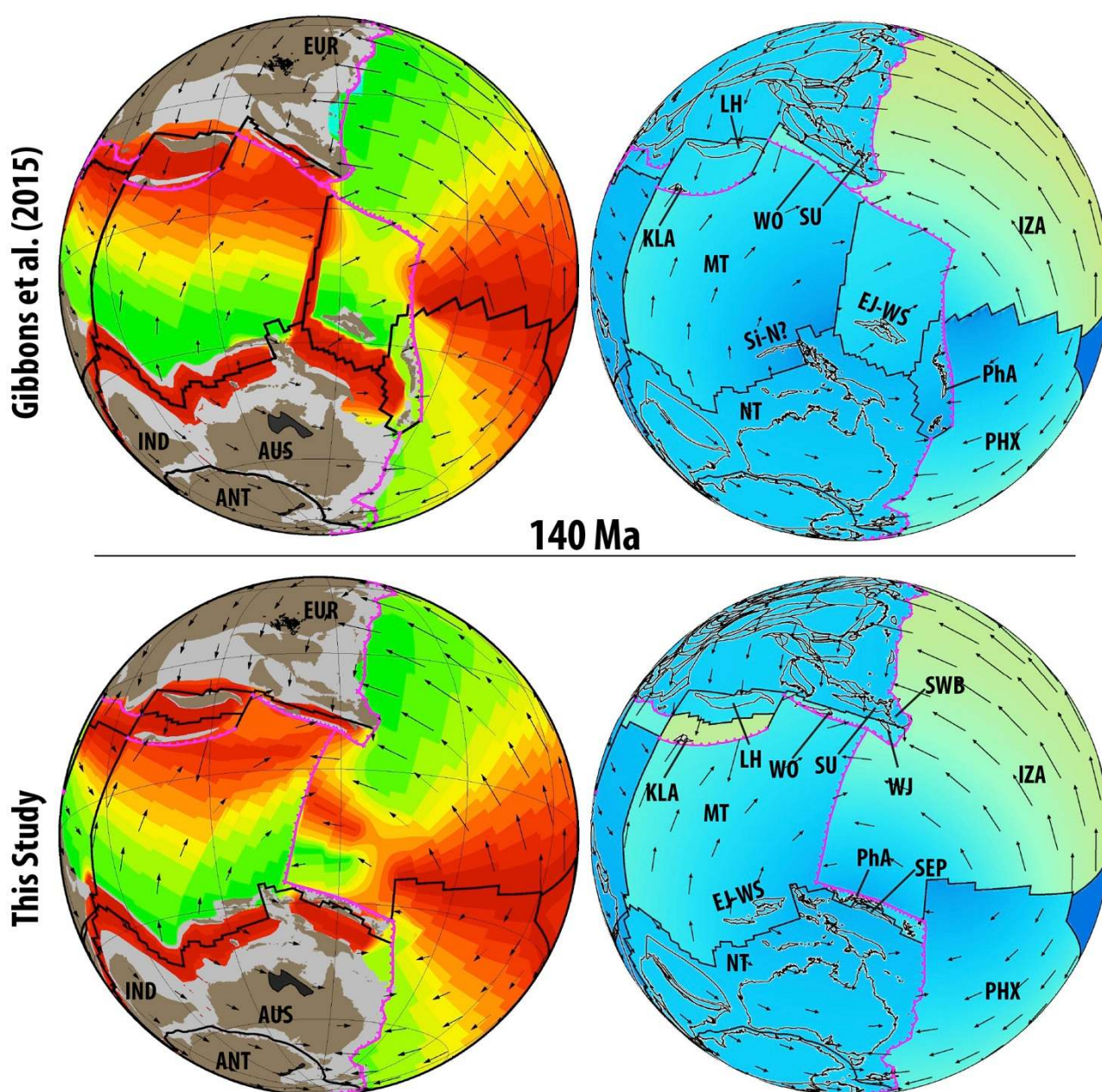
<i>Model</i>	<i>All continental fragments originating from northern Gondwana in the Late Jurassic eastern Tethys</i>	<i>Argoland fragment</i>
Audley-Charles et al. (1988)	South Tibet (Lhasa), West Burma, Malaya, Sumatra, East and West Borneo fragments, West Sulawesi	West Burma
Metcalf (1994)	West Burma, Sikuleh, Natal, West Sulawesi, Mangkalihat, Banda Allochthons	West Burma
Heine and Müller (2005)	West Burma	West Burma
Hall (2012)	Southwest Borneo core, East Java, West Sulawesi	East Java and West Sulawesi
Zahirovic et al. (2014) Gibbons et al. (2015)	Sikuleh, Natal, East Java, Southeast Borneo, West Sulawesi	Sikuleh, Natal and other possible fragments that may be in the Mawgyi Nappe along West Burma
This Study	East Java, Eastern Borneo, Mangkalihat, West Sulawesi and Sepik (New Guinea)	East Java, Eastern Borneo, Mangkalihat and West Sulawesi

873

874 The ~155 Ma onset of seafloor spreading in the Argo segment of the north Gondwana margin
875 is consistent with Jurassic sedimentary rift-drift sequences (Pigram and Panggabean, 1984), and
876 mafic rocks that are as old as 158 Ma on West Sulawesi (Polvé et al., 1997), likely representing the
877 drift of the East Java and West Sulawesi continental fragments (Zahirovic et al., 2014). The early
878 seafloor spreading history is preserved in the Argo Abyssal Plain, with the youngest marine
879 magnetic anomaly of M10Ny (Gibbons et al., 2013) representing an age of 128.9 Ma, after which
880 the seafloor spreading history is unconstrained. As discussed extensively in Zahirovic et al. (2014),
881 and summarised below in Section 3.4, the East Java and West Sulawesi fragments may have
882 collided with an intra-oceanic arc in the mid-Cretaceous (Wakita, 2000), and sutured to Sundaland
883 by 80 Ma. However, the Neo-Tethyan full seafloor spreading velocity required by the ~115 Ma arc-
884 continent collision approaches ~25 cm/yr between ~128 and 115 Ma (see Supplementary Fig. 1),

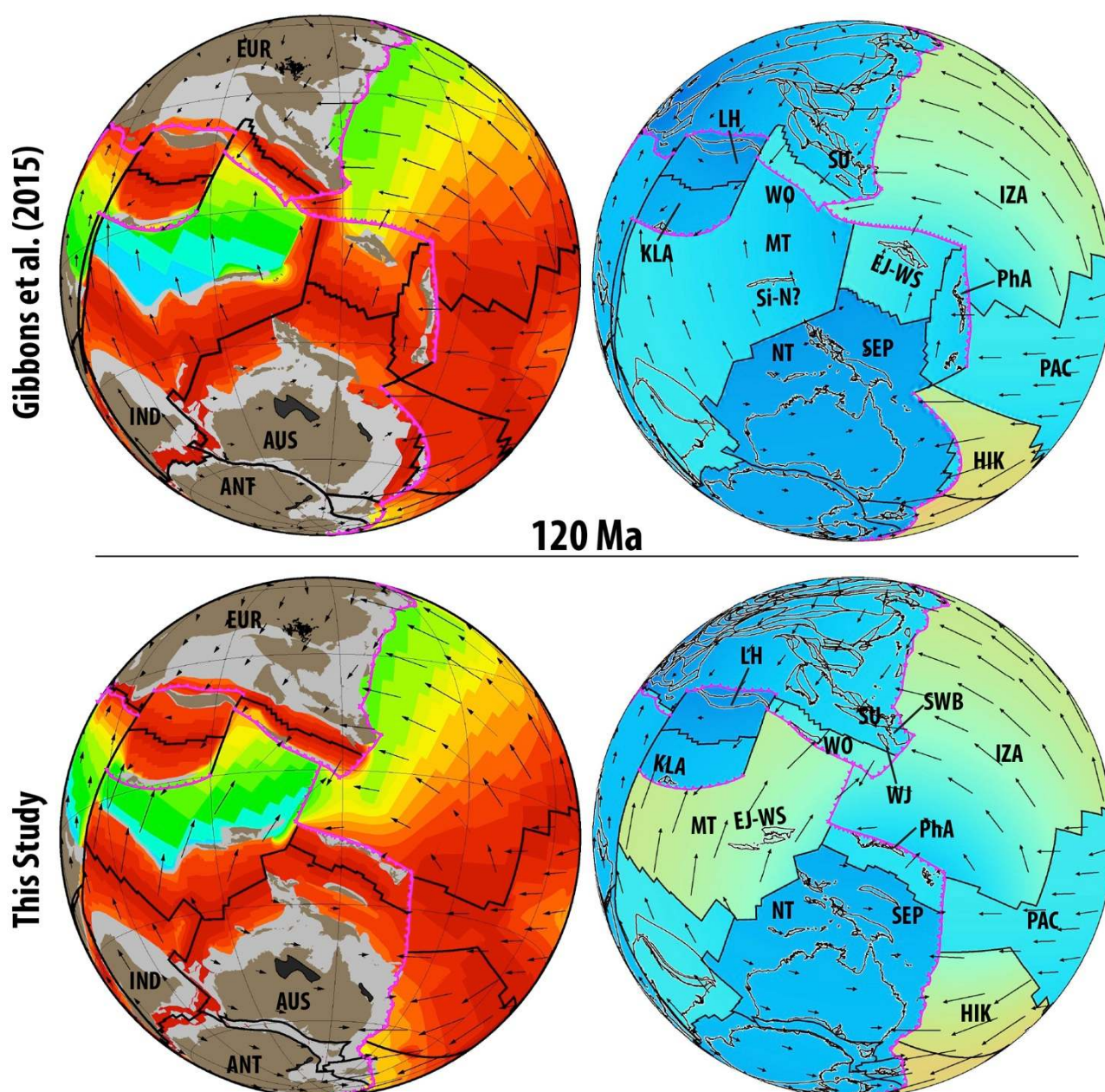
885 which is likely to be an upper limit for plate velocities in the post-Pangea timeframe (Stampfli and
886 Borel, 2002; V  rard et al., 2012; Zahirovic et al., 2015). An alternative explanation for the ~115 Ma
887 peak in very high pressure (VHP) metamorphic rocks in the Luk Ulo-Meratus Suture Zone
888 (Parkinson et al., 1998) (Fig. 2), includes the initiation of subduction of the Woyla/Barito back-arc
889 basins, which reduces the synthetic seafloor spreading velocities to ~11 cm/yr (Figs. 10-11). We
890 adopt the latter option that does not introduce a geodynamically implausible velocity spike in
891 Tethyan plate velocities.

892



893

894 **Fig. 9.** Ongoing Meso-Tethyan subduction leads to the opening of the Kohistan-Ladakh (KLA) and
895 Woyla (WO) back-arc basins, as well as the Neo-Tethys (NT) along northern Gondwana. The
896 Philippine Archipelago (PhA) is detached from the Sepik Terrane (SEP) through a northward ridge
897 jump and continued rollback of the Izanagi slab.
898



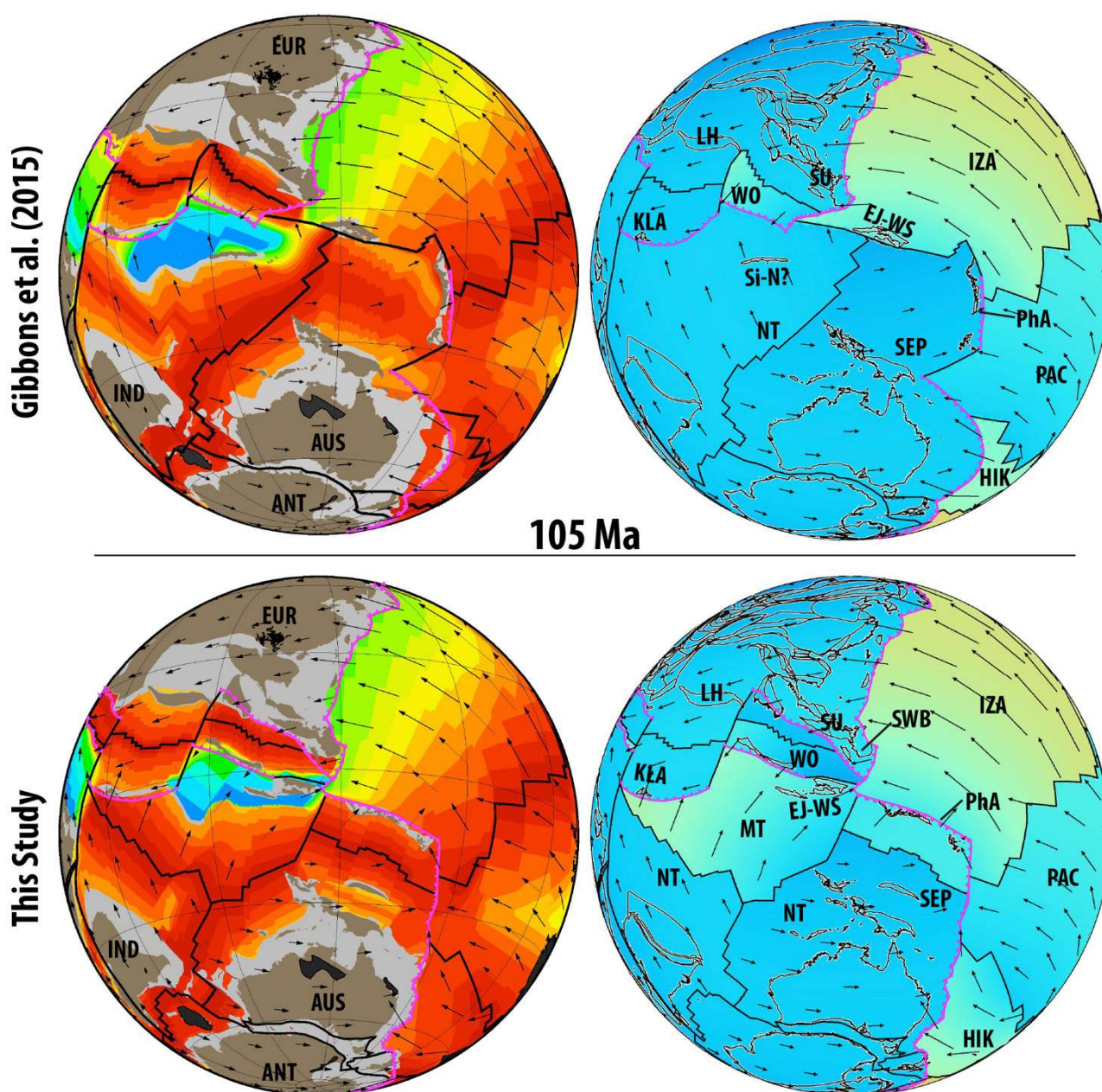
899
900 **Fig. 10.** In the models of Zahirovic et al. (2014) and Gibbons et al. (2015) the Neo-Tethyan ridge
901 system is abandoned by 120 Ma. In this study, seafloor spreading continues because of ongoing
902 subduction of the Meso-Tethyan Plate. Although the oldest preserved seafloor spreading constraints

for the Neo-Tethys are ~128 Ma in the Argo Abyssal Plain, we impose continued seafloor spreading in the Neo-Tethys that is driven by northward slab pull. HIK – Hikurangi Plate.

3.2 Active margin evolution in the Lhasa segment

The Late Jurassic is characterized by the asynchronous development of an active margin along southern Eurasia that was consuming the Meso-Tethyan ocean basin along a north-dipping subduction zone (Fig. 8). Along southern Lhasa, subduction-related calc-alkaline granites and granitoids ranging in age from ~170 to 137 Ma indicate the onset of north-dipping Meso-Tethyan Andean-style subduction (Zhang et al., 2012). The onset of subduction-related magmatism within the Kohistan Arc, which has no continental basement (Burg, 2011; Jagoutz and Schmidt, 2012), at ~154 Ma in the form of the Matum Das tonalite (Schaltegger et al., 2003) suggests the rollback of a Meso-Tethyan slab (e.g., Pettersen and Windley, 1985; Pudsey, 1986) and the possible origin of Kohistan and Ladakh as fore-arc oceanic crust, following the generic model of forearc formation proposed by Flower and Dilek (2003) and Stern et al. (2012). Further east along the present-day suture zone, the interpreted intra-oceanic Zedong Terrane records latest Jurassic ages of subduction-related igneous suites including a dacite breccia dated as 161.0 ± 2.3 Ma, a number of samples with an age of ~156 Ma (andesite dyke, andesite breccia and quartz diorite), and an andesitic dyke with an age of 152.2 ± 3.3 Ma (McDermid et al., 2002). The Kohistan-Ladakh, Zedong and more-broadly Neo-Tethyan intra-oceanic subduction zone likely became established through continued southward slab rollback between ~150 and 120 Ma, which is marked by a magmatic hiatus in the Gangdese Batholith on Lhasa until ~110 Ma (Ji et al., 2009; Wen et al., 2008b). However, while the magmatic evolution of the Kohistan-Ladakh intra-oceanic arc is well-studied, its paleo-latitudinal position remains controversial and poorly constrained. Burg (2011) and Gibbons et al. (2015) place Kohistan on the equator at ~100 Ma (Fig. 11) based on the magnetisation of mid-Late Cretaceous

929 red beds (Zaman and Torii, 1999), suggesting a maximum southward extent for the Neo-Tethyan
 930 intra-oceanic arc. In addition, although Kohistan and Ladakh form the only significant preserved
 931 remnants of the Early Cretaceous intra-oceanic arc within the Yarlung-Tsangpo Suture Zone,
 932 additional ophiolites with intra-oceanic affinity are embedded in the suture zone east of Kohistan
 933 and Ladakh (Aitchison et al., 2000; Hébert et al., 2012).



934
 935 **Fig. 11.** The change in the motion of India from largely counterclockwise in the Early Cretaceous to
 936 largely northward, is recorded in fracture zone bends in the Wharton Basin at ~105-100 Ma
 937 (Matthews et al., 2012). In this study, the Neo-Tethyan ridge is consumed at the Kohistan-Ladakh

938 (KLA) intra-oceanic subduction zone from ~105 Ma, leading to a greater northward slab pull acting
939 on the Indian Plate (IND), which we interpret as causing the change in India Plate motion. The
940 collision of the East Java-West Sulawesi continental fragments possibly impeded subduction at the
941 Woyla Arc at ~105 Ma, and led to obduction of the Meratus ophiolite in the Cenomanian-Turonian
942 (~100-93 Ma) (Pubellier et al., 2004; Yuwono et al., 1988). The Kohistan-Ladakh and Woyla arcs
943 likely occupied near-equatorial latitudes by ~100 Ma, with both back-arc systems subducted
944 northward from ~115 Ma in the Sunda segment and from ~110 Ma along Lhasa, resulting in two
945 coeval north-dipping subduction zones in the Neo-Tethys (see Section 3.2).

946

947 The Aptian to Albian (~126-100 Ma) Yasin Group sedimentary sequence on the Kohistan-
948 Ladakh Arc are intercalated with syn-tectonic arc volcanics, and subsequent intrusions of diorites
949 and granodiorites (Pudsey et al., 1985; Rehman et al., 2011). A large portion of the magmatic
950 products were emplaced during a key timeframe between ~110 and 90 Ma (Petterson and Windley,
951 1985; Rehman et al., 2011; Schärer et al., 1984), with significant magmatic accretion forming the
952 Sapat Complex on the Kohistan Arc between ~105 and 99 Ma (Bouilhol et al., 2011). This short-
953 lived “trenchward migration of the hot mantle source” (Bouilhol et al., 2011) may indicate the
954 arrival of the Neo-Tethyan mid-oceanic ridge with slab window formation, consistent with the
955 ~95 Ma high-temperature granulite metamorphism in the Jijal Complex and the peak metamorphic
956 event in the Kamila Amphibolite unit (Petterson, 2010). The demise of the Neo-Tethyan mid-
957 oceanic ridge between ~110 and 90 Ma along the Kohistan-Ladakh intra-oceanic arc (Fig. 11) likely
958 had substantial geodynamic implications for the region at the time, resulting in stronger northward
959 slab pull acting on the Indian Plate. Although the slab window likely temporarily impeded
960 subduction, the progressively increasing northward slab pull from ~105 Ma likely resulted in a
961 major change in the direction and speed of the Indian Plate, observable in the significant bends
962 observed in the Wharton Basin fracture zones (e.g., Wallaby-Zenith Fracture Zone) at ~105-100 Ma
963 that required a ~50° clockwise reorientation of the Indo-Australian spreading system (Matthews et

964 al., 2012), and possibly triggered a regional plate-reorganization event (Matthews et al., 2011). In
965 addition, the onset of northward slab pull on the Indian Plate from ~100 Ma may explain the
966 paleomagnetic observations of rifting within Greater India in the Late Cretaceous (van Hinsbergen
967 et al., 2012).

968 The intersection of the Neo-Tethyan ridge with the Kohistan-Ladakh intra-oceanic
969 subduction zone, as modelled in this study, may have temporarily interrupted subduction due to the
970 decrease of negatively buoyant oceanic lithosphere entering the trench, with convergence
971 accommodated along the active continental Eurasian margin from ~110 Ma rather than along the
972 intra-oceanic subduction zone. The Gangdese Batholith recorded a major pulse of granitic
973 magmatism from ~109 to 80 Ma (Ji et al., 2009), indicating the resumption of Andean-style
974 subduction along Lhasa that is contemporaneous with intra-oceanic subduction along Kohistan-
975 Ladakh, and hence signifies the onset of two simultaneous north-dipping subduction zones in the
976 Neo-Tethys from ~110 Ma.

977 The Late Cretaceous evolution of the Kohistan-Ladakh Arc has conflicting interpretations.
978 Conventional models suggest a Late Cretaceous collision and suturing of Kohistan-Ladakh to
979 Eurasia (Clift et al., 2002; Debon et al., 1987; Treloar et al., 1996), whereas more recent works,
980 which have incorporated detailed geochronology and structural interpretations of Kohistan, have
981 concluded that instead of suturing to Eurasia, the Late Cretaceous is punctuated by an arc rifting
982 and splitting episode by ~85 Ma (Bouilhol et al., 2011; Burg, 2011; Burg et al., 2006), which
983 suggests Neo-Tethyan slab rollback rather than collisional processes. The ~75-60 Ma magmatic gap
984 in the Gangdese Batholith (Chung et al., 2005; Wen et al., 2008b) may imply that the majority of
985 India-Eurasia convergence was accommodated by subduction along Kohistan-Ladakh rather than
986 by subduction along Lhasa. A scenario that precludes Kohistan-Ladakh collision with Eurasia in the
987 Late Cretaceous requires that an intra-oceanic arc first accreted onto Greater India (Chatterjee et al.,
988 2013). A similar model proposes that the Muslim Bagh Ophiolite represents the Kohistan-Ladakh
989 forearc and was obducted onto the leading edge of Greater India at ~65 Ma in near-equatorial

latitudes, which resulted in the cessation of calc-alkaline magmatism on Kohistan-Ladakh during ~65-61 Ma (Khan et al., 2009). This scenario requires the accompanying suturing between Kohistan-Ladakh and Greater India along the Indus Suture to occur earlier than the closure of Shyok Suture. Such a scenario is consistent with the plate reconstructions presented in this study, in which Greater India reaches equatorial latitudes at ~65 Ma. A recent stratigraphic analysis presented in Hu et al. (2015) suggests the India-Eurasia collision was underway by 59 ± 1 Ma, which we interpret as the initial arc-continent collision, consistent with the tectonic evolution of the Kohistan-Ladakh Arc. The major slowdown in spreading across the Central and Southeast Indian Ridges at ~52 Ma (Chron 23o, Cande et al., 2010) may indicate the complete abandonment of the intra-oceanic subduction zone, and the completion of the initial arc-continent collision between Greater India and the Neo-Tethyan intra-oceanic arc. Recent geochemical analyses of granitoids from the Kohistan-Ladakh Arc indicate a major change in magma chemistry (Nd and Hf isotopes) and the arrival of the Greater Indian continental margin into the subduction zone by 50.2 ± 1.5 Ma (Bouilhol et al., 2013), which is consistent with the cessation of intra-oceanic subduction by this time.

The continent-continent collision between Greater India and Eurasia likely occurred at ~47 Ma, recorded in the marked slowdown of seafloor spreading at Chron 21o along the Southeast Indian Ridge (Cande and Patriat, 2015) and the contemporaneous formation of an Indian Ocean microplate near the Ninetyeast Ridge (Matthews et al., 2016). Suturing along the Shyok Suture Zone between the two continents was likely complete by 40.4 ± 1.3 Ma (Bouilhol et al., 2013), which accounts for the ~60-40 Ma Andean-style emplacement of the Linzizong Volcanics in Lhasa (Chung et al., 2005). The ~47-40 Ma continent-continent collision timing is consistent with an additional slowdown and change in spreading direction along the Central and Southeast Indian Ridges, the inception of a short-lived Indian Ocean microplate (Matthews et al., 2016), and the abandonment of the Wharton Ridge sometime between ~43 and 36 Ma (see discussion in Gibbons et al., 2015).

1016

1017 **3.3 Convergence along the West Burma and Sumatra margin segment**

1018

1019 Eastern Sumatra, as part of the Sibumasu ribbon terrane, docked with the Eurasian margin
1020 sometime in the Late Triassic to Early Jurassic (Metcalf, 2011), and has since recorded Meso- and
1021 Neo-Tethyan subduction and accretion histories. The Woyla Terrane, which accreted to Sumatra in
1022 the Late Cretaceous (Morley, 2012a), plays a key role in elucidating the geodynamic setting of the
1023 Sumatran active margin since the Late Jurassic. However, the nature of the Woyla Terrane crust and
1024 the subduction polarity and history has given rise to a number of competing models for the tectonic
1025 evolution of Sumatra. The Jurassic to Cretaceous Woyla Group of sedimentary and volcanic units
1026 has previously been interpreted as an arc built on re-worked continental basement (Barber and
1027 Crow, 2003; Cameron et al., 1980), largely due to the presence of a tin geochemical signature in the
1028 Sikuleh granitoids (Fig. 2) that may have been interpreted as analogous to the Southeast Asian tin
1029 belts that were built on continental crust (e.g., Bangka and Billiton Islands; Searle et al., 2012).
1030 Parts of the Woyla basement near Sikuleh, Natal and Bengkulu are composed of quartzite and
1031 phyllite (Acharyya, 1998), and overprinted by widespread granitoid intrusions largely Late
1032 Cretaceous in age (Barber and Crow, 2003), leading some authors to interpret these micro-blocks as
1033 Gondwana-derived continental fragments (Görür and Sengör, 1992; Haile, 1979; Metcalfe, 1994;
1034 Metcalfe, 2002; Metcalfe and Irving, 1990). The paleomagnetic study of a Jurassic limestone
1035 sample by Haile (1979) suggests that the crust in the vicinity of Sikuleh (Locality H in Haile, 1979)
1036 was at 26°S in the Jurassic. This result was used by Metcalfe (1994) to suggest a Gondwana origin
1037 for the proposed micro-continental fragment.

1038 The continental nature of the Sikuleh part of the Woyla Terrane (Si, Fig. 2) is rejected by
1039 Barber and Crow (2003), who instead propose an intra-oceanic arc origin. The Woyla Group
1040 consists, at least in part, of accreted fragments that include seamounts, reef fragments, ophiolites
1041 and associated ocean floor sedimentary sequences (Barber and Crow, 2003; Wajzer et al., 1991),

1042 but no clear continental basement can be identified, much like the Kohistan-Ladakh Arc in the
1043 central Neo-Tethys. Paleontological constraints from a single foraminifera specimen within the
1044 Batang Natal Megabreccia provide a Late Triassic age (Wajzer et al., 1991), and suggest that the
1045 oceanic crust that was consumed in the Woyla intra-oceanic subduction system in the Cretaceous
1046 was at least Late Triassic in age, consistent with the age of Meso-Tethyan oceanic crust subducted
1047 along the Sumatra segment predicted by our reconstructions for the Cretaceous (Fig. 10). In
1048 addition, the accretion of highly disrupted lenses of oceanic crust and sedimentary sequences onto
1049 the Woyla Terrane is consistent with the observations of accreted oceanic plate stratigraphy further
1050 east in the Luk Ulo-Meratus Suture Zone between East Java-West Sulawesi and the core of Borneo
1051 (Wakita, 2000; Wakita and Metcalfe, 2005).

1052

1053 ***3.3.1 Development of the Woyla intra-oceanic arc***

1054

1055 The Woyla Terrane, largely represented by the Woyla Group of sedimentary sequences and
1056 intrusions, likely developed on an active intra-oceanic margin (with possible continental basement)
1057 in the Early Cretaceous (Figs. 9-11), separated from mainland Sumatra by a marginal sea (Rock et
1058 al., 1983; Wajzer et al., 1991). However, the origin of the Woyla Arc has recently been debated,
1059 with a model proposing a Gondwana origin for both the Woyla and the Kohistan-Ladakh Arc (Hall,
1060 2012) as the result of continued rollback of a south-dipping subduction zone (Fig. 4b-c).
1061 Alternatively, the model of Zahirovic et al. (2014), and the one presented here, invoke a southern
1062 Eurasia origin of the Kohistan-Ladakh and Woyla intra-oceanic island arcs. The scenario invoking
1063 south-dipping subduction along northern Gondwana in the Late Jurassic could be corroborated by
1064 the preservation of contemporaneous arc rocks on Greater India (Tethyan Himalayas) or the NW
1065 Australian Shelf, which are not yet documented. The scenario invoking north-dipping Meso-
1066 Tethyan subduction to detach the Argoland continental fragments and open the Neo-Tethys in the
1067 latest Jurassic can be corroborated by the subduction history along Lhasa, West Burma (Myanmar)

1068 and Sundaland. Subduction is suggested to have initiated along the West Burma block at ~163-
1069 152 Ma by jadeite geochronology (Shi et al., 2008; Shi et al., 2014). This age is similar to that of
1070 the 154 Ma Matum Das tonalite within the Kohistan-Ladakh arc (Schaltegger et al., 2003) to the
1071 west. The formation of the Naga Ophiolite during ~156-150 Ma, based on Kimmeridgian-lower
1072 Tithonian cherts (Baxter et al., 2011), suggests a close temporal and geodynamic association
1073 between the Kohistan-Ladakh (Lhasa segment), Mawgyi (West Burma segment) and Woyla
1074 (Sumatra segment) intra-oceanic arcs along which Meso-Tethyan oceanic crust began subducting in
1075 the latest Jurassic.

1076

1077 **3.3.2 Subduction of the Woyla back-arc basin**

1078

1079 The resumption of Andean-style subduction in the central Neo-Tethys along Lhasa is well-
1080 constrained to ~109 Ma, based on the onset of subduction-related magmatism in the Gangdese
1081 Batholith (Ji et al., 2009). However, the timings of subduction initiation along West Burma and
1082 Sumatra are less well constrained. An Albian (~113-100 Ma) unconformity on West Burma
1083 (Morley, 2012a) may indicate compression related to subduction initiation, which is
1084 contemporaneous with observations in Lhasa, and the supra-subduction formation of the Andaman
1085 Ophiolite at 95 ± 2 Ma (Pedersen et al., 2010) may suggest the onset of rollback and extension in
1086 the overriding plate. Here we interpret the ~115 Ma peak in Ultra- and Very-High Pressure
1087 metamorphics in the Luk-Ulo Suture Zone (Figs. 10-12) (Parkinson et al., 1998) as indicators of
1088 subduction initiation of the Woyla back-arc basin to account for the Albian unconformity on West
1089 Burma. The 105 to 90 Ma dioritic and granodioritic intrusions into the Wuntho-Popa Arc (Mitchell
1090 et al., 2012), west of the Sagaing Fault, suggest continuity of the contemporaneous Lhasa
1091 subduction zone into the West Burma segment of the margin. However, subduction to consume the
1092 Woyla back-arc basin may (also) have been south-dipping as argued in Morley (2012a).

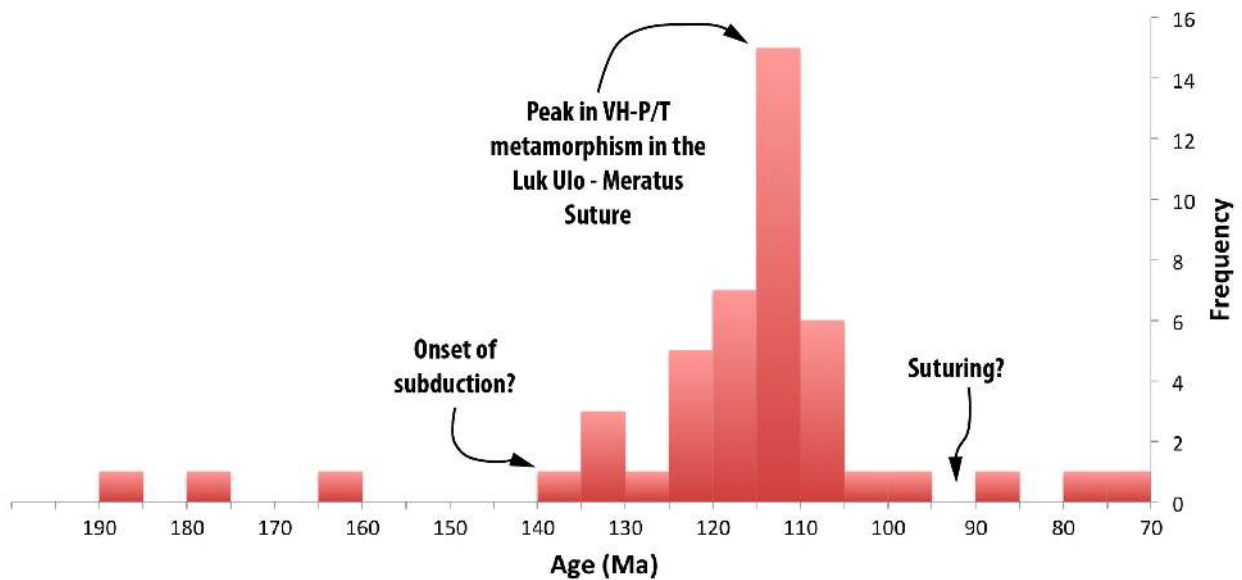


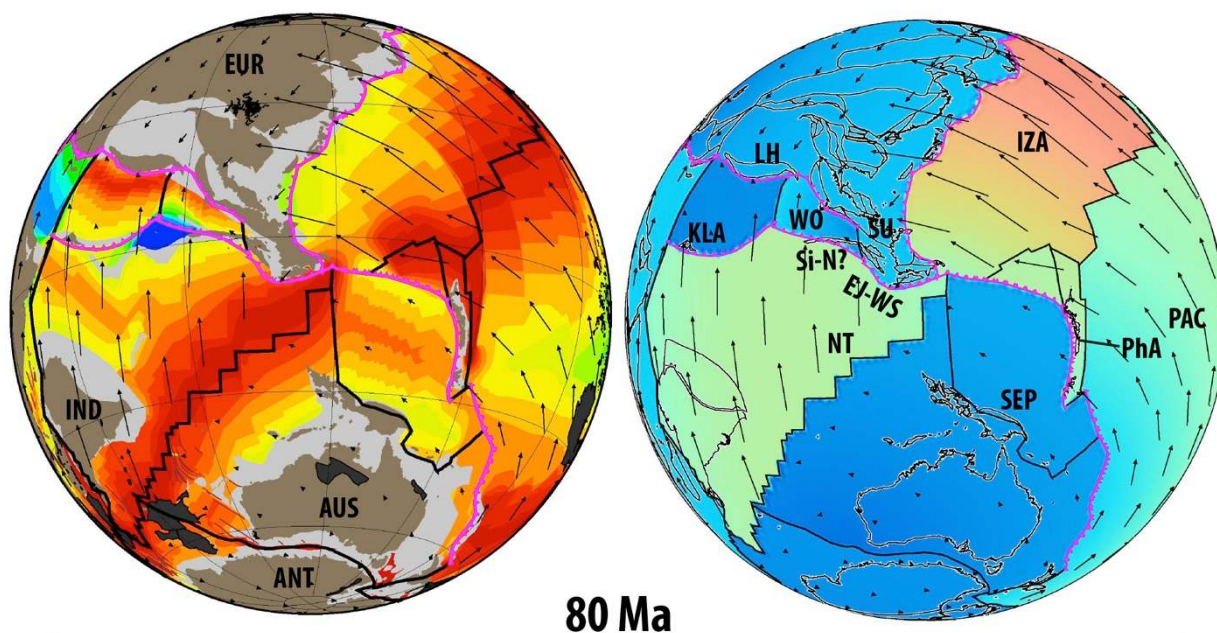
Fig. 12. Very High and Ultra High Pressure (VHP/UHP) metamorphic rocks in the Luk Ulo-Meratus suture on Java and Borneo (Fig. 2) record well-established subduction from at least ~140 Ma. A significant spike at ~115 Ma has been previously interpreted as a collision between East Java-West Sulawesi and the Woyla intra-oceanic arc (Gibbons et al., 2015; Zahirovic et al., 2014). However, in the refined plate reconstructions presented herein, the origin of East Java from the Argo Abyssal Plain would require excessive seafloor spreading rates, and instead we interpret the peak in VHP/UHP metamorphism to represent the onset of Woyla back-arc subduction along West Burma and Sundaland. Figure modified from Parkinson et al. (1998).

Although the Kohistan-Ladakh Arc is loosely constrained to near-equatorial paleo-latitudes during the mid-Cretaceous (Burg, 2011), no latitudinal constraints exist for the Woyla Arc. However, some constraints are available for the closure of the Woyla back-arc basin, and the collision of the intra-oceanic arc with Sumatra (Figs. 13-14). The Woyla Group is intruded by a number of Late Cretaceous igneous bodies, including the 84.7 ± 3.6 Ma (K-Ar) Batu Madingding diorite and the 78.4 ± 2.5 Ma (K-Ar) andesite in the southwest Batang Natal section (Wajzer et al., 1991), after which a significant magmatic gap is interpreted to represent collision of the Woyla Terrane with Sumatra. Hall (2012) argued that no subduction occurred on the Woyla/Sumatra segment of the Tethyan margin between 90 and 45 Ma (Fig. 4c), largely due to the presence of a

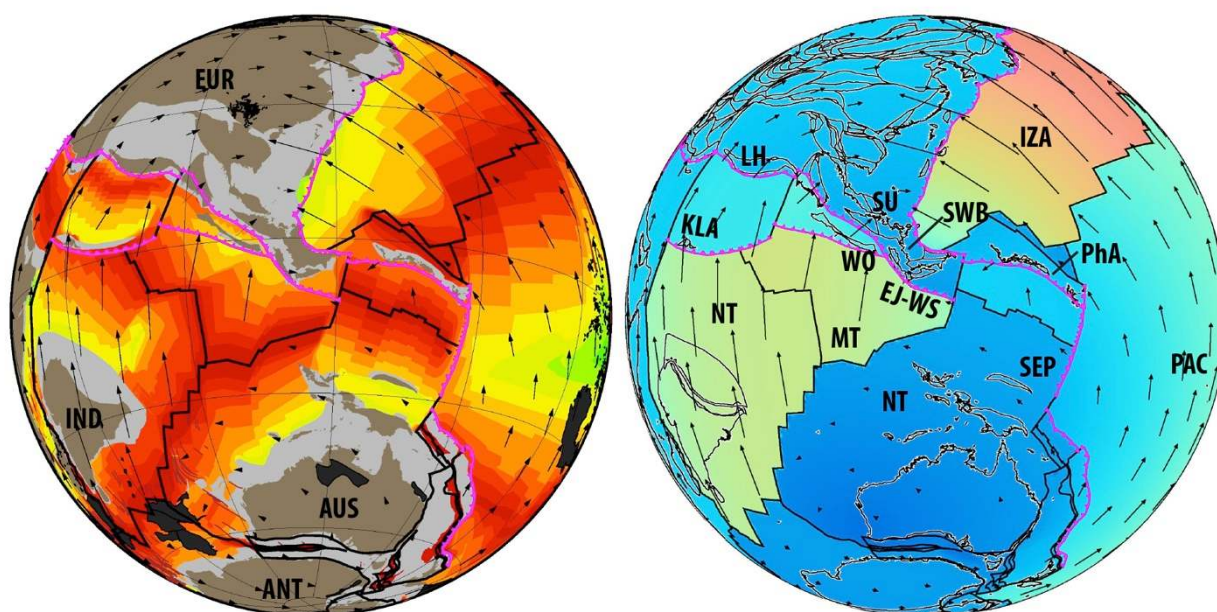
1112 regional unconformity that was interpreted to signify the absence of subduction-related dynamic
1113 subsidence on the overriding plate (Clements et al., 2011). However, only a ~10-15 Myr magmatic
1114 gap associated with a hiatus in subduction between ~75 and 62 Ma (Fig. 15) can be accounted for in
1115 the volcanic record on Sumatra (McCourt et al., 1996; Zahirovic et al., 2014). However, some of
1116 these (~10 Myr) magmatic gaps may be due to sampling issues, and future work may reveal more
1117 continuous subduction histories. The choice to impose a ~45 Myr (Hall, 2012) rather than a ~10-
1118 15 Myr Zahirovic et al. (2014) subduction hiatus has significant geodynamic implications for the
1119 region, where the continued northward motion of the Indian Plate needs to be accommodated by an
1120 oceanic transform that cuts across older oceanic lithosphere and pre-existing structural fabric in the
1121 reconstructions of Hall (2012) (Fig. 4c).

1122

Gibbons et al. (2015)



This Study



1123

1124

1125

1126

1127

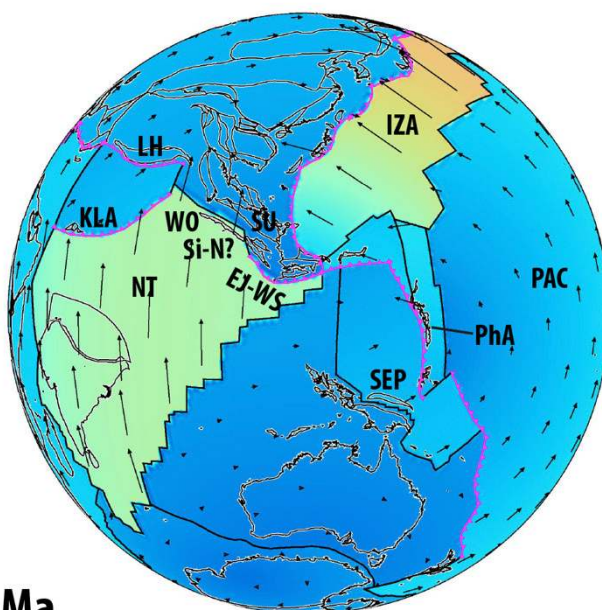
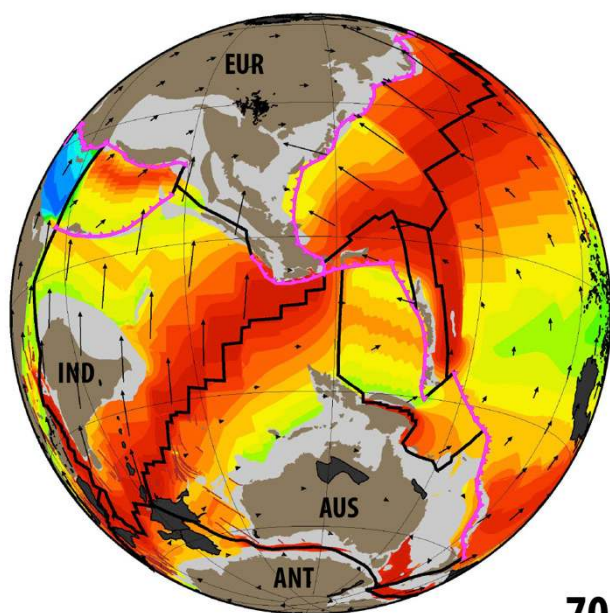
1128

1129

1130

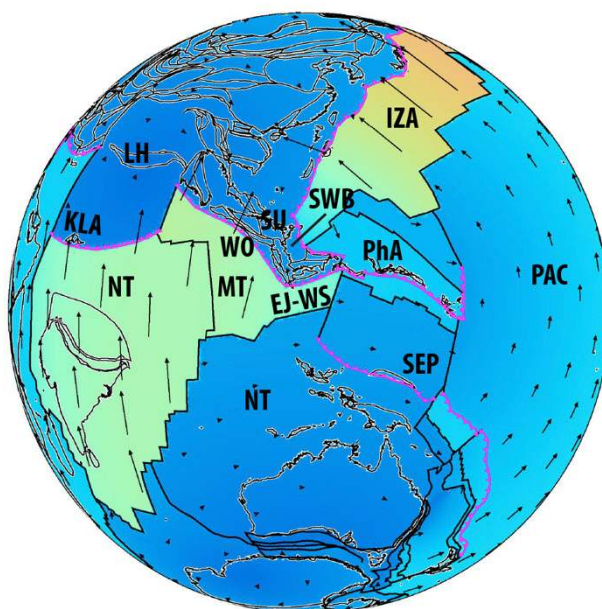
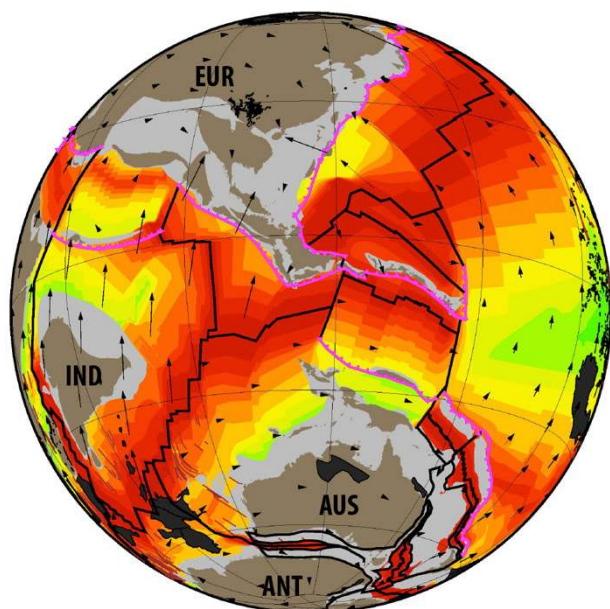
Fig. 13. India's northward motion accelerated from ~80 Ma. The subduction polarity likely reversed along the Philippine Arc and suturing of the East Java and West Sulawesi continental fragments to the Southwest Borneo Core was complete by this time. The Woyla Terrane was approaching the Sumatran margin by this time. Additional polygons in the lower panels for Australian-Antarctic and Lord Howe-Tasman Sea regions represent areas of deforming continental crust.

Gibbons et al. (2015)



70 Ma

This Study



1131

1132 **Fig. 14.** The Woyla Arc collided with Sundaland (SU) by ~75 Ma, and impeded subduction in this
 1133 segment of the margin for ~10 Myr. The Meso-Tethyan Plate was still likely being subducted along
 1134 the Sunda Trench based on the refined plate reconstructions, with Wharton Ridge arrival near
 1135 eastern Sundaland between ~70 and 60 Ma in both reconstructions. In this study, we reconstruct the
 1136 subduction of the Sepik oceanic gateway from ~71 Ma based on the age of the Emo volcanics
 1137 (Worthing and Crawford, 1996).

1138

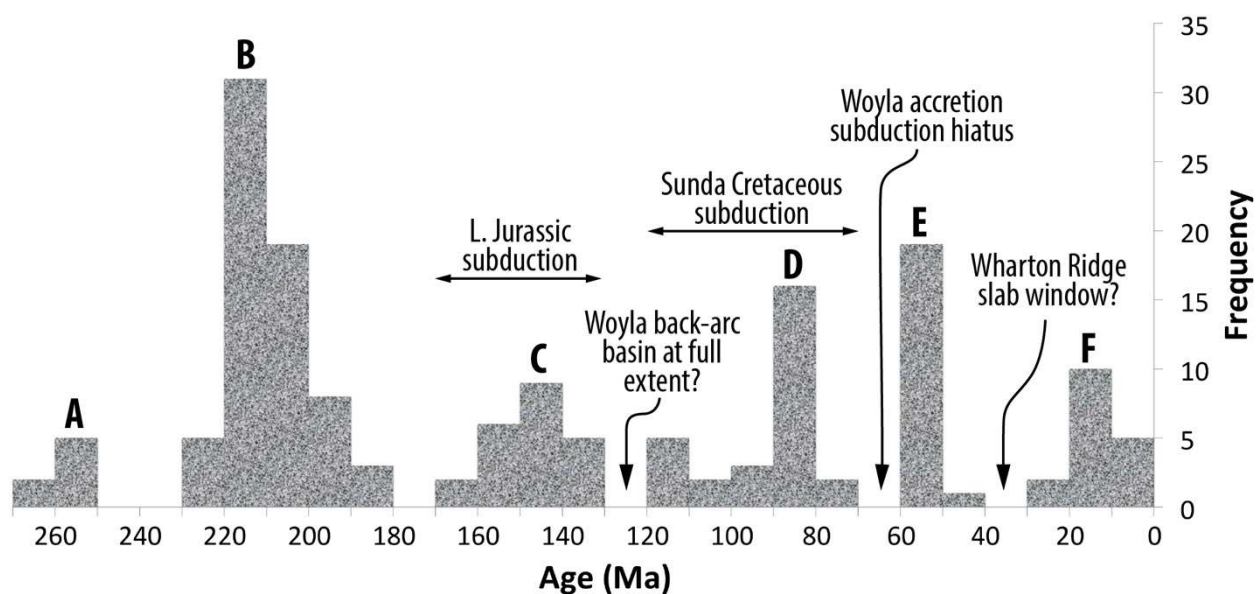


Fig. 15. A synthesis of arc volcanism on Sumatra, adapted from McCourt et al. (1996), highlights a number of short-lived magmatic hiatuses likely related to back-arc basin rifting and/or collisional processes that impeded subduction along the Sumatran continental margin.

The post-Cretaceous history of the Sumatran margin is less controversial, with magmatism related to the subduction of the Neo-Tethys and Indian oceans (Mccourt et al., 1996), and widespread basin rifting and flooding occurring since Paleocene times on Sundaland (Doust and Sumner, 2007). One important geodynamic consideration for the Sumatra margin is the interaction of the (extinct) Wharton Ridge with the Java-Sunda trench, with the model of Whittaker et al. (2007) suggesting a long-lived slab window sweeping westward from eastern Sundaland (near Java) from ~75 Ma to the present. Such a scenario implies a time-dependent along-trench thermal anomaly affecting the Sundaland continent, and more importantly, the subduction of young oceanic crust (and hence thinner oceanic lithosphere) has important implications on the long-wavelength mantle-driven topography on the overriding plate (e.g., Flament et al., 2015, for Patagonian uplift associated with the Chile Triple Junction; Guillaume et al., 2009). The combination of a subduction hiatus in the Late Cretaceous, as well as the subduction of very young oceanic crust in the Eocene along the Java-Sunda trench would likely result in widespread regional dynamic uplift that has been

1157 proposed by Clements et al. (2011) to account for a widespread Late Cretaceous to Paleocene
1158 regional unconformity across Sundaland, as explored in Zahirovic et al. (In Review).

1159

1160 **3.4 Accretionary history of the Java and Borneo margin segment**

1161

1162 A key region recording the evolution of Southeast Asia in the context of Eurasian, Tethyan
1163 and (proto-) Pacific convergence is the Sundaland continental promontory. The core of Sundaland
1164 is composed of north-eastern Sumatra, West Java and the Southwest Borneo block (Hall, 2012;
1165 Metcalfe, 1988; Metcalfe, 2011; Zahirovic et al., 2014). The promontory is largely Phanerozoic
1166 continental crust (Hall, 2011), with accreted intra-oceanic and allochthonous continental fragments
1167 – some, like East Java, carrying Archean zircon signatures (Smyth et al., 2007). The continental
1168 fragments making up Sundaland have largely Tethyan-Gondwanan affinities based on
1169 paleontological, stratigraphic and paleo-magnetic constraints, as reviewed in Metcalfe (2006).

1170

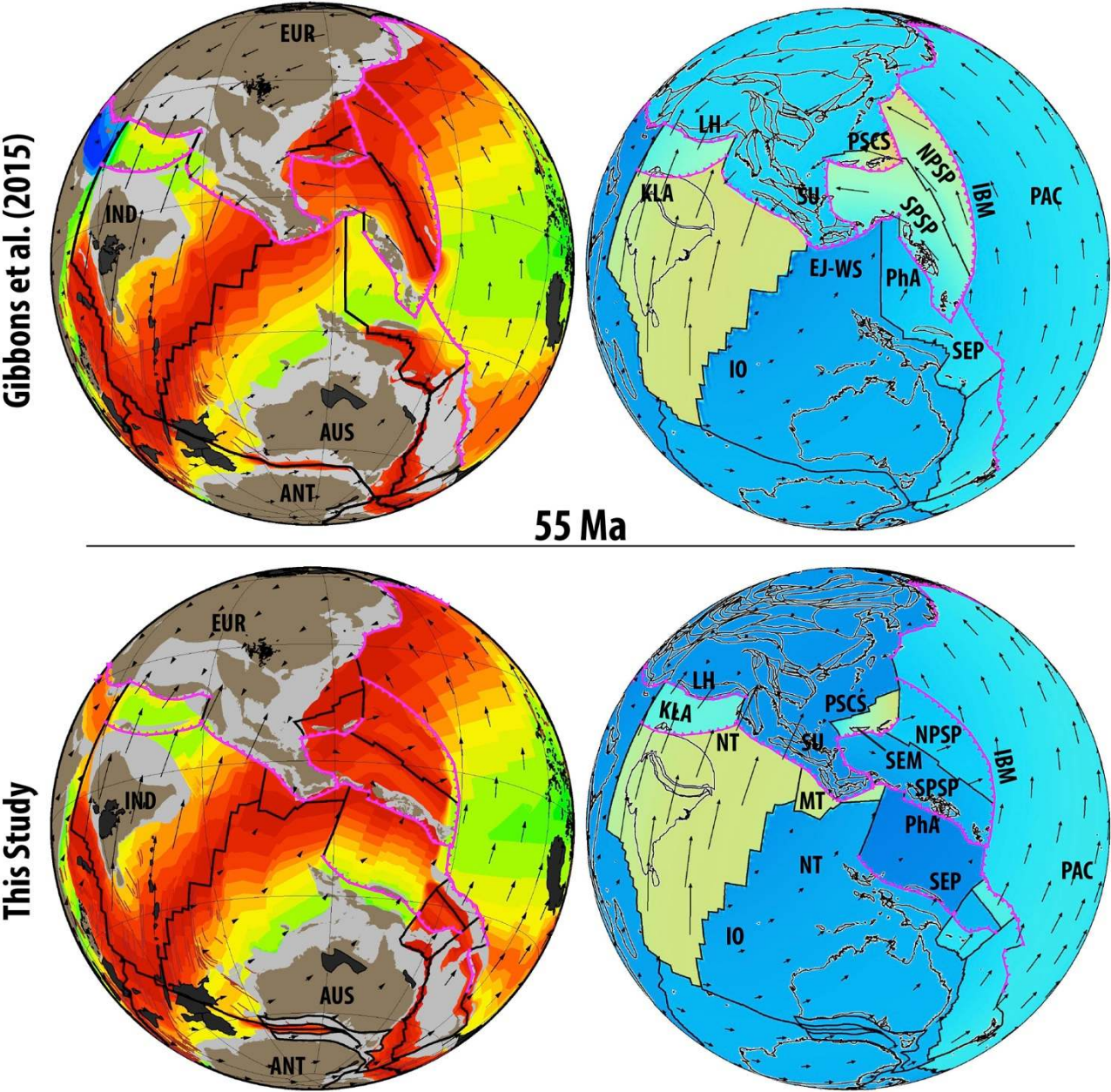
1171 **3.4.1 Subduction and accretion history of southern Sundaland**

1172

1173 The onset of Late Jurassic subduction in the eastern Tethys is best represented by the ~180-
1174 165 Ma schists found within the Meratus Complex on the eastern periphery of the Southwest
1175 Borneo core, as well as the presence of Bajocian (~170 Ma) and younger radiolarians embedded in
1176 the Meratus Suture Zone (Wakita et al., 1998). Zircons shed into the Ciemas and Bayah Formations
1177 on West Java, have ages of 160 Ma and younger (Clements and Hall, 2007), and likely represent the
1178 onset of subduction along this margin. The Late Jurassic-Early Cretaceous age of subduction onset
1179 on this segment is consistent with the establishment of a major subduction system along southern
1180 Eurasia, spanning at least from western Lhasa to the easternmost Tethyan margin on eastern
1181 Sundaland (see previous sections for full chronology). A continuous record of very-high-pressure
1182 (VHP) metamorphic rocks (Fig. 12), including greenschists, blueschists, granulites, eclogites and

1183 jadeite-bearing metamorphics from ~140 Ma in the Luk-Ulo and Meratus region of Sundaland
1184 (Parkinson et al., 1998) suggests a well-established subduction zone in the Early Cretaceous. The
1185 VHP metamorphism peak at ~115 Ma has previously been interpreted as an arc-continent collision
1186 of Gondwana-derived continental fragments (including East Java, West Sulawesi, Mangkalihat, and
1187 eastern Borneo) with the eastward continuation of the Woyla Arc (Zahirovic et al., 2014). However,
1188 in this study we prefer an interpretation of Woyla back-arc basin subduction initiation at this time to
1189 account for the UHP/VHP metamorphism, as discussed in earlier sections.

1190 A significant spike in the zircon age spectra at ~100 Ma (Clements and Hall, 2007) may
1191 indicate the arrival of the East Java-West Sulawesi in the vicinity of Sundaland. The obduction of
1192 the Meratus Ophiolite in the Cenomanian/Turonian between ~100 and 93 Ma (Pubellier et al., 2004;
1193 Yuwono et al., 1988) is consistent with the Cenomanian radiolarians found in the Meratus Complex
1194 (Wakita et al., 1998). The final closure of the Barito Sea back-arc basin along southern Sundaland
1195 occurred by ~80 Ma based on the lack of volcanic-derived zircons in fore-arc sandstones (Clements
1196 and Hall, 2011; Wakita, 2000). A Late Cretaceous to Paleocene (~72 to 65 Ma) unconformity on
1197 southwest Sulawesi (Milsom, 2000) may indicate collisional (uplift/denudation) processes, a
1198 subduction hiatus, or a combination of both. A resumption of subduction likely occurred in the
1199 Paleocene (Yuwono et al., 1988), with ~65-58 Ma (K-Ar) subduction related rocks (Guntoro,
1200 1999), a 63 Ma tuff reported on South Sulawesi (van Leeuwen, 1981), and continuous calc-alkaline
1201 and tholeiitic volcanism occurring between 51 and 17 Ma on the Western and northern arm of
1202 Sulawesi (Elburg et al., 2003). Ongoing subduction and major deformation (Figs. 16-17), largely
1203 due to the arrival of the Australian continental margin, namely the Sula Spur (Figs. 18-19), started
1204 with the obduction of the East Sulawesi Ophiolite at ~20 Ma (Oligocene to Miocene) in a continent-
1205 continent collision setting (Bergman et al., 1996). The subsequent compressional deformation, and
1206 widespread oroclinal bending of Sundaland are discussed at length in Hutchison (2010) and
1207 Zahirovic et al. (2014), and are summarised in the following sections.



1209

1210 **Fig. 16.** The 55 Ma reconstruction marks the initial stages of contact between Greater India and the

1211 Kohistan-Ladakh Arc to close the Indus Suture Zone, leading to major changes in spreading rate

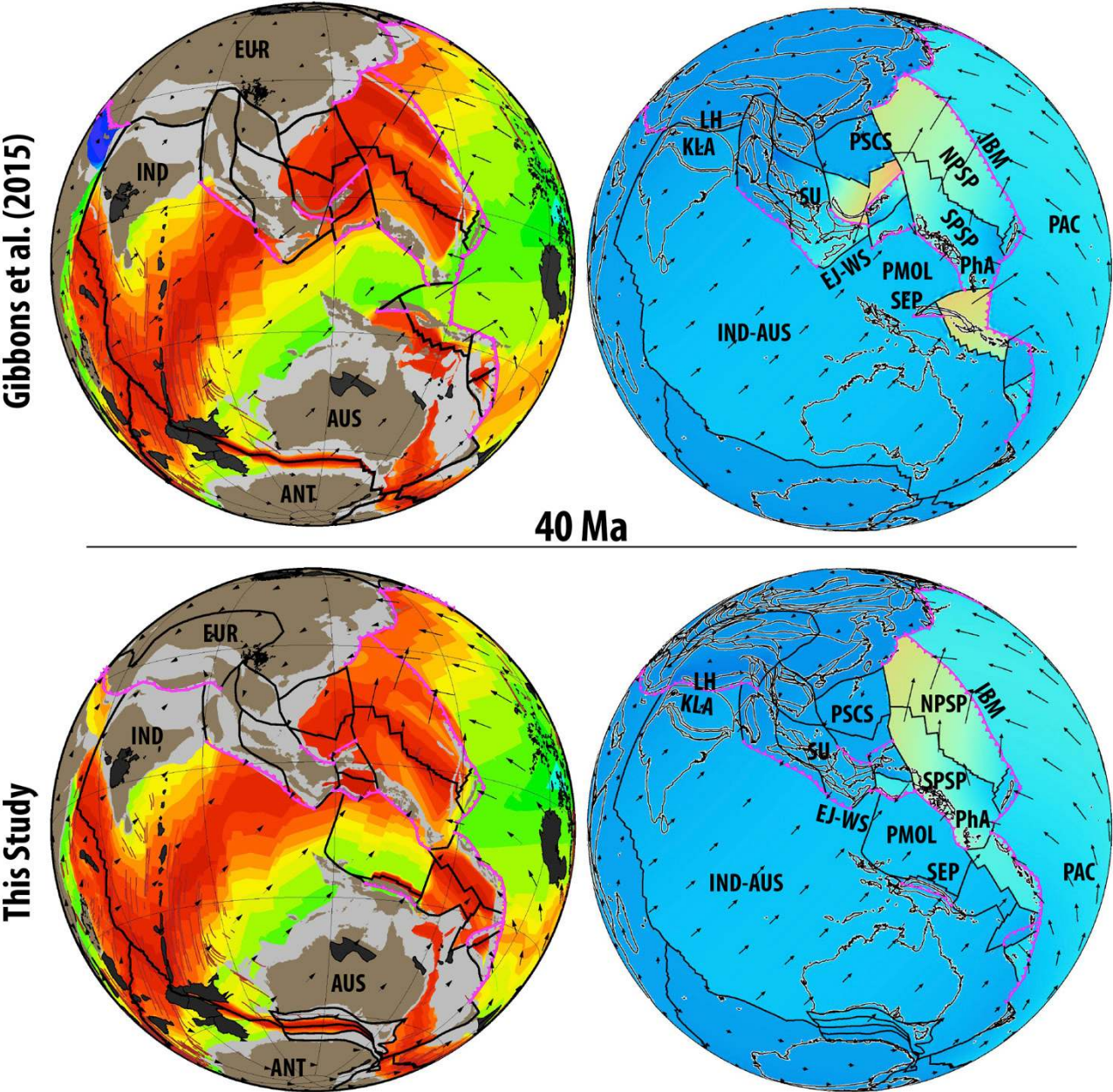
1212 and direction on the India-Antarctica ridge system. The rollback of the Izanagi slab opens the Proto

1213 South China Sea (PSCS) from ~60 Ma in a Tyrrhenian-style back-arc system. Subduction is

1214 initiated at ~55 Ma along the Izu-Bonin-Marina Arc (IBM) to consume Pacific (PAC) oceanic crust.

1215 IO – Indian Ocean, NPSP – North Philippine Sea Plate, SPSP – South Philippine Sea Plate, SEM –

1216 Semitau Block.

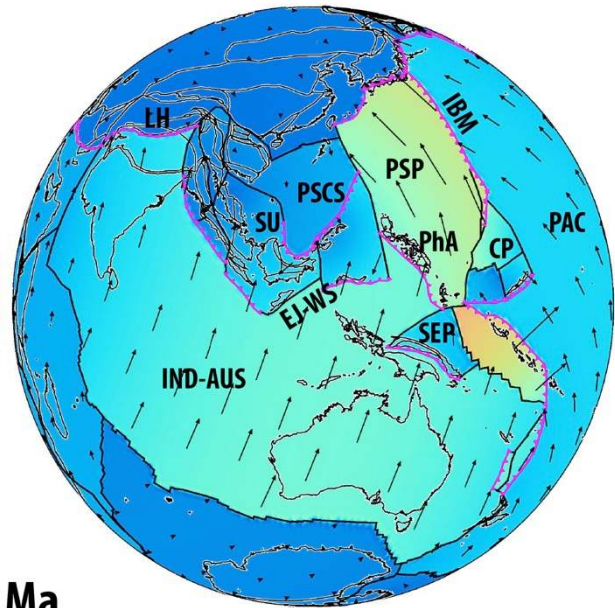
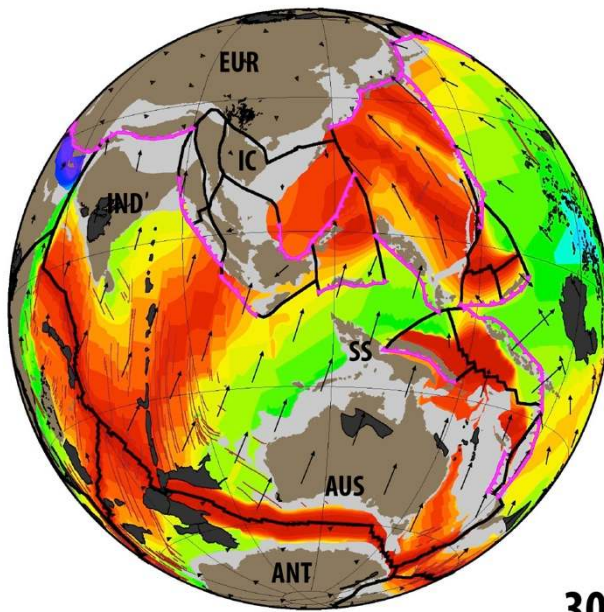


1218

1219 **Fig. 17.** Continent-continent collision between India and Eurasia likely initiated by ~47 Ma, leading
1220 to final closure of the Yarlung-Tansgpo and Shyok suture zones (see Fig. 1). The rollback of the
1221 Izanagi slab opens the Proto South China Sea and transfers the Semitau and Mindoro continental
1222 fragments from the South China margin onto northern Borneo, leading to a mid Eocene collision.
1223 The Sepik oceanic gateway is almost consumed along a north-dipping subduction zone, north of
1224 which the Proto Molucca Plate (PMOL) is consumed contemporaneously along the Philippine Arc.

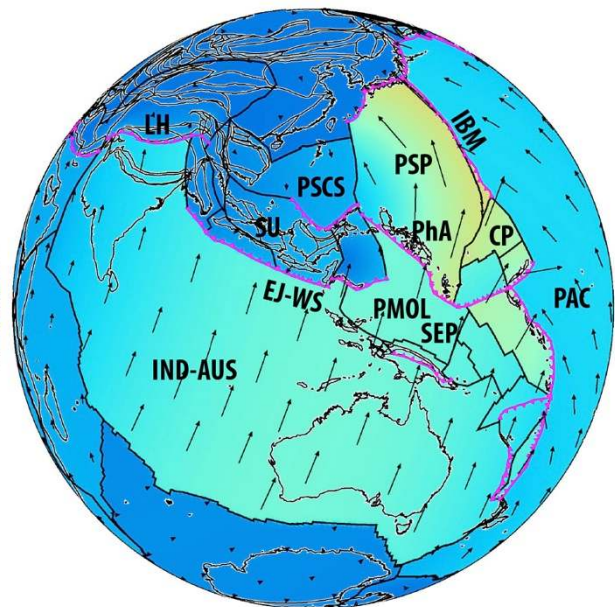
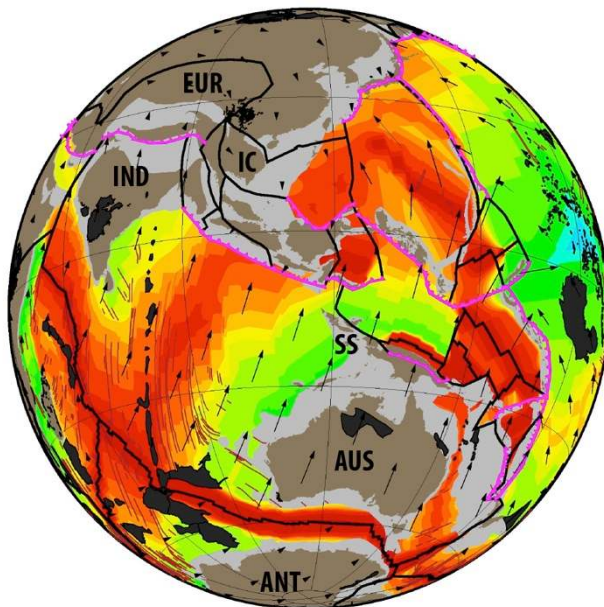
1225

Gibbons et al. (2015)



30 Ma

This Study



1226

1227

1228

1229

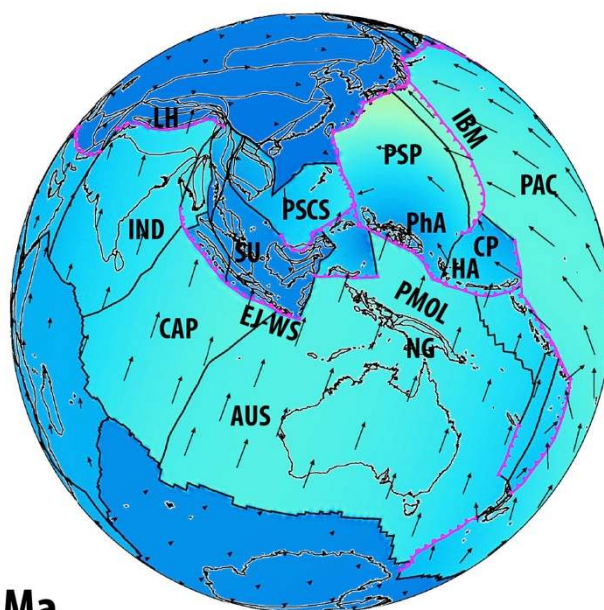
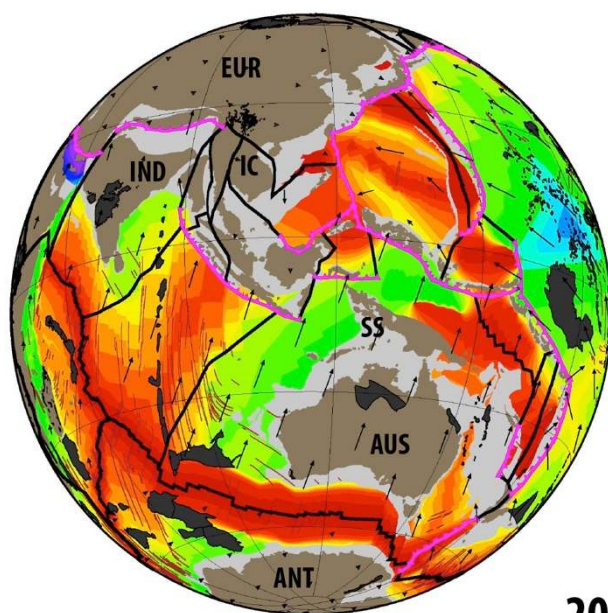
1230

1231

1232

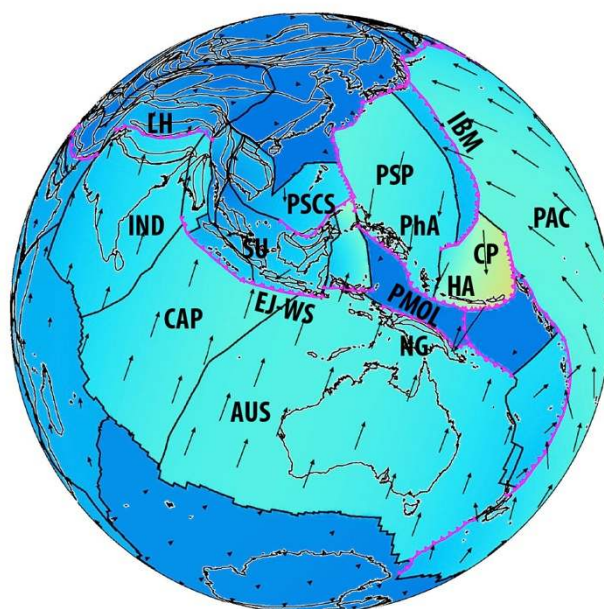
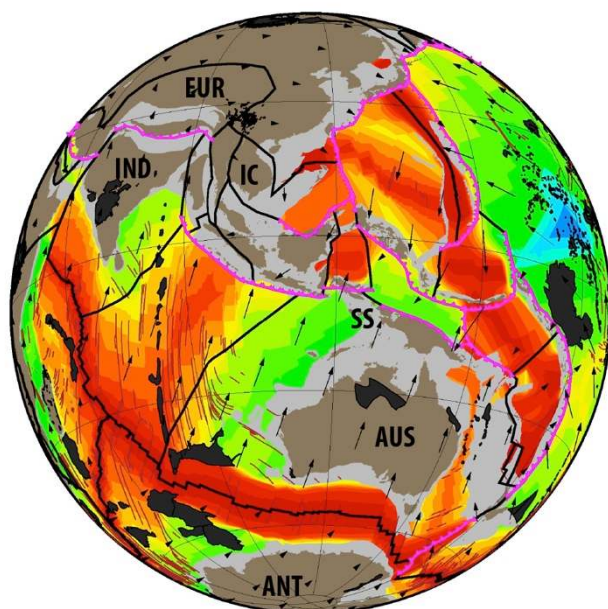
Fig. 18. India's continued, although slowed, northward advance results in the clockwise rotation and lateral extrusion of Indochina (IC), leading to the first stages of oroclinal bending in western Sundaland. The Sepik Terrane docks with the New Guinea margin, and the Sula Spur (SS) continental promontory on the northern Australian margin approaches Sundaland. CP – Caroline Plate, PSP – Philippine Sea Plate.

Gibbons et al. (2015)



20 Ma

This Study



1233

1234

1235

1236

1237

1238

1239

1240

1241

Fig. 19. The extrusion of Indochina due to India's northward motion, together with the collision between Sula Spur and West Sulawesi results in the oroclinal bending of Sundaland, resulting in major counterclockwise rotation of Borneo relative to Sumatra and the Malay Peninsula. South-dipping subduction initiates by ~20 Ma to account for the Maramuni Arc volcanics on New Guinea, with coeval north-dipping subduction of the Proto Molucca Plate (PMOL) accommodating southward motion of the Caroline Plate (CP) and the Halmahera Arc (HA).

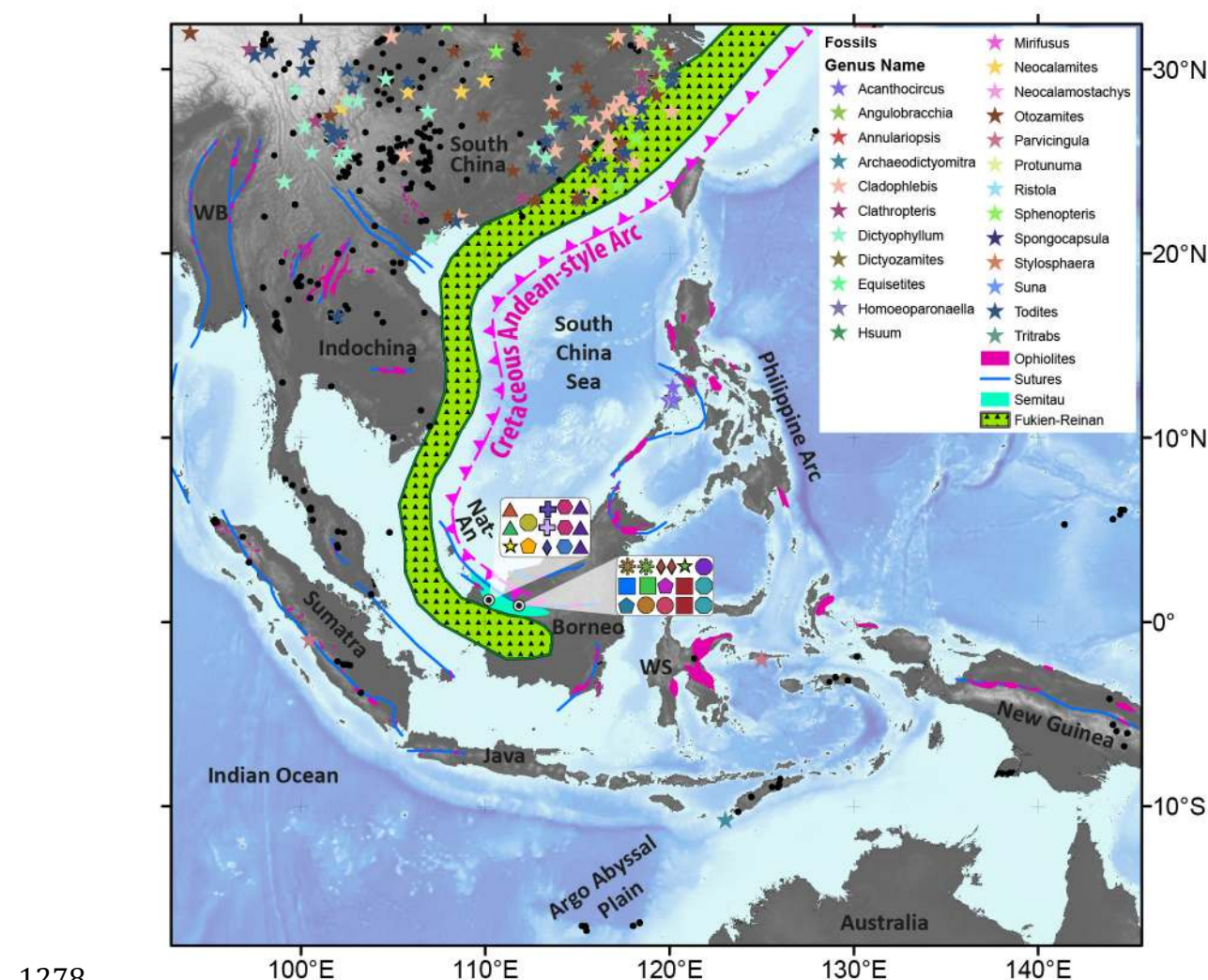
1242 **3.4.2 *Northern Sundaland collisions***

1243

1244 The geological record on the Sundaland continental promontory captures the geodynamic
1245 interaction between the Tethyan and proto-Pacific oceanic domains, and holds clues as to how the
1246 present-day complexity of plate boundaries developed. Most notably, an ongoing topic of interest
1247 relates to how the east Asian margin transitioned from purely Andean-style subduction (Fig. 20) in
1248 the Late Cretaceous (Shi and Li, 2012), to one that is presently dominated by a labyrinthine network
1249 of intra-oceanic active margins connected by splayed transforms, ridge segments and diffuse plate
1250 boundaries (Bird, 2003). Although much of the proto-Pacific plates have been recycled into the
1251 mantle, the preserved flanks of the seafloor spreading history have been used to restore the lost
1252 plates, assuming seafloor spreading symmetry (Seton et al., 2012). However, the location and
1253 evolution of subduction zones is difficult to constrain, with the only clues coming from
1254 paleomagnetic constraints, arc volcanics and present-day mantle structure (Hall and Spakman,
1255 2002; Miller et al., 2006; Queano et al., 2007; Zhao et al., 2007).

1256 Although a key component of the intra-oceanic system is the Philippine Sea Plate, which is
1257 discussed in Section 3.5.1, the transition from Andean-style to intra-oceanic subduction north of
1258 Sundaland is most likely controlled by back-arc basin opening processes in the Late Cretaceous
1259 (Morley, 2012a). In the model proposed in Zahirovic et al. (2014), and adopted here, the
1260 emplacement of the Fukien-Reinan massif (Fig. 20) from Andean-style subduction ceases in the
1261 Late Cretaceous (Jahn et al., 1976), and was replaced with extension and back-arc basin opening
1262 (Li, 2000) due to rollback of the Izanagi slab (Figs. 13-14, 16). Such a scenario is consistent with
1263 the onset of Late Cretaceous tectonic subsidence in East Asian basins (Yang et al., 2004), as well as
1264 the crustal and biogeographic affinity between continental fragments wedged in northern Borneo
1265 and the Philippine Archipelago, namely the Semitau and Mindoro blocks, and their likely origin on
1266 the South China continental margin (Fig. 20) in the Late Cretaceous (Zahirovic et al., 2014). The
1267 rollback induced extension in the overriding plate (Schellart and Lister, 2005) likely progressed to

back-arc basin opening, following the analogue of the Tyrrhenian back-arc system in the Mediterranean that detached and carried continental blocks to eventually collide as allochthons with a distant margin (Doglioni, 1991; Jolivet et al., 1999; Rehault et al., 1987). In the case of the Proto South China Sea, the Semitau and Mindoro fragments were likely detached from the East Asian margin by ~65 Ma, based on the onset of tectonic subsidence (Yang et al., 2004) and the ~59 Ma emplacement of supra-subduction zone ophiolites on Mindoro (Yumul et al., 2009). The continued rollback transferred Semitau and Mindoro southward, resulting in an Eocene collision with the northern Borneo margin to produce the Sarawak Orogeny (Cullen, 2010; Fyhn et al., 2010; Hutchison, 1996; Hutchison, 2004), after which southward subduction consumed the Proto South China Sea to emplace widespread volcanism on northern Borneo (Soeria-Atmadja et al., 1999).



1279 **Fig. 20.** Triassic and Jurassic fossil occurrences from the global Paleobiology Database (now
1280 Fossilworks) from Semitau (northern Borneo), represented by coloured symbols. The same fossils
1281 are also found elsewhere in Asia, with the strongest biogeographic affinity with mainland South
1282 China. The curved Fukien-Reinan massif (green hatched region) represents the Cretaceous Andean-
1283 style east Asian margin, which was replaced with an intra-oceanic setting in the Late Cretaceous.
1284 The curvature of the Andean-style magmatic arc also supports strong oroclinal bending of
1285 Sundaland in post-Cretaceous times. Nat-An – Natuna–Anambas Arc, WB – West Burma, WS –
1286 West Sulawesi. Figure adapted from Zahirovic et al. (2014).

1287

1288 The slab pull from south-dipping Proto South China Sea subduction along northern Borneo,
1289 along with the clockwise (CW) extrusion of Indochina resulting from the India-Eurasia collision
1290 (Fuller et al., 1991; Tapponnier et al., 1982), may have led to significant adjustments in the plate
1291 boundary forces acting on Sundaland. The ~32 Ma onset of seafloor spreading along the South
1292 China margin (Fig. 18) detached the Dangerous Grounds-Reed Bank continental blocks to open the
1293 South China Sea (Lee and Lawver, 1994; Lee and Lawver, 1995), with collision of the continental
1294 fragments with northern Borneo and South Palawan at ~15 Ma resulting in ophiolite obduction and
1295 the Sabah Orogeny (Hutchison, 2004; Hutchison et al., 2000), as well as choking the north Borneo
1296 subduction system and shutting down seafloor spreading in the South China Sea (Briais et al.,
1297 1993). This southward collision was wedged between the India-Eurasia collision from ~47 Ma (see
1298 Section 3.2) and the collision of the Australian northern margin with eastern Sundaland from ~25
1299 Ma (Bergman et al., 1996; Hall, 2002). This arrangement of plate boundaries, and the driving
1300 forces, presumably had significant consequences for the rotational history of Borneo and the
1301 deformation of Sundaland.

1302

1303

1304

1305 3.4.3 *Sundaland oroclinal bending*

1306

1307 The large counterclockwise (CCW) rotation of Borneo, relative to stable Sundaland, in the
1308 Cenozoic has drawn a range of interpretations and led to a number of competing models (see
1309 discussion in Zahirovic et al. (2014)). Each model of Borneo rotation has consequences for the
1310 deformation history on Sundaland (in particular, the basins of the Sunda Shelf and Java Sea), as
1311 well as understanding the mechanism that led to the 90° CCW rotation of Borneo relative to
1312 Sundaland in the Mesozoic, including up to 50° CCW rotation since 25 Ma (Fuller et al., 1999). In
1313 the absence of large transform faults, such as the Red River Fault bounding northern Indochina,
1314 within the Java Sea or the Sunda Shelf, Hutchison (2010) proposed a model of oroclinal bending for
1315 the rotation of Borneo as a mechanism to explain the deformation of the Sundaland continental
1316 promontory.

1317 Hutchison (2010) synthesised the paleomagnetic evidence, as well as observations of curved
1318 lineaments observed in the gravity anomalies of Sundaland and the curvature of the Natuna and
1319 Anambas Cretaceous paleo-arc (Fig. 20) to infer that wholesale bending of Sundaland
1320 accommodated the CW rotation of Indochina and the CCW rotation of Borneo (Fuller et al., 1999;
1321 Fuller et al., 1991). The curved lineaments (Fig. 21) are most likely to be successive generations of
1322 ancient volcanic arcs (Hutchison, 2010), with the most obvious example being the curved arc
1323 belonging to the Middle to Late Triassic tin belt granites on Bangka and Billiton islands, as well as
1324 the previously-mentioned Natuna-Anambas Cretaceous Arc. Zahirovic et al. (2014) expanded on
1325 the work of Hutchison (2010) and used filtered Bouguer anomalies (Balmino et al., 2012) to extract
1326 geometrical constraints on the oroclinal bending (Fig. 21), and constructed a kinematic oroclinal
1327 bending model that accounts up to ~78° CCW rotation of Borneo since ~50 Ma.

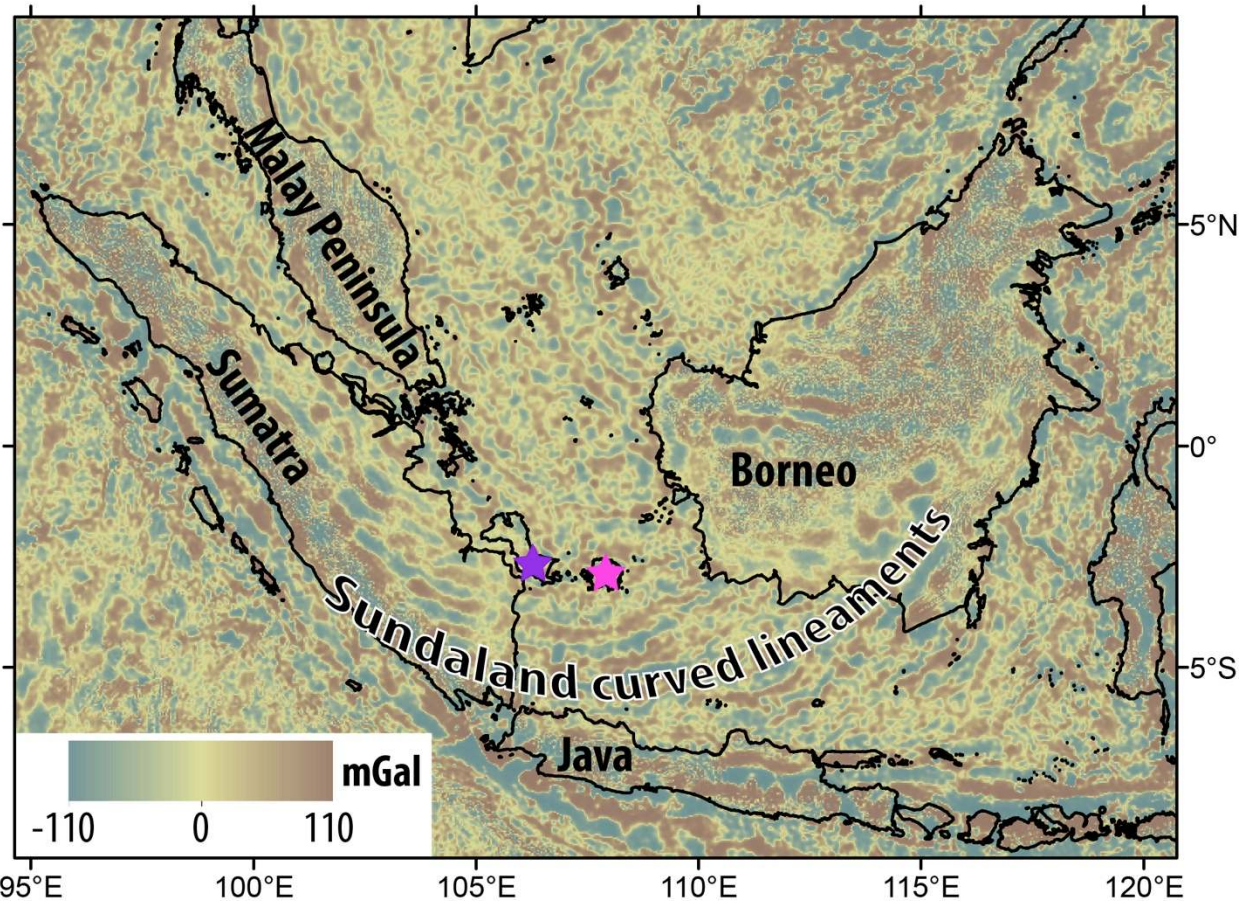


Fig. 21. The band-pass-filtered (150 to 10 km) Bouguer gravity anomalies from the 1 min World Gravity Map (Balmino et al., 2012) highlights the large-scale structures and the curved lineaments on Sundaland, resulting from oroclinal bending as proposed by Hutchison (2010). Bangka Island – purple, Belitung (Billiton) Island – pink.

One important distinction between the oroclinal bending of Sundaland and classical models of oroclinal bending largely relates to the tightness of the oroclinal folds and the deformation experienced by the continental crust (Carey, 1955; Eldredge et al., 1985). In the case of Sundaland, the hinge of the orocline is likely to be in the Sunda Shelf west of Borneo, with a wide region of bending rather than tight oroclinal bends that are typically reported for Kazakhstan (Abrajevitch et al., 2008) and the Mediterranean (Rosenbaum, 2014). Although the boundaries of the Sundaland continental promontory experienced compression during oroclinal bending, the Java Sea and Sunda Shelf were dominated by extension from Eocene times to the mid Miocene, after which a major

1342 phase of basin inversion dominated the tectonic regime of Sundaland to the present (Doust and
1343 Sumner, 2007; Pubellier and Morley, 2014).

1344

1345 **3.5 New Guinea and the Philippines**

1346

1347 **3.5.1 *Origin and evolution of the Philippine Archipelago***

1348

1349 Tectonic reconstructions of the transfer of Gondwana-derived terranes following the
1350 breakup of Pangea are limited by the lack of preserved seafloor, but are typically supplemented
1351 with high-quality and well-constrained onshore geological data that helps reconstruct the synthetic
1352 seafloor spreading histories. However, the region east of Sundaland, which includes the Philippines
1353 and New Guinea are considerably more complicated, as they straddle the Tethyan and (proto-)
1354 Pacific tectonic domains, resulting in a complex interaction dominated by back-arc basin formation
1355 processes and multiple phases of collision, obduction and subduction that consumed them.

1356 One early synthesis of the tectonic evolution of the post-Eocene West Pacific was carried
1357 out by Jolivet et al. (1989), who modelled the plate motions in six stages (56, 43, 32, 20, 12 and
1358 3 Ma), and importantly, provided finite rotation poles that define their time-dependent plate circuit.
1359 In the reconstructions of Jolivet et al. (1989), and subsequent models (Hall et al., 1995a; Lee and
1360 Lawver, 1995; Pubellier et al., 2003; Queano et al., 2007; Zahirovic et al., 2014), the Philippine Sea
1361 Plate develops in near-equatorial southern latitudes during the Eocene (Hall et al., 1995a; Hall et al.,
1362 1995b; Richter and Ali, 2015), and is isolated from the surrounding plate circuits by a network of
1363 plate boundaries (including subduction zones and transforms) for much of the time. This tectonic
1364 isolation, and lack of preserved seafloor spreading linking the Philippine Sea Plate directly to the
1365 Pacific, Eurasian or Australian plates leads to difficulties in reconstructing the absolute and relative
1366 plate motions of this region that links the Pacific with the Indian oceans. However, the seafloor
1367 spreading history within the Philippine Sea Plate itself has been well-documented, including the

opening of the West Philippine Basin between ~55 and 33 Ma (see Hilde and Chao-Shing (1984), Deschamps and Lallemand (2002), and references therein) and the back-arc opening of the Shikoku and Parece Vela back-arc basins between ~29 and 15 Ma from Philippine Sea Plate rotation (Sdrolias et al., 2004) and Izu-Bonin-Mariana trench rollback (Kobayashi, 2004).

Although the seafloor spreading history of the Philippine Sea Plate is confined to post-Eocene times, the Philippine Arc has recorded a much longer history of subduction, with the earliest supra-subduction zone (SSZ) rocks from the Late Jurassic. The SSZ ophiolites from the Philippine Arc have ages of 156.3 ± 2.0 Ma and 150.9 ± 3.3 Ma (Lagonoy Ophiolite), and 142 ± 4 Ma (Gag Island, Halmahera) from the synthesis of Encarnación (2004). They are discussed at length in Zahirovic et al. (2014). Recent work by Deng et al. (2015) reported mid-Cretaceous, 126 ± 3 Ma and 119 ± 2 Ma (U-Pb), SSZ volcanics from Cebu Island. These ages are consistent with the minimum 99.9 ± 7.0 Ma (Ar-Ar) age of the Calaguas Ophiolite (Geary et al., 1988; Geary and Kay, 1989), and the 100 ± 4 Ma arc rocks reported from Obi Island on Halmahera (Hall et al., 1995b), suggesting continuous Early Cretaceous subduction along the Philippine Arc. To reconcile the likely southern hemisphere origin of the Philippine Arc and the Late Jurassic-Early Cretaceous temporal similarity with north Gondwana rifting events, Zahirovic et al. (2014) proposed a SSZ origin in the vicinity of New Guinea, recently independently suggested by Deng et al. (2015). The multiple generations of ophiolites may suggest a tectonic scenario similar to the current multi-generation opening of back-arcs along the Izu-Bonin-Mariana system, and may explain the origin of the Daito and Oki-Daito ridges as paleo-arc features in the north West Philippine Basin.

3.5.2 *Nature of the New Guinea margin since the Late Jurassic*

To accommodate the northern Gondwana rifting episode in the Late Jurassic, Zahirovic et al. (2014) placed the East Java-West Sulawesi continental fragments along New Guinea as the simplest end-member of transferring blocks north towards Sundaland, but acknowledged that an

Argo Abyssal Plain origin (NW Australian shelf) would also be possible due to the lack of preserved seafloor spreading histories to constrain a pre-drift fit. In this study, we implement the Argo origin end-member scenario, which is consistent with the zircon age spectra linking East Java to the NW Australian shelf (Sevastjanova et al., 2015; Smyth et al., 2007). The 158-137 Ma ages of mafic rocks, some of which are associated with pillow basalts, on West Sulawesi (Polvé et al., 1997) are consistent with the oldest oceanic crust (155 ± 3.4 Ma) in the Argo Abyssal Plain on the NW Australian Shelf (Gradstein and Ludden, 1992). By shifting these continental fragments west along northern Gondwana, the New Guinea margin can accommodate the source of the Philippine Archipelago to have formed along its margin. The benefit of such a scenario is that it accounts for the origin of (likely) Jurassic age SSZ ophiolites within the Central Ophiolite Belt in New Guinea (Monnier et al., 2000). However, the Late Jurassic-Early Cretaceous ($\sim 157 \pm 16$ Ma) and Late Cretaceous (66 ± 1.6 Ma) are unpublished ages from Permana (1998), reported in Pubellier et al. (2003), and require further corroboration. What is known is that at least part of the New Guinea margin was an active margin in Early Cretaceous times, as indicated by the Early Cretaceous volcanism and the Kondaku Tuffs (Dow, 1977; Rickwood, 1954), and likely represents the continuation of the long-lived east Gondwana active margin.

To what extent the Late Jurassic-Early Cretaceous active margin extended west into the Indonesian portion of New Guinea remains poorly constrained. In the east, the protolith of the Bena Bena metamorphics is partly Late Triassic (221 Ma) in age, and is intruded by Jurassic granite of 172 Ma in age (Davies, 2012). In the west, the Bird's Head region experienced granitoid emplacement in the Early Jurassic with one sample yielding an age of 197 ± 3 Ma (K-Ar) (Pieters et al., 1983), 205 ± 5 Ma in the P'nyang-1 exploration well in western Papua New Guinea (Valenti, 1993), and the 210 ± 25 Ma Mangole Volcanics on Banggai-Sula (Charlton, 2001). These results suggest that the trench along western New Guinea may have undergone rollback by the Late Jurassic to explain Early Cretaceous volcanics confined only to eastern New Guinea. Such a scenario is also consistent with the sedimentary history that records syn-rift sedimentation in the

1420 Early-Middle Jurassic, followed by a post-breakup unconformity and the formation of a
1421 diachronous passive margin along much of New Guinea (Pigram and Panggabean, 1984), with the
1422 exception of continued Early Cretaceous arc volcanism in the east.

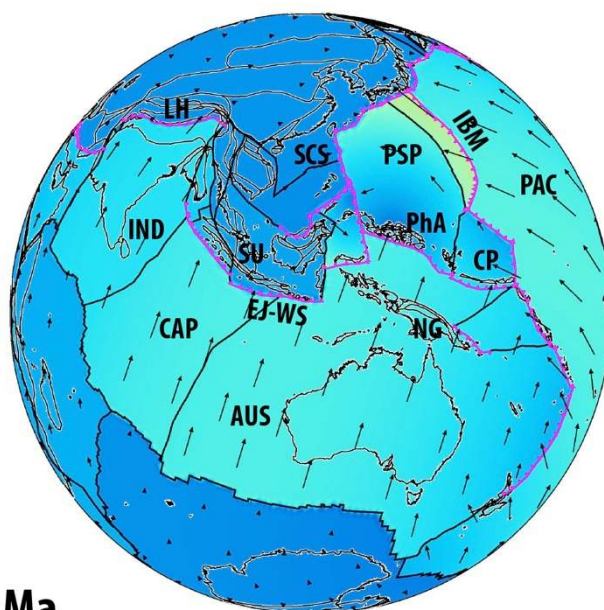
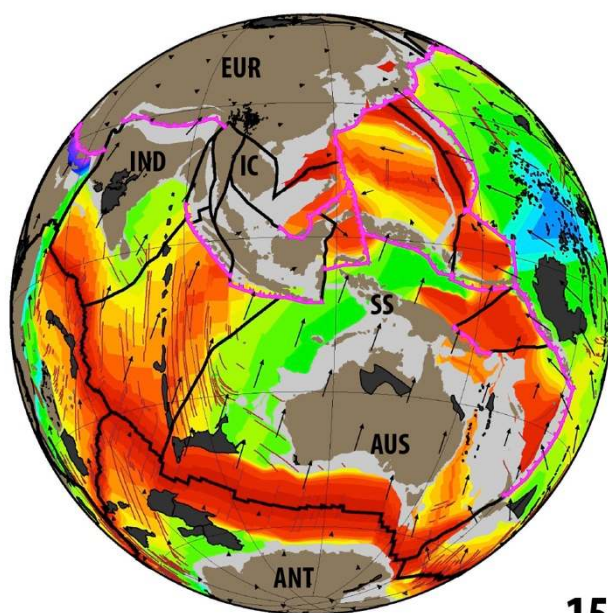
1423 Although the Early-Middle Jurassic rift-drift sequence is well preserved on New Guinea,
1424 few constraints exist to identify which (if any) continental terranes rifted from this margin (Hill and
1425 Hall, 2003; Pigram and Symonds, 1991). Apart from the East Java and West Sulawesi blocks
1426 (Zahirovic et al., 2014), parts of the Sepik Terrane may represent a para-allochthon that detached
1427 from the margin in the Jurassic, as invoked in this study, to open a somewhat-narrow oceanic basin
1428 and form the Late Jurassic SSZ ophiolites (Permana, 1998; Pubellier et al., 2003) exposed along the
1429 Central Ophiolite Belt in New Guinea (Fig. 3). Even though the Sepik Terrane is the largest
1430 accreted block on the New Guinea margin, the composite nature of the Sepik crust – with both
1431 continental and intra-oceanic arc fragments (Klootwijk et al., 2003) – leads to an enigmatic tectonic
1432 evolution. The New Guinea margin experienced at least two collisional phases; one in the late
1433 Eocene (Hall, 2002) to mid Oligocene (Crowhurst et al., 1996; Pigram and Symonds, 1991), and
1434 another major collision responsible for compressional deformation in the Mobile Belt during the
1435 late Miocene (Hall, 2002; Hill and Hall, 2003; Hill and Raza, 1999). However, the collisional
1436 history of the Sepik Terrane remains controversial in terms of whether the terrane first collided with
1437 one or more intra-oceanic arcs and subsequently welded to New Guinea, or whether the converse is
1438 true.

1439 Although the size of the oceanic basin that separated the Sepik Terrane from mainland New
1440 Guinea remains uncertain, the longevity of the oceanic basin can be inferred from subduction-
1441 related metamorphics that are distributed along the Central (Irian) Ophiolite Belt (Fig. 3), and
1442 eastward into the April Ultramafics and the Marum Ophiolite. The ~68 Ma high-temperature
1443 metabasites and ~44 Ma blueschists in the West Papuan Ophiolite (Weyland Overthrust) indicate
1444 that subduction of the Sepik oceanic basin was underway (Davies, 2012), which is consistent with
1445 ~45 to 40 Ma glaucophane (K-Ar) and 28 to 25 Ma (K-Ar) phengite ages (Baldwin et al., 2012) in

1446 the April Ultramafics. The Balantak Ophiolite on the East and Southeast Sulawesi Arm records ages
1447 of ~96-32 Ma (Monnier et al., 1995), with a paleo-latitudinal constraint of $17 \pm 4^\circ\text{S}$ at 80 Ma
1448 (Mubroto et al., 1994) suggesting that these ophiolites formed somewhere between Sundaland and
1449 the New Guinea margin. Such a scenario is consistent with north-dipping subduction of the Sepik
1450 oceanic basin, which may have generated supra-subduction zone ophiolites that were subsequently
1451 obducted onto Sulawesi. The Maastrichtian (~71 to 66 Ma, stratigraphic correlation and dating
1452 using foraminifera) Emo volcanics (Worthing and Crawford, 1996) were likely emplaced in a back-
1453 arc setting from north-dipping subduction along the Sepik Terrane, with final docking likely taking
1454 place by ~30 Ma (Findlay, 2003; Zahirovic et al., 2014), based on the 35 to 31 Ma (Ar-Ar)
1455 amphibolite age of the Emo metamorphics (Worthing and Crawford, 1996) and the cooling histories
1456 of exhumed blocks (Crowhurst et al., 1996).

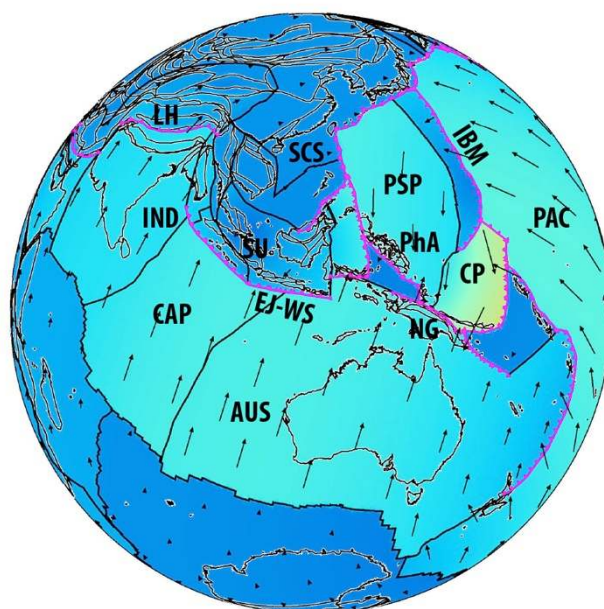
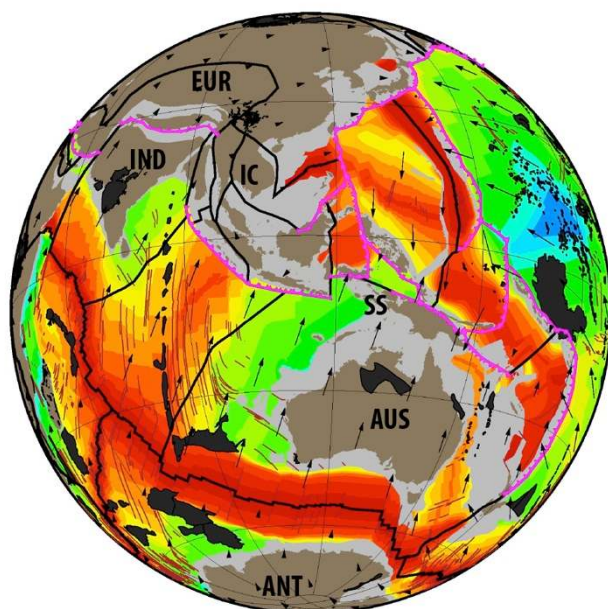
1457 Following the docking of the Sepik composite terrane, south-dipping subduction was likely
1458 established (Figs. 19, 22) to account for the ~18 to 8 Ma Maramuni Arc volcanism (Hill and Hall,
1459 2003; Page, 1976), followed by post-collisional volcanism to at least ~1 Ma (Holm et al., 2014; van
1460 Dongen et al., 2010). The approaching Halmahera Arc, attached to the southern portion of the
1461 Caroline Plate, likely collided with the northern New Guinea margin by ~14 Ma (Figs. 22-23),
1462 leading to a major compressional phase in the Mobile Belt, that has been inferred from apatite
1463 fission track geochronology (Hill and Raza, 1999; Kendrick, 2000). Although the New Guinea
1464 margin is a key component of the Australian, Pacific and Eurasian convergence zone, more work is
1465 required to resolve competing tectonic scenarios for this margin (van Ufford and Cloos, 2005).
1466 However, additional insights can be made from interpretations of mantle structure from seismic
1467 tomography, as well as testing end-member scenarios using coupled plate kinematic and numerical
1468 mantle convection modelling of the New Guinea margin.

Gibbons et al. (2015)



15 Ma

This Study



1469

1470

1471

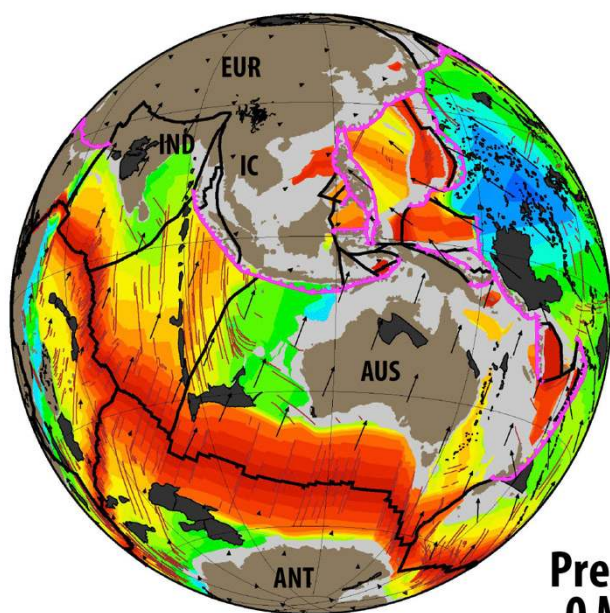
1472

1473

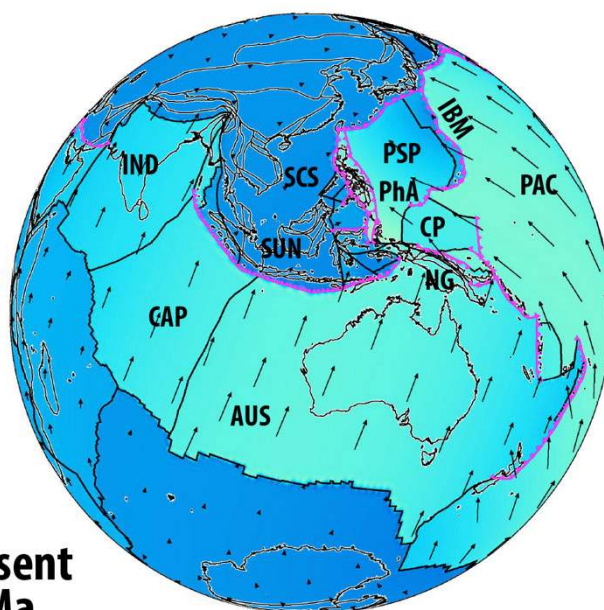
1474

Fig. 22. The 15 Ma timestep records the transition to compressional tectonics on Sundaland and New Guinea. The arrival of the Dangerous Grounds-Reed Bank continental fragment shuts down Proto South China Sea subduction along Borneo, and results in ophiolite obduction in Palawan and orogenesis on Borneo. In the refined reconstructions, the Halmahera Arc collides with New Guinea at ~15 Ma to result in major compression in the New Guinea Mobile Belt.

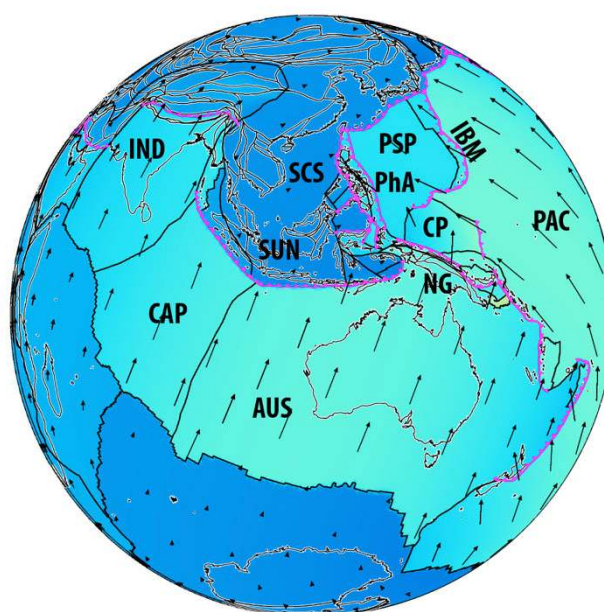
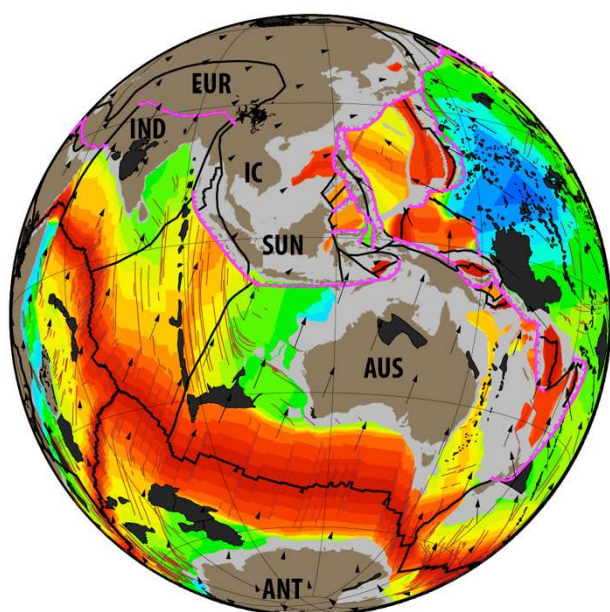
Gibbons et al. (2015)



Present
0 Ma



This Study



1475

1476

1477

1478

1479

1480

1481

1482

1483

Fig. 23. The present-day tectonic configuration of Southeast Asia is the result of long-lived Indo-Australian, Eurasian and Pacific convergence accommodated by the subduction of Tethyan ocean basins and back-arcs. The northward motion of India is significantly slower than in the early Eocene, with intra-plate diffuse deformation in the Capricorn (CAP) Plate since ~20 Ma.

4 Insights from age-coded slabs in seismic tomography

In light of the complex tectonic evolution of Southeast Asia and the Tethyan-Pacific oceanic linkages, we interpret high velocity seismic anomalies from the P-wave model of Li et al. (2008) to

1484 obtain insights into the subduction history (Fig. 24). Although assuming constant and vertical slab
1485 sinking is a simplification, it is arguably a reasonable assumption for the late Cenozoic where large
1486 lateral slab advection would be limited, as indicated by previous estimates of less than ~1-2 cm/yr
1487 of mid-mantle lateral flow in the Tethyan realm (Becker and Faccenna, 2011; Zahirovic et al.,
1488 2012). We compare the plate reconstructions with age-coded depth slices of high velocity seismic
1489 anomalies, applying a sinking rate of 2 cm/yr in the lower mantle, and end-member estimates of 3
1490 and 8 cm/yr in the upper mantle (see Methods). The proposed lower mantle slab sinking rates for
1491 the Tethyan realm are larger (~2 cm/yr) than estimated global averages (1.2-1.3 cm/yr in
1492 Butterworth et al., 2014; van der Meer et al., 2010), and may reflect the suction exerted by deep
1493 slabs in this slab graveyard area (Conrad and Lithgow - Bertelloni, 2004).

1494 The plate reconstructions in our base model (Zahirovic et al., 2014) were calibrated for the
1495 Philippine Sea Plate and Sundaland using a similar method (assuming sinking rates of 3 and
1496 1.2 cm/yr in the upper and lower mantle, respectively). However, in the refined reconstructions, we
1497 do not modify the Sundaland oroclinal bending model, but modify the position of the Philippine Sea
1498 Plate since ~30 Ma to ensure collision of the Halmahera Arc with New Guinea at ~15 Ma, to
1499 account for the onset of widespread compression in the New Guinea Mobile Belt (Hill and Hall,
1500 2003). Consequently, the match between Sundaland subduction zones and age-coded slabs from
1501 tomography is not surprising. Modifications to fit the Philippine Sea Plate to surface geology since
1502 ~30 Ma, rather than seismic tomography, presents a case study to test whether both geological and
1503 seismic tomographic constraints can be accommodated simultaneously.

1504

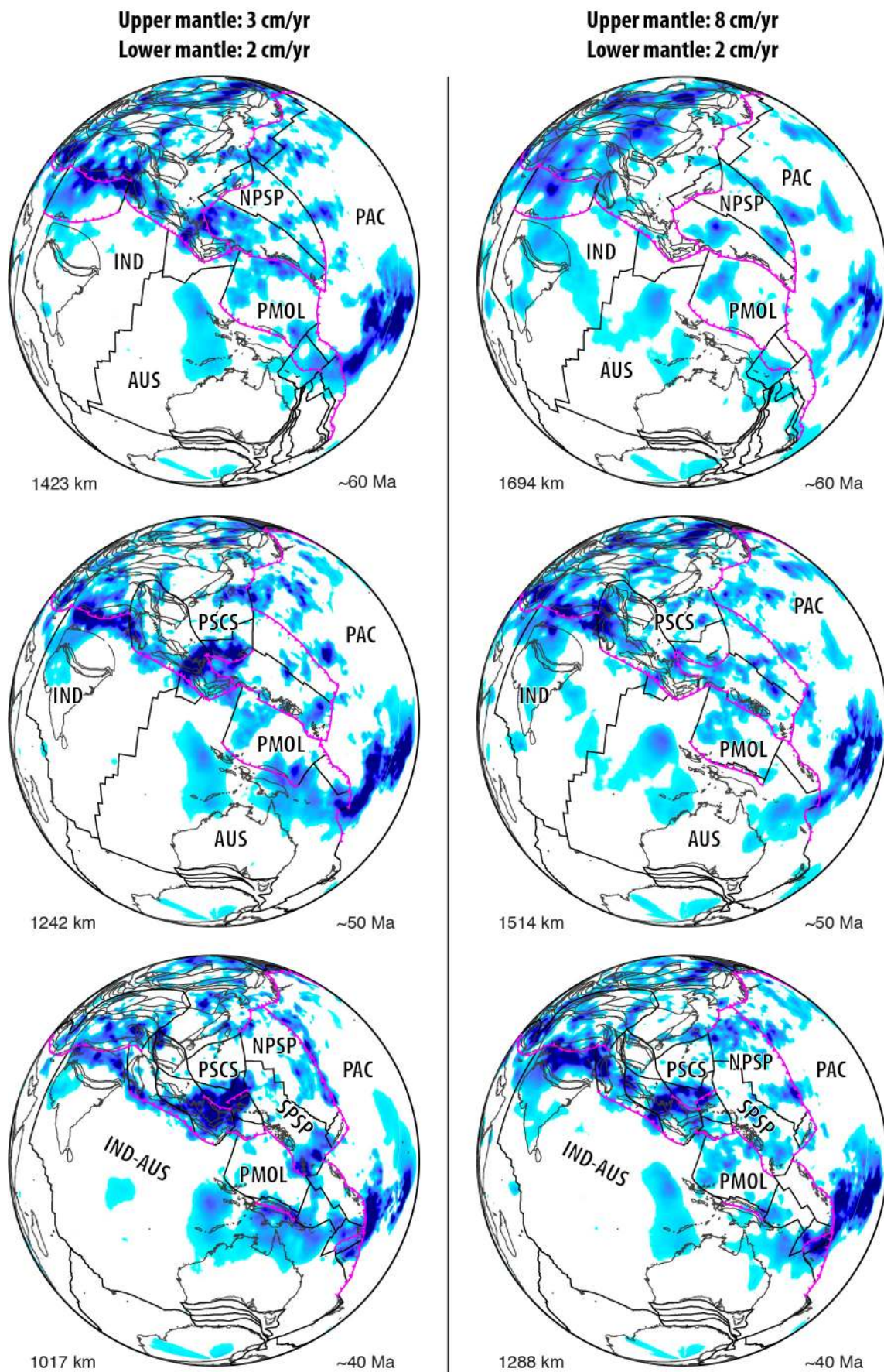
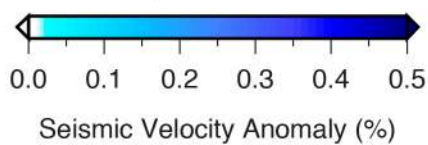
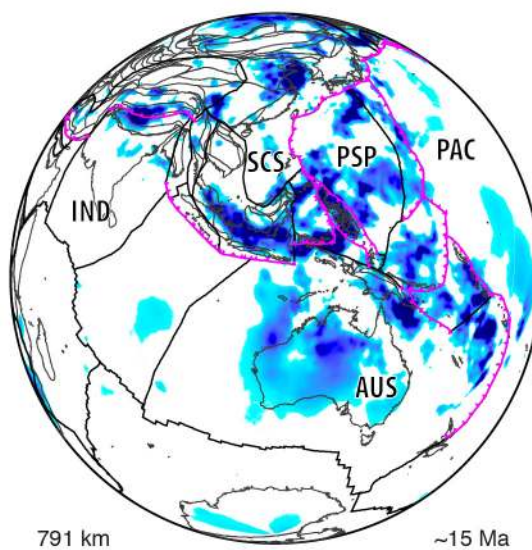
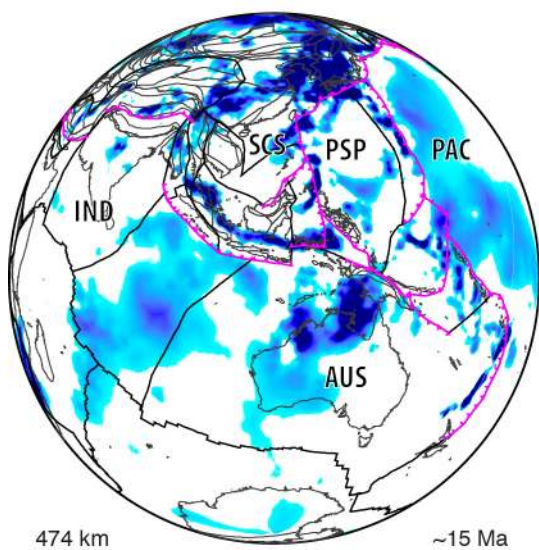
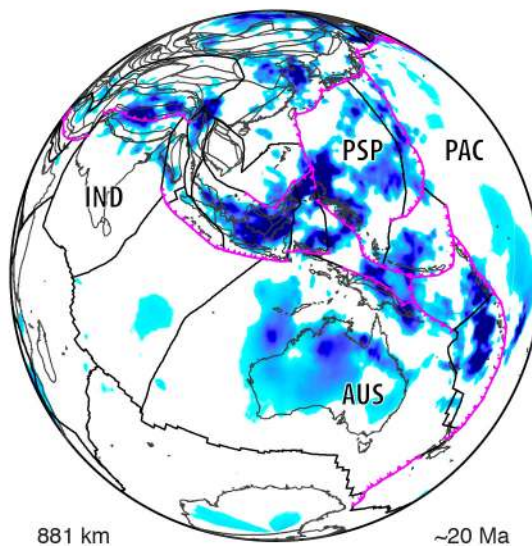
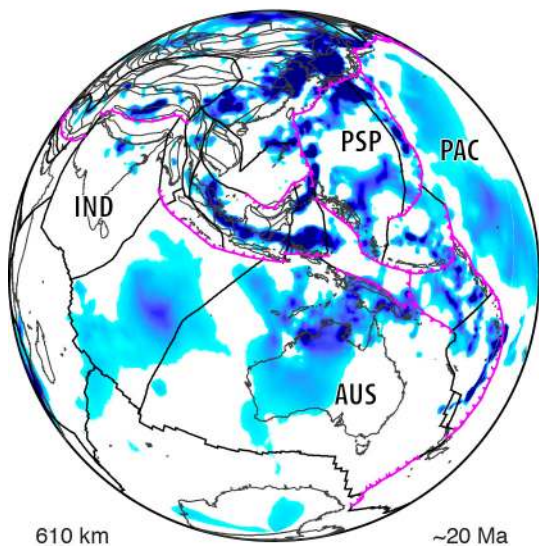
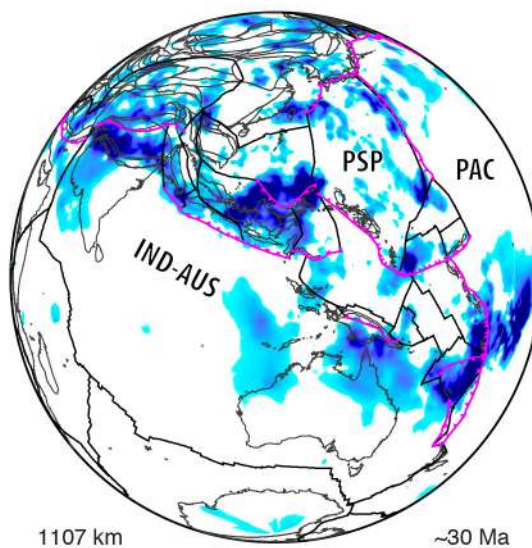
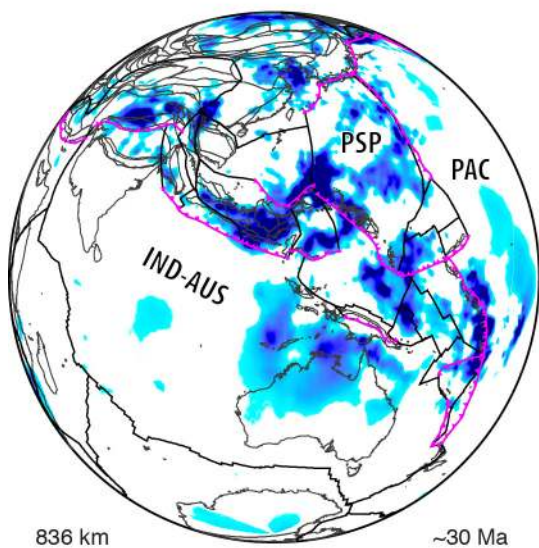


Fig. 24. Fast seismic velocity anomalies from the Li et al. (2008) P-wave seismic tomography model compared to our refined plate reconstructions. Ages are attributed to depths assuming that

1508 the average vertical sinking rate of slabs is ~ 2 cm/yr in the lower mantle, and 3 cm/yr (left) and 8
1509 cm/yr (right) in the upper mantle. Additional polygons in Australian-Antarctic and Lord Howe-
1510 Tasman Sea regions represent areas of deforming continental crust. See Supplementary
1511 Animations 5 and 6.

Upper mantle: 3 cm/yr
Lower mantle: 2 cm/yr

Upper mantle: 8 cm/yr
Lower mantle: 2 cm/yr



1513 **Fig. 24.** (continued)

1514

1515 At ~60 Ma (Fig. 24), the scenario invoking a slower sinking rate in the upper mantle better
1516 reproduces the Sunda slab, as well as the subduction of the Proto Molucca Plate (PMOL) beneath
1517 the Philippine Arc and the rollback-induced opening of the Proto South China Sea. The match with
1518 the Sunda and Philippine slabs is not surprising, as a slower sinking rate was also used to calibrate
1519 the position of these blocks in our base plate motion model (Zahirovic et al., 2014). Both slab
1520 sinking scenarios reproduce the Andean-style subduction along southern Eurasia consuming the
1521 Kohistan-Ladakh and Woyla back-arc basins, as implemented in the reconstructions based on the
1522 near-equatorial latitudes from paleomagnetic estimates. At ~50 Ma, the slower sinking rate matches
1523 the oroclinal bending of Sundaland and subduction of the Proto South China Sea, which is again
1524 expected due to calibration of the reconstructions with tomography. However, the match to
1525 subduction of the Sepik oceanic basin north of New Guinea is not imposed, and suggests the large
1526 E-W slab presently beneath Australia is likely sourced from this subduction system (Schellart and
1527 Spakman, 2015). Interestingly, the gap in the Sunda slab along Sumatra in both sinking rate end-
1528 members, coinciding with the modelled location of the Wharton Ridge, supports the slab window
1529 scenario proposed by Whittaker et al. (2007).

1530 The 40 and 30 Ma timesteps in the age-coded seismic tomography depth slices support
1531 ongoing subduction along northern Borneo (Fig. 24), and waning subduction in the India-Eurasia
1532 segment of the active margin. The ~20 and 15 Ma reconstructions (Fig. 19 and 21) highlight the
1533 requirement of south-dipping subduction along New Guinea to account for the Maramuni Volcanics
1534 (Fig. 24), as well as contemporaneous north-dipping subduction along the Halmahera Arc, which is
1535 terminated after ~15 Ma following the arc-continent collision on northern New Guinea. The
1536 collision of Dangerous Grounds-Reed Bank with northern Borneo at ~15 Ma also choked the north
1537 Borneo subduction zone, and likely resulted in Proto South China Sea slab breakoff. The ~15 Ma
1538 reconstruction using the faster sinking rate, and corresponding to a 791 km depth slice, shows a

1539 discrete slab volume along northern Borneo that we interpret as the Proto South China Sea slab
1540 (Fig. 24).

1541 The seismic tomographic interpretation highlights that the refinement of the New Guinea
1542 margin (namely the Maramuni subduction zone) and the adjustment to the Philippine Sea Plate
1543 (namely the position of the Halmahera Arc) since ~30 Ma can accommodate both the geological
1544 and the tomographic constraints. Neither sinking rate scenarios produce consistent matches
1545 throughout the plate reconstruction timeframe, likely due to the complex time-varying slab sinking
1546 rates and regional interactions of slabs in a spherical mantle shell. However, the assumption of
1547 vertical sinking of slabs is likely to be an acceptable estimate of trench locations in the Cenozoic for
1548 slabs that are still attached to the subducting plate, or slabs that have experienced little stagnation or
1549 folding in the mantle transition zone. The numerical computations described in the following
1550 section provide a more consistent approach to tracking slabs in the mantle resulting from the
1551 complex subduction history in the Tethys, east and Southeast Asia, and New Guinea.

1552 **5 Numerical modelling results**

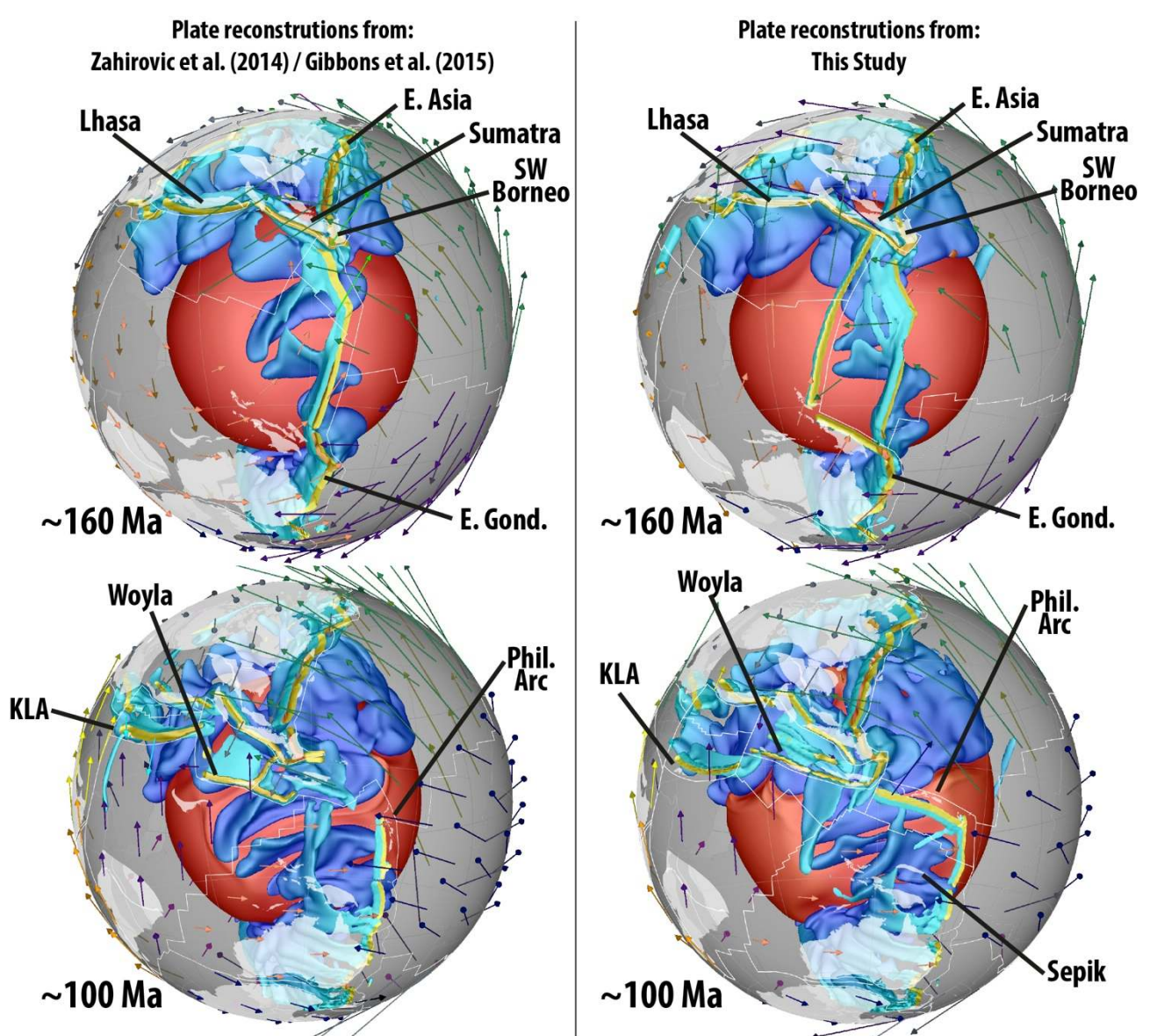
1553

1554 **5.1 Large-scale post-Jurassic mantle evolution of the Tethyan tectonic domain**

1555

1556 We present the first synthesis of post-Jurassic Tethyan plate reconstructions and
1557 geodynamics in a 4D (space and time) global context. We ran five cases of coupled plate kinematic
1558 and geodynamic numerical experiments, mainly to test end-member plate reconstructions, and
1559 present 3D snapshots of two experiments that compare the Zahirovic et al. (2014) model with
1560 refinements for the Neo-Tethys, Philippine Sea Plate and New Guinea presented in this study (Fig.
1561 25). Although the mantle convection models are initiated at 230 Ma during the time of Pangea
1562 stability, we present only the post ~160 Ma timeframe applicable to the refined plate
1563 reconstructions. At ~160 Ma, the dominant feature of the mantle is the circum-Pangea subduction

1564 girdle, as well as the southern Eurasian active margin consuming Meso-Tethyan oceanic lithosphere
 1565 (Fig. 25a). The tectonic scenario presented invokes the northward continuation of East Gondwana
 1566 subduction along New Guinea and connecting to the East Asian subduction of the Izanagi Plate. By
 1567 ~140 Ma the rollback of the Lhasa trench opens the Kohistan-Ladakh back-arc basin, with a slower
 1568 opening and southward position of ~10°N in our base model by 100 Ma (Zahirovic et al., 2014),
 1569 compared with the equatorial position implemented in this study following Burg (2011) and
 1570 Gibbons et al. (2015).



1571
 1572 **Fig. 25a.** Snapshots of mantle structure including sinking slab volumes (blue) and thermochemical
 1573 upwellings (red) from the core-mantle boundary are visualised in GPlates using the mantle
 1574 temperature predictions from the CitcomS numerical experiments of mantle flow depicting Case 4

1575 (left) and 5 (right). The snapshots compare the large-scale mantle evolution in the latest Jurassic
1576 and Early Cretaceous from Tethyan subduction along Lhasa and the Kohistan-Ladakh Arc (KLA),
1577 as well as recycling of proto-Pacific lithosphere along the East Asian, East Gondwana and
1578 Philippine Arc subduction zones. Plate boundaries (white), velocities (coloured arrows) and
1579 reconstructed present-day coastlines (translucent white) are plotted. Subduction zones are yellow
1580 regions, and slab colouring is a function of depth from light blue (shallow slabs) to darker blue
1581 (deep slabs). These snapshots highlight the global nature of our numerical experiments, with
1582 complex interactions of slabs as they sink in the mantle shell. The experiments allow us to track the
1583 sinking trajectory (vertical and lateral) of the slabs to identify their source from the present-day
1584 mantle prediction, which are compared to the mantle structure imaged using P- and S-wave seismic
1585 tomographic techniques. Central co-ordinate is 10°S, 115°E.

1586

1587 As our modelling domain is spherical, and because the flow is constrained to follow surface
1588 velocities that include net rotation of the lithosphere, lateral mantle flow may influence the
1589 trajectory of sinking slabs. As subducting slabs sink in the mantle, the core-mantle boundary
1590 becomes draped with older slabs that sweep the hotter material into the large-scale Pacific and
1591 African upwellings (Bower et al., 2013; McNamara and Zhong, 2005) (Fig. 25). In addition, mantle
1592 flow advects slabs laterally, with notable southward (and somewhat westward) translation of the
1593 Paleo-Tethyan slabs, and eastward advection of the east Asian slabs (Fig. 25). India's collision with
1594 the Kohistan-Ladakh Arc ceases intra-oceanic subduction by ~50 Ma in our model, resulting in the
1595 Andean-style subduction of the Kohistan-Ladakh back-arc basin along southern Lhasa (Fig. 25b).
1596 The ~47 Ma continent-continent collision temporarily shuts down subduction, causing a slab break-
1597 off event, followed by ongoing subduction of the Greater Indian mantle lithosphere (Capitanio et
1598 al., 2010). Australia's northward motion results in the northern margin, including New Guinea,
1599 overriding the Southeast Asian slab graveyard from ~30 Ma following the docking of Sepik, and
1600 the initiation of south-dipping Maramuni subduction from ~20 Ma.

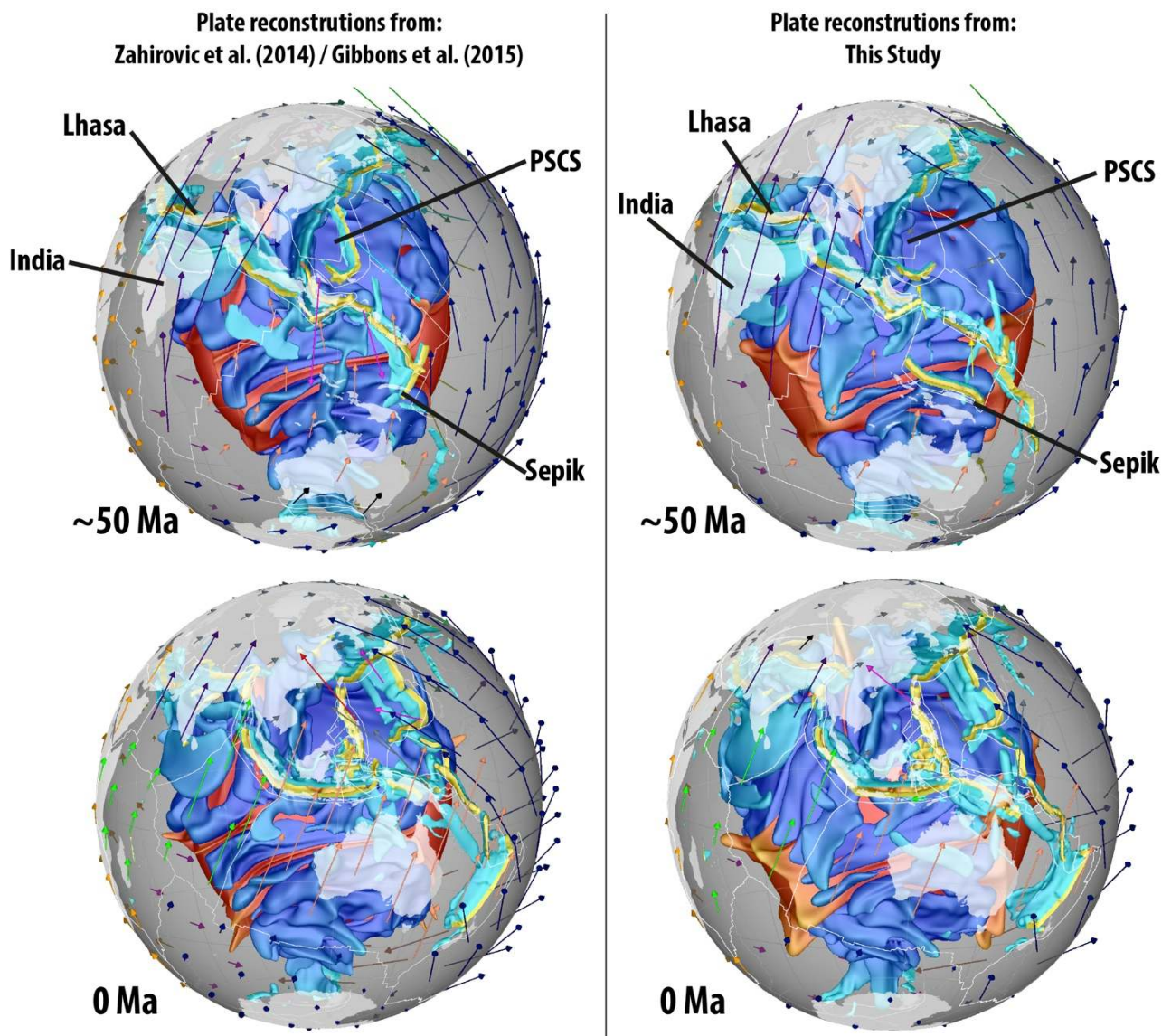


Fig. 25b. Coupled plate reconstructions and mantle flow models in the Eocene and present-day, highlighting the draping of subducted slabs along the core-mantle boundary and the self-organisation of the African and Pacific large-scale upwellings as a result of post-Pangea subduction. These models are interrogated regionally using vertical profiles in Figs. 26-29. Centre co-ordinate is 10°S, 115°E. See Supplementary Animation 7 consistent with right panels.

The large-scale evolution of slab sinking and lateral advection, as well as the evolution of the large-scale upwellings, can be depicted in 3D hemispherical views of the mantle, while regional cross-sections of the numerical experiments provide a more detailed approach to interrogating the

1611 spatio-temporal geodynamic evolution of key subduction zones from post-Jurassic plate
1612 reconstructions.

1613

1614 **5.2 Regional interpretations of mantle evolution**

1615

1616 To capture the detailed evolution of subduction, vertical cross-sections of the mantle are
1617 presented in a plate frame of reference (i.e., fixed to the overriding plate, Figs. 26-29). Such time-
1618 dependent sections help understand the sinking trajectory of subducted slabs, as well as interpreting
1619 sinking rates and lateral mantle flow resulting from the post-Jurassic plate reconstructions. For the
1620 geological reasoning underpinning the reconstructions, please refer to Section 3 and Table 3.

1621 **5.2.1 *India-Eurasia convergence***

1622

1623 The India-Eurasia segment is best represented by a largely north-south profile at present-day
1624 that is reconstructed with Lhasa (Fig. 26). At ~160 Ma, the Paleo-Tethyan slab has detached and is
1625 sinking through mid-mantle depths at ~1.5 cm/yr (Fig. 26a,h), while the Meso-Tethys is being
1626 actively consumed northward beneath Lhasa in both plate reconstruction scenarios. Both tectonic
1627 scenarios include southward slab rollback and the establishment of a Kohistan-Ladakh (Tethyan)
1628 back-arc basin, reaching to ~10°N in the base model (Zahirovic et al., 2014) and the equator at
1629 ~100 Ma in this study (Fig. 26c,j). Using the base reconstructions, the Meso-Tethyan slab only
1630 penetrates the mantle transition zone at ~100 Ma and begins sinking into the lower mantle by
1631 ~90 Ma (Fig. 26, Supplementary Animation 7). In the refined reconstructions the slab enters the
1632 mantle transition zone by ~120 Ma, and enters the lower mantle by ~110 Ma. This reflects greater
1633 convergence rates due to the combined effect of greater slab rollback in the refined reconstructions,
1634 as well as continued seafloor spreading north of India during this timeframe. In the base
1635 reconstructions, the seafloor spreading north of India is abandoned by ~120 Ma, leading to lower
1636 convergence rates across the Kohistan-Ladakh Tethyan trench (Fig. 10). This results in the

subduction of larger volumes of older, and therefore thicker, oceanic lithosphere, while in the refined reconstructions subducted volumes along the Kohistan-Ladakh Arc system in the Early to mid-Cretaceous are smaller because the oceanic lithosphere associated with the Neo-Tethyan seafloor spreading north of India by ~100 Ma is younger and thinner (Fig. 26j). Once the Tethyan slab has entered the lower mantle, the sinking rate in the refined reconstruction is only ~1.4 cm/yr (between 100 and 89 Ma), while it is ~2.5 cm/yr in the base reconstructions (between 89 and 79 Ma) likely due to the larger subducted volumes.

The intersection of the Neo-Tethyan mid-oceanic ridge with the Kohistan-Ladakh subduction zone in the mid-Cretaceous would likely lead to slab breakoff and the formation of a slab window. However, our model does not capture the complexity of a subduction hiatus that would be associated with a slab window along Kohistan-Ladakh in the mid-Cretaceous. Perhaps due to the arrival of buoyant oceanic crust at the intra-oceanic subduction system, north-dipping subduction becomes established along Lhasa and begins to consume the Kohistan-Ladakh back-arc basin, eventually resulting in two Late Cretaceous north-dipping subduction zones in the Neo-Tethys (see Section 3.2). The mid-ocean ridge from the Kohistan-Ladakh back-arc is subducted in the Late Cretaceous in both reconstruction scenarios, with no interruption in subduction assumed in the base reconstructions. In the alternative reconstructions we impose a subduction hiatus along Lhasa from 80 to 65 Ma, which leads to slab breakoff. This slab window may be linked to adakitic volcanism at ~80 Ma (Wen et al., 2008a), followed by a ~75-60 Ma magmatic gap, in the Gangdese Batholith (Chung et al., 2005; Ji et al., 2009; Wen et al., 2008b).

In both reconstruction scenarios, Greater India collides with Kohistan-Ladakh by ~50 Ma, inducing Neo-Tethyan slab break-off at ~5-10°N. Since the Kohistan-Ladakh Arc is at equatorial latitudes in the refined reconstructions in the mid-Cretaceous, one may expect the collision with India to occur by ~60 Ma. As the magmatic chemistry change is much later, at 52 Ma (Bouilhol et al., 2013), the model includes some advance of the intra-oceanic subduction system between ~60 and 52 Ma. In the base reconstructions, the Kohistan-Ladakh Arc is closer to Eurasia at pre-

collision times, meaning that relatively little trench advance is required. However, in both instances, the Tethyan slab is anchored in the lower mantle, leading to India overriding the sinking slabs. Andean-style subduction of the Kohistan-Ladakh back-arc along southern Lhasa is temporarily shut off by the ~47-40 Ma continent-continent collision, after which subduction of Greater India (continental) mantle lithosphere continues to present-day in the refined reconstructions. The Meso- and Neo-Tethyan slabs are predicted at present to be approximately at mid-mantle depths (~1000 to 2000 km), with a latitudinal range of ~0 to 35°N, using the base model plate reconstructions (Fig. 30, IND-EUR). More generally, the base plate reconstruction in modelled Case 4 reproduces a number of discrete slabs at mid-mantle depths, with a large latitudinal range, which is consistent with the interpretations of the mantle structure by van der Voo et al. (1999b) (Fig. 5).

Although the numerical model that uses the refined reconstructions presented in this study has the same radial viscosity profile, the Meso- and Neo-Tethyan slabs are predicted to be shallower at ~800 to 1500 km depths, as opposed to ~1000 to 2000 km depths predicted using the base reconstructions (Fig. 26g,n). This is likely due to the subduction of smaller volumes of younger Tethyan oceanic lithosphere north of India in the Cretaceous, resulting in less negative buoyancy. In addition, the required trench advance also results in folding of the Tethyan slab at the mantle transition zone, leading to generally shallower penetration into the lower mantle. In the post-collision timeframe, the Tethyan slab sinks at a rate of ~0.65 cm/yr (from 38 to 0 Ma) using the base reconstructions, and ~0.25 cm/yr (from 39 to 0 Ma) using the refined reconstructions where the slab is almost stagnant at ~1000 km depth (Supplementary Animation 7). The time-varying sinking rates in the lower mantle highlight the role active subduction has in adding negatively buoyant slab volumes into the mantle, and the role of thermal diffusion of slabs in reducing negative buoyancy of subducted lithosphere. A slightly deeper depth range (~1000 to 2000 km) provides a better match to the equivalent P- and S-wave tomography slice (Fig. 30, IND-EUR), as is obtained with the base plate reconstructions (Gibbons et al., 2015; Zahirovic et al., 2014), with the potential that slabs may extend further south of the equator based on the S-wave model.

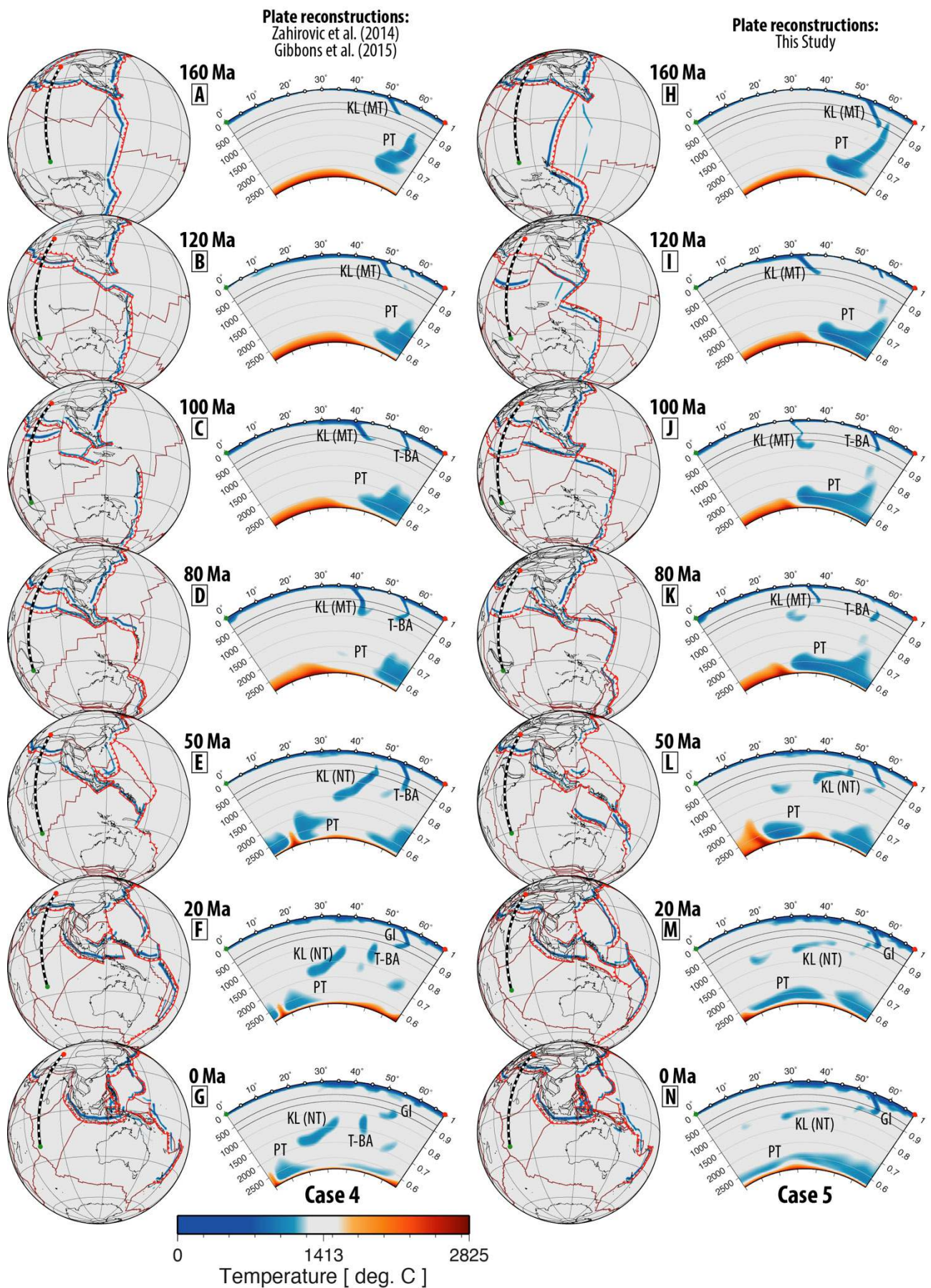


Fig. 26. Time-dependent evolution of the India-Eurasia convergence zone, with a representative vertical slice reconstructed with Lhasa to capture the evolution of the Kohistan-Ladakh (KL) and

1692 Tethyan (T-BA) intra-oceanic subduction zones modelled in Zahirovic et al. (2014) and Gibbons et
1693 al. (2015) (left), and compared to the subduction histories implied in the revised plate
1694 reconstructions presented in this study (right). The cross-sections depict the temperature field from
1695 the numerical mantle flow models, and the globes show the position of the vertical slices through
1696 time, the plate reconstruction and the predicted mantle temperature field at ~400 km depth. The
1697 background mantle temperature is ~1413°C, and the small tick marks on the temperature scale
1698 represent temperature intervals of 250°C. Great circle angular distance along the vertical profile is
1699 shown on the x-axis. The left y-axis represents depth in kilometres, and on the right represents non-
1700 dimensional Earth radius. The plate reconstructions are plotted in an Orthographic projection with
1701 centre co-ordinate of 15°S, 115°E. GI – Greater India (continental) mantle lithosphere, MT – Meso-
1702 Tethys slab, NT – Neo-Tethys slab, PT – Paleo-Tethys slab. See Supplementary Animation 8.

1703

1704 **5.2.2 *Woyla and Sumatra active margin evolution***

1705

1706 The Sumatra segment of the Sunda margin accommodates northward subduction of the
1707 Meso-Tethys in the Late Jurassic, with rollback of the slab opening the Woyla back-arc to near-
1708 equatorial latitudes (Fig. 27), similar to the development of the Kohistan-Ladakh Arc further to the
1709 west. In the base reconstructions, the rollback imposed is faster and the maximum southward extent
1710 of subduction is ~0-10°S (Fig. 11). This leads to a smaller volume of subducted slabs folded in the
1711 mantle transition zone. Although the base reconstruction maintains convergence across the Woyla
1712 subduction zone, there is significant trench advance between ~100 and 75 Ma, leading to a similar
1713 smearing effect of slabs in the transition zone. Although trench advance occurs at present-day along
1714 the Izu-Bonin-Mariana Trench (Becker et al., 2015; Carlson and Mortera-Gutiérrez, 1990;
1715 Mathews, 2014), the modelled values in our base reconstructions are likely excessive, with a more
1716 geodynamically reasonable evolution of trench migration in the refined reconstructions.

1717

1718 Subduction continues along Sumatra to consume the Woyla back-arc basin, and is
1719 interrupted for ~10 Myr between accretion of the Woyla Arc onto the Sumatran margin between
1720 ~75 and 65 Ma in the base reconstructions. Due to the convergence required between the Tethyan-
1721 Indian Ocean and Eurasia, we impose a shorter ~5 Myr hiatus in subduction between 75 and 70 Ma
1722 to induce slab breakoff that may have occurred due to Woyla Terrane accretion. Our assumption of
1723 slab breakoff is simplistic and based on the magmatic gap, and more realistic slab breakoff timings
1724 of 5-10 Myr after collision (Li et al., 2013; van Hunen and Allen, 2011) will need to be considered
1725 in future refinements of the model in this region.

1726 In both tectonic reconstructions, subduction at the Sunda Trench is initiated at ~70-65 Ma,
1727 and persists to present-day. The slab is predicted to have penetrated the lower mantle by ~50 Ma,
1728 after which the collision of India with Eurasia, and subsequent rotation of Indochina and much of
1729 Sundaland from ~30 Ma leads to a kink in the slab in the mantle transition zone (410 to 660 km,
1730 Fig. 27g,n). Although the kink results from the constant slab dip imposed in the slab assimilation,
1731 this slab kink is imaged by the P- and S-wave seismic tomography analysed here, and also recently
1732 discussed in Hall and Spakman (2015). The numerical experiments of mantle flow also reproduce
1733 the latitudinal range of the subducted slab (Fig. 30, SUM), as well as a gap in the slab at depths
1734 greater than ~1500 km, consistent with earlier interpretations of the Sunda slab (Widiyantoro and
1735 van der Hilst, 1996). The mantle convection models predict the Woyla/Meso-Tethys slab at ~1500
1736 to 2000 km depths at ~10°S along the Sumatran vertical slice (Fig. 30, SUM), and ~20°S along the
1737 Java-Borneo Sundaland slice (Fig. 30, SUN), which is likely to be equivalent to fast seismic
1738 velocities in P- and S-wave tomography at ~1500-2000 and ~1200-1600 km depth along the
1739 Sumatran and Java-Borneo vertical slices, respectively.

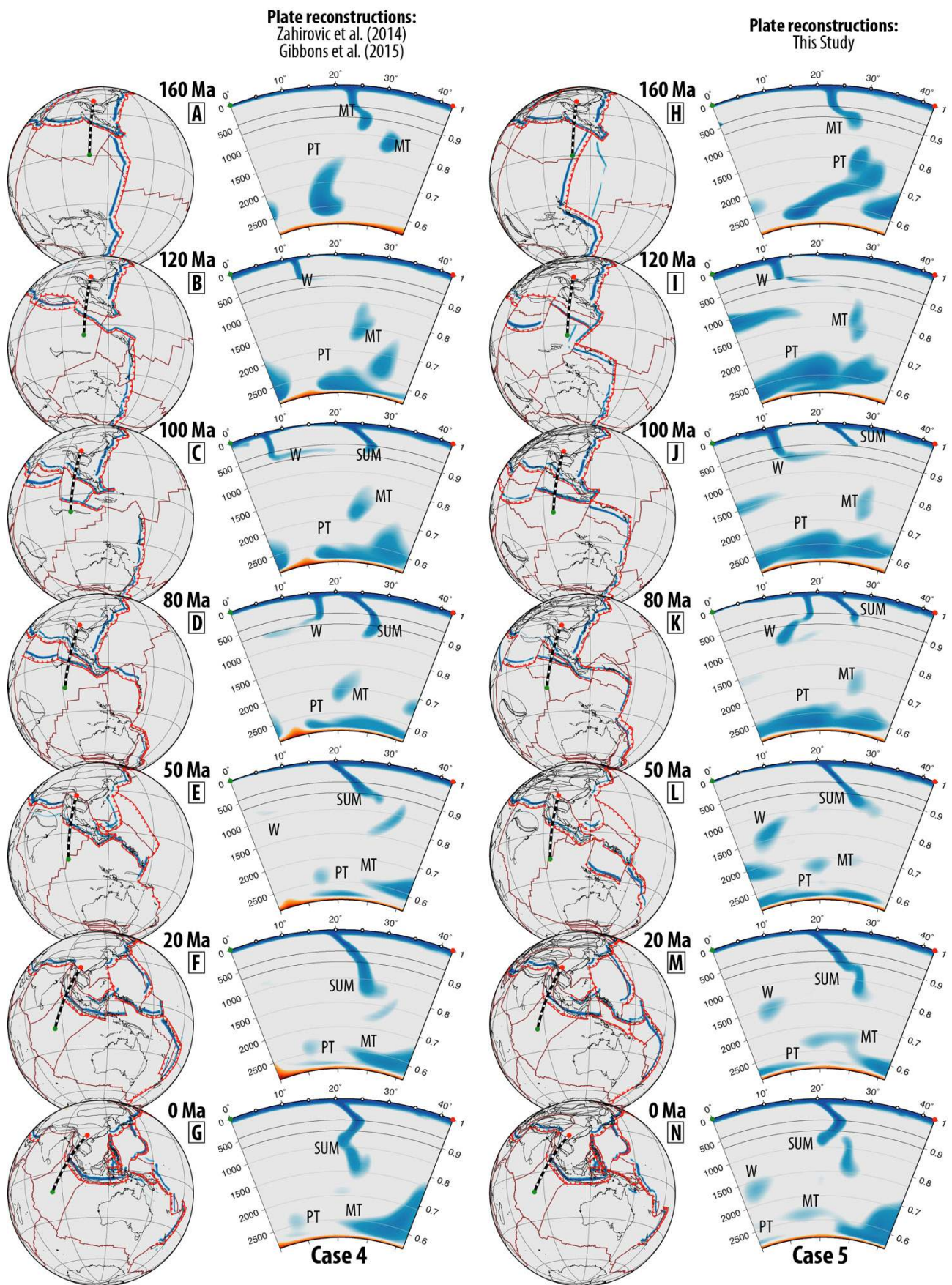


Fig. 27. Reconstructed vertical profiles across northwest Sumatra highlighting the evolution of the Woyla intra-oceanic and Sunda subduction zones through time, with both numerical experiments

1743 predicting a significant kink in the Sumatran portion of the Sunda slab (SUM) when the slab dip is
1744 held constant during the clockwise rotation and extrusion of Indochina. MT – Meso-Tethys slab,
1745 NT – Neo-Tethys slab, PT – Paleo-Tethys slab, W – Woyla slab. See Supplementary Animation 9.

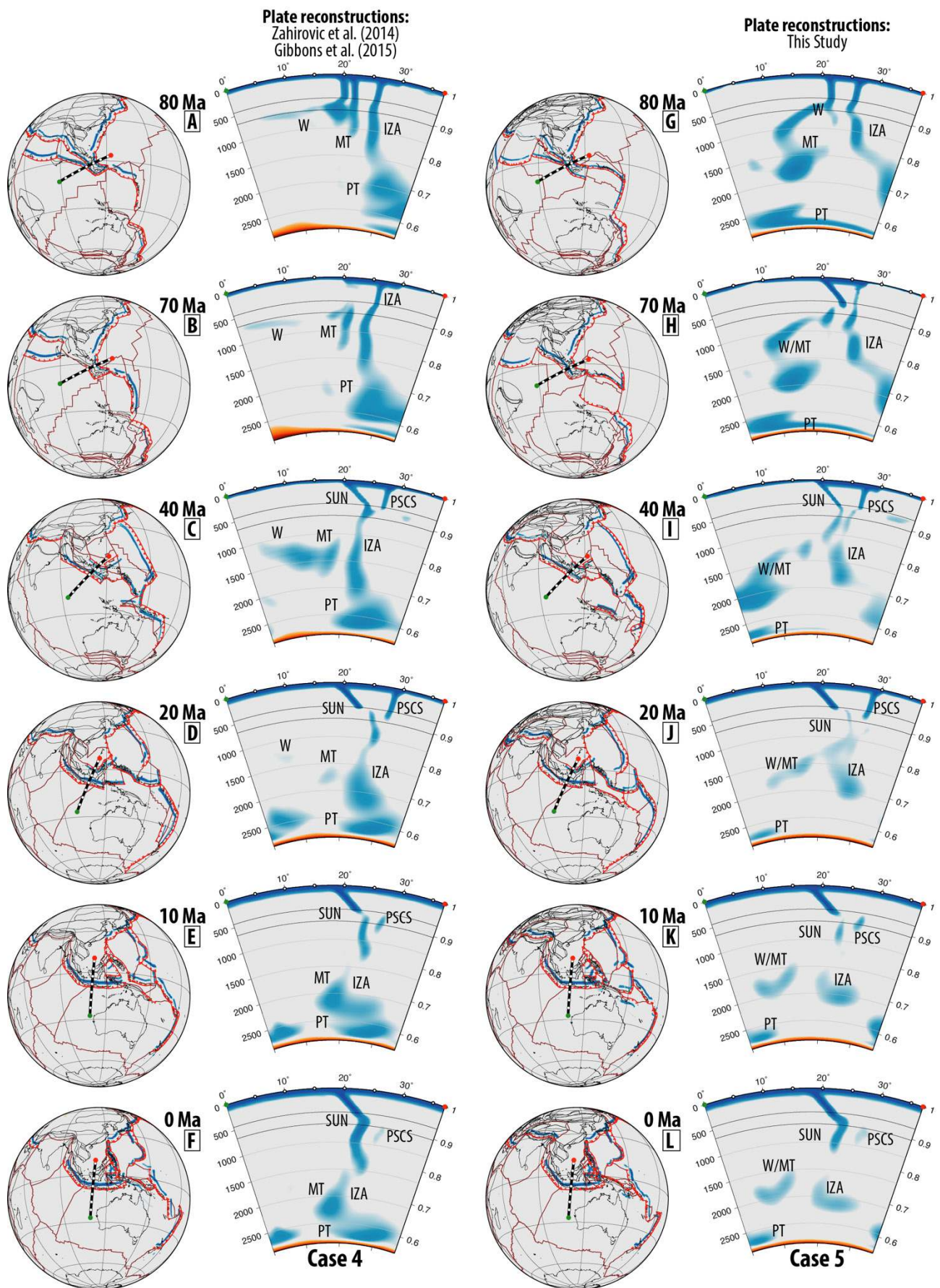
1746

1747 **5.2.3 *Java and Borneo subduction history***

1748

1749 Similar to the Sumatra margin, the Java segment of the Sunda Trench accommodates
1750 subduction of the Meso-Tethys and the Woyla back-arc basin during the Cretaceous (Fig. 28).
1751 However, as this segment represents the Sundaland continental promontory, south-dipping
1752 subduction of the Izanagi Plate is contemporaneous to the Tethyan subduction history. As a result,
1753 the mid- and lower mantle slabs are likely to be a mixture of Pacific- and Tethyan-derived slabs.
1754 The accretion of the Woyla Arc temporarily shuts off subduction in this segment in the Late
1755 Cretaceous at ~70 Ma in the base reconstructions (Fig. 28b,h), followed by the accretion of the
1756 Semitau continental fragment and Proto South China Sea Arc onto northern Borneo at ~45 Ma in
1757 both reconstruction scenarios (Fig. 28c,i). The late Eocene is dominated by renewed north-dipping
1758 Sunda subduction and south-dipping subduction of the Proto South China Sea. Although the Sunda
1759 subduction continues to the present-day, the Proto South China Sea subduction is interrupted at
1760 ~15 Ma with the docking of the Dangerous Grounds-Reed Bank continental fragment along
1761 northern Borneo, which leads to the abandonment of the South China Sea seafloor spreading. The
1762 refined reconstructions imply a longer-lived Meso-Tethyan Plate that is completely consumed by
1763 ~45 Ma, leading to much younger oceanic crust and thinner oceanic lithosphere subducted at the
1764 Sunda Trench than in the base reconstructions. This leads to the subduction of smaller slab volumes
1765 between ~60 and 30 Ma for the refined reconstructions that predict a smaller and shallower slab that
1766 penetrates to ~1200 km depth at present. In contrast, the base reconstructions lead to a larger Sunda
1767 slab at depths of ~1500 km (Fig. 30, SUN), which is consistent with the interpretations of P- and S-
1768 wave seismic tomography. The kink in the slab observed in the Sumatra segment (Fig. 30, SUM) is

1769 much less pronounced in the Java region (Fig. 30, SUN), especially when compared to the results
1770 using our base plate reconstruction. A gap in the slab is also reproduced for depths greater than
1771 ~1500 km, with older Tethyan and Izanagi slab fragments reproduced near the core-mantle
1772 boundary when comparing to the S-wave seismic tomography (Fig. 30, SUN). The Proto South
1773 China Sea slab is predicted at ~600-1000 km depths, while P- and S-wave tomographic images
1774 indicate a slab stagnating at the base of the 410-660 km mantle transition zone.
1775



1776

1777 **Fig. 28.** Reconstructed vertical slice through eastern Sundaland, capturing the subduction of the

1778 Meso- and Neo-Tethyan, as well Indian Ocean, basins. The Sunda slab is predicted to reach a

1779 maximum depth of ~1500 km along southern Sundaland in the base reconstructions, and ~1200 km
1780 in the refined reconstructions, while a small Proto South China Sea slab is predicted just beneath the
1781 660 km upper-lower mantle transition. See Supplementary Animation 10.

1782

1783 **5.2.4 *New Guinea margin evolution***

1784

1785 Further east along the New Guinea Tethyan segment, the Early Cretaceous Sepik oceanic
1786 basin is consumed at a north-dipping subduction zone from ~40 Ma (Fig. 29b) in the base model
1787 reconstructions, while in our refined model subduction starts earlier at ~71 Ma (Fig. 29g) to account
1788 for the ~71 to 66 Ma Emo volcanics (Worthing and Crawford, 1996) that likely formed in the back-
1789 arc of this subduction system. North-dipping subduction along the Sepik Terrane is interrupted at
1790 ~30 Ma in both plate reconstruction scenarios, based on the timing of docking of the composite
1791 terrane at the New Guinea margin. We impose slab breakoff during the collision, leading to a slab
1792 that is entrained in the upper part of the lower mantle (660-1000 km depths) for both reconstruction
1793 scenarios. In the base model, north-dipping subduction is then accommodated along the Halmahera
1794 Arc, which forms the southern boundary of the Caroline Plate, and is accreted to the New Guinea
1795 margin diachronously from west to east by ~5 Ma. In the refined reconstructions, a south-dipping
1796 subduction zone is implemented (Fig. 29j) to account for the ~18 to 8 Ma Maramuni Arc volcanics
1797 (Hill and Hall, 2003; Page, 1976), as well as simultaneous north-dipping subduction along the
1798 Halmahera Arc. Both subduction zones are abandoned progressively from ~15 Ma, resulting from
1799 the collision of the Halmahera Arc with the New Guinea margin.

1800 The numerical experiments of mantle flow assimilating the base plate motion model predict
1801 two slabs at depths between ~500 and 1000 km (Fig. 30, PNG), with the southernmost slab at
1802 ~20°S belonging to the Sepik oceanic basin, and the northern slab at 0 to 5°S resulting from the
1803 subduction of the Solomon Sea along the Halmahera Arc. With the addition of the Maramuni
1804 subduction zone in the refined plate reconstructions (~20 to 10 Ma, Fig. 29), an additional slab is

1805 predicted at slightly deeper depths of ~900 to 1500 km at ~15°S. The Sepik oceanic basin slab is
1806 predicted to be further south in the refined plate reconstruction scenario, at depths of ~700 to
1807 1000 km and latitude of ~30°S (Fig. 30, PNG). This difference in latitude is largely due to the
1808 earlier onset of Sepik oceanic gateway subduction at ~71 Ma in the refined reconstructions, leading
1809 to the slab entering the lower mantle at more southerly latitudes, as opposed to the younger age of
1810 ~40 Ma subduction onset using the base reconstructions (Fig. 29b). The refined plate
1811 reconstructions result in a much better fit with the mantle structure than the base model, with the
1812 ~30°S position of the Sepik oceanic gateway slab corresponding to the fast seismic anomaly
1813 interpreted beneath Lake Eyre in eastern Australia, recently interpreted in Schellart and Spakman
1814 (2015). However, a slab at ~1300 to 1800 km depths at present-day (PNG, Fig. 30), and latitudes
1815 between ~10°S and the equator, is not accounted for in either model of mantle flow – suggesting the
1816 Cretaceous plate reconstruction needs additional refinement.

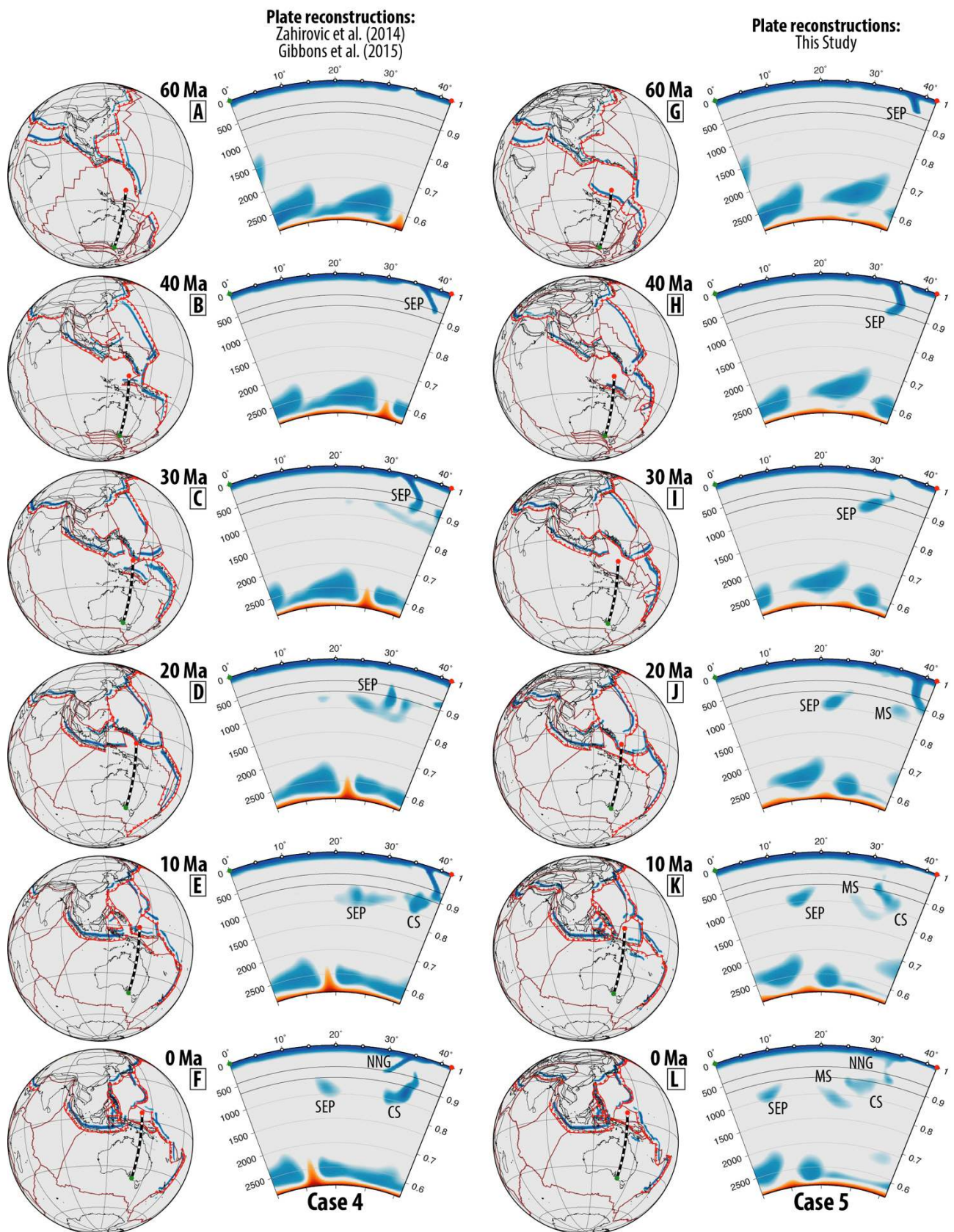
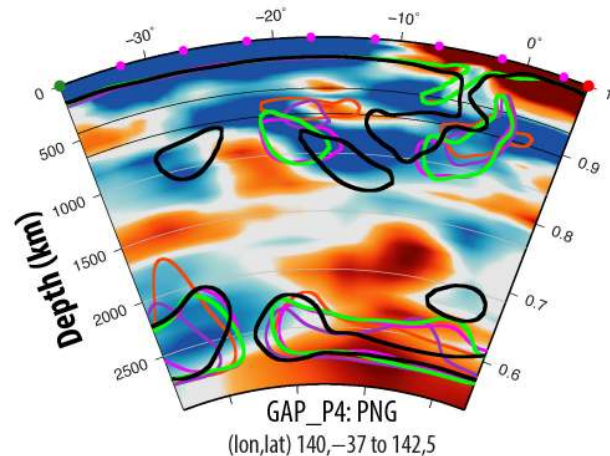
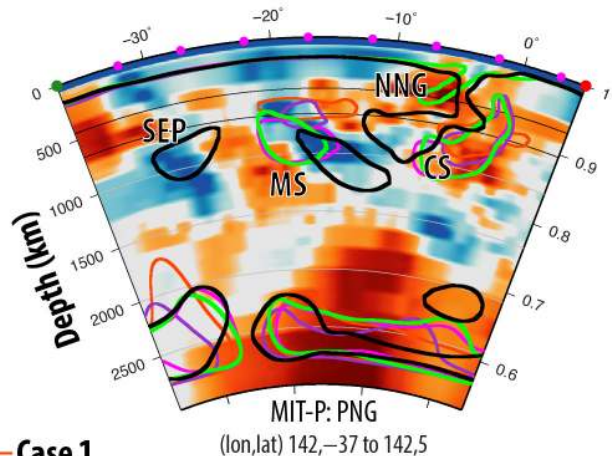
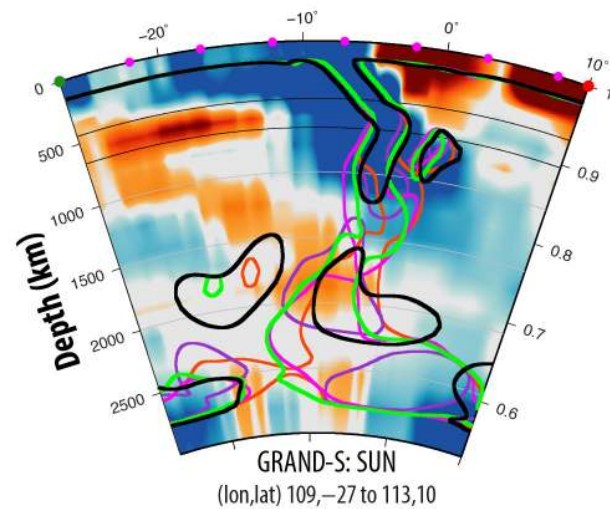
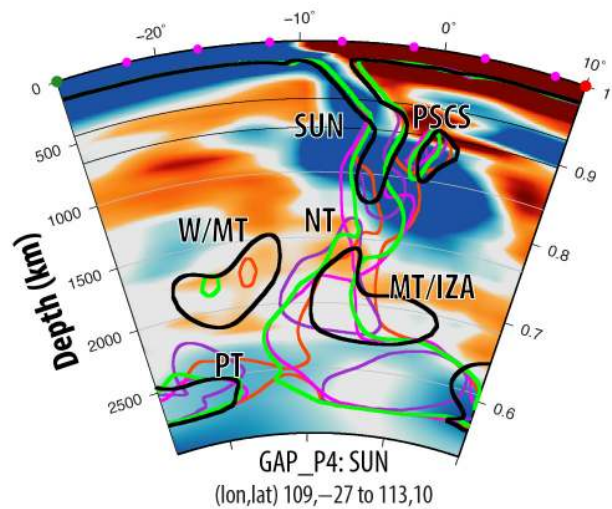
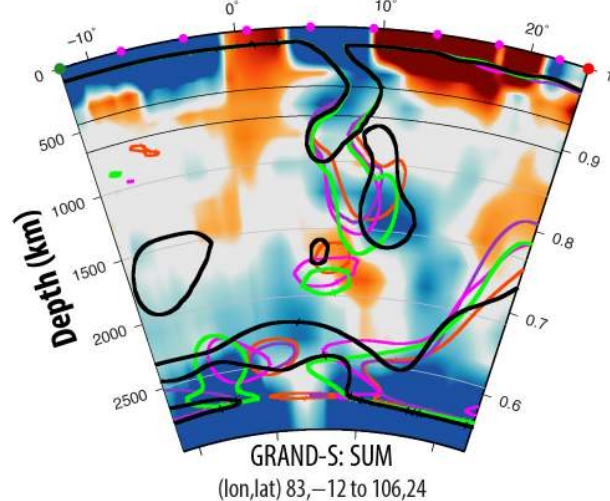
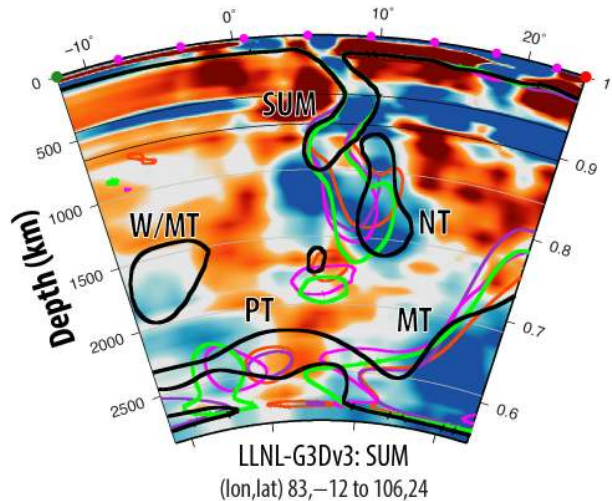
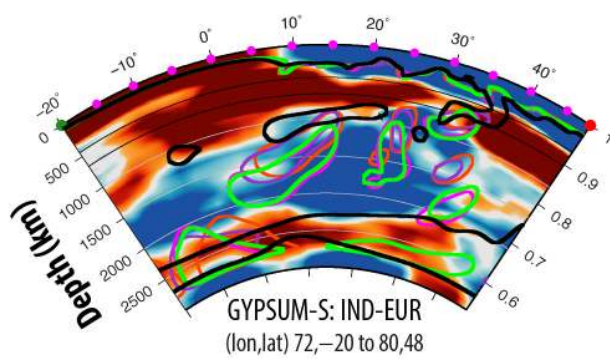
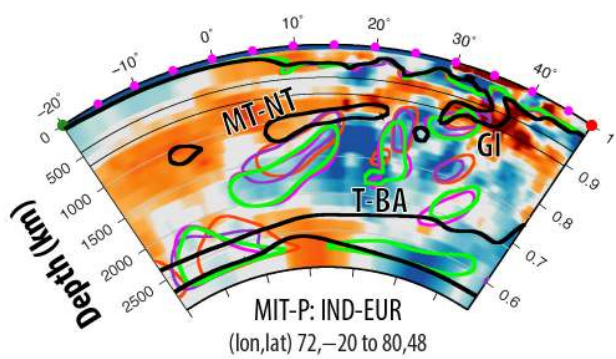


Fig. 29. Reconstructed representative profile through Australia and New Guinea, highlighting that the revised plate reconstructions account for additional slab volumes above mid-mantle depths. The southernmost slab is related to the subduction of the Sepik oceanic gateway (SEP) between ~71 and

1821 30 Ma, while Maramuni subduction (MS) has taken place since ~20 Ma, coeval with north-dipping
1822 subduction along the Halmahera Arc to produce the Caroline/Proto Molucca slab (CS). See
1823 Supplementary Animation 11.

1824

1825



- Case 1
- Case 2
- Case 3
- Case 4
- Case 5

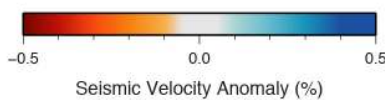


Fig. 30. Present-day mantle structure along vertical slices through India (IND-EUR), northwest Sumatra (SUM), eastern Sundaland (SUN) and Australia-New Guinea (PNG) using P- and S-wave seismic tomography models, superimposed with the predicted slabs (coloured lines) from five computations of mantle flow. Case 1 to 4 uses the Zahirovic et al. (2014) plate reconstruction, but varies the radial viscosity profile of the mantle. Case 5 uses the plate reconstruction presented in this study, and the preferred viscosity structure used in Case 4. Slabs from the numerical models are defined as regions 10% colder than the background mantle temperature. The P-wave seismic tomographic models used are the MIT-P (Li et al., 2008), GAP_P4 (Obayashi et al., 2013) and LLNL-G3Dv3 (Simmons et al., 2015). Both P- and S-wave models from Simmons et al. (2010) are used, as well as the S-wave model from Grand (2002). The x-axis of the vertical section represents latitude. Table 4 lists the differences between Cases 1 to 5. The start and end coordinates for each profile are included on each cross-section, and plotted geographically in Figs. 26-29 and Supplementary Fig. 2.

6 Discussion

We have demonstrated the strength of using coupled plate tectonic reconstructions and numerical models of mantle flow to test competing kinematic scenarios in the absence of preserved seafloor spreading histories. In addition, the global nature of the models removes the edge effects associated with Cartesian box models of mantle convection, and allows us to track the origin and trajectory of sinking slabs, and therefore their sinking rates, which can then be compared to the mantle structure interpreted from P- and S-wave seismic tomography (Fig. 30).

6.1 Intra-oceanic subduction in the Meso- and Neo-Tethys

1851 In the India-Eurasia segment of the Tethyan margin, a number of important geodynamic
1852 implications arise from the Neo-Tethyan seafloor spreading history and the evolution of intra-
1853 oceanic subduction zones along southern Eurasia. Although early plate reconstructions of the
1854 Tethys incorporated intra-oceanic subduction and an initial collision between Greater India and the
1855 Kohistan-Ladakh Arc at or before ~53 Ma (Patriat and Achache, 1984), this two-stage India-Eurasia
1856 collision scenario was abandoned based on subsequent work that argued that Kohistan and Ladakh
1857 first collided with Eurasia in the Late Cretaceous along the Shyok Suture Zone (Clift et al., 2002;
1858 Debon et al., 1987; Treloar et al., 1996). However, recent work requires near-equatorial position of
1859 the Kohistan-Ladakh Arc in the Late Cretaceous (Burg, 2011; Chatterjee et al., 2013; Zaman et al.,
1860 2013; Zaman and Torii, 1999), and an initial arc-continent collision between Greater India and the
1861 Neo-Tethyan intra-oceanic arc sometime between ~60 and 50 Ma (Aitchison et al., 2007; Bouilhol
1862 et al., 2013; Khan et al., 2009). Our results favour a ~60 Ma arc-continent collision if the near-
1863 equatorial paleo-latitudes of Kohistan-Ladakh are robust, as a younger collision requires more
1864 significant advance of the Kohistan-Ladakh intra-oceanic trench before Greater India enters the
1865 subduction zone, terminating the subduction of oceanic lithosphere. The Kohistan-Ladakh back-arc
1866 basin was then subducted along southern Lhasa at an Andean-style margin, with final Shyok
1867 suturing occurring by 40 Ma (Bouilhol et al., 2013; Gibbons et al., 2015; Zahirovic et al., 2014).

1868 The geodynamic implications of a well-established intra-oceanic system in the Neo-Tethys,
1869 suggest a scenario that is much like the present-day Izu-Bonin-Mariana Arc in the west Pacific. The
1870 paleo-latitudinal position of the intra-oceanic arc largely determines the timing of Neo-Tethyan
1871 ridge subduction, as well as the plate driving forces acting on the Indian Plate. In our
1872 reconstruction, the Neo-Tethyan mid-oceanic ridge is consumed at the Kohistan-Ladakh subduction
1873 zone from ~105 Ma (Figs. 11 and 26c,j). Subduction of the southern Neo-Tethyan flank of the
1874 spreading system from ~100 Ma would have been associated with progressively strengthening
1875 northward slab pull, to which we attribute the change towards largely northward convergence with

1876 Eurasia that is best represented by the ~110-90 Ma fracture zone bends in the Wharton Basin
1877 (Gibbons et al., 2015; Matthews et al., 2011; Matthews et al., 2012).

1878 The role of two coeval north-dipping subduction zones in the Neo-Tethys (Fig. 26) were
1879 suggested to have contributed to the ~80 Ma acceleration of India in Gibbons et al. (2015), which
1880 has recently been proposed as a mechanism for India's rapid northward advance using numerical
1881 techniques quantifying plate driving forces in Jagoutz et al. (2015). Although the arrival of the
1882 Reunion Plume head south of India at ~65 Ma possibly played a role in India's acceleration (Cande
1883 and Stegman, 2011; van Hinsbergen et al., 2011), the effects were likely short-lived (~5-10 Myr),
1884 and post-date by 15 Myr the initial acceleration of India from ~80 Ma. India's northward
1885 acceleration resulting from greater slab pull (and slab suction) may have induced stronger large-
1886 scale mantle return flow, possibly triggering the ascent of the Reunion Plume from the margin of
1887 the lower mantle African super-swell (Fig. 25). The recent data compilations of the surface geology,
1888 as well as new plate reconstructions and numerical approaches, suggest that a two-stage collision
1889 between India and Eurasia is more likely than a single continent-continent collision, and that the
1890 Tethyan tectonic evolution was punctuated by generations of back-arc basins and intra-oceanic
1891 subduction systems more similar to the present-day West Pacific, than a simpler long-lived Andean-
1892 style margin.

1893

1894 **6.2 Southeast Asia and New Guinea**

1895

1896 Southeast Asia, and in particular Sundaland and New Guinea, played an important role in the
1897 convergence history of Australia, Eurasia and the Pacific. In this study we have shown that our
1898 plate reconstructions are compatible, at least to the first-order, with fast seismic anomalies imaged
1899 by seismic tomography. In particular, the numerical methods suggest that the extrusion and
1900 clockwise rotation of Indochina from ~30 Ma is likely responsible for the Sunda slab kink beneath
1901 west Sumatra. The models reproduce the depth of the Sunda slab beneath Sumatra and Borneo,

1902 which supports subduction initiation from ~65 Ma, rather than from ~45 Ma (Hall, 2012). If the
1903 1600 km deep Sunda slab represents subduction since 45 Ma (Hall and Spakman, 2015), then an
1904 average whole-mantle sinking rate of 3.5 cm/yr is required, while our post-65 Ma subduction
1905 history would require average sinking rates of 2.5 cm/yr, which is more consistent with previous
1906 studies of sinking rates in numerical models (Butterworth et al., 2014; Steinberger et al., 2012). The
1907 constraints from the subduction-related volcanic history of Sumatra (McCourt et al., 1996) result in
1908 a predicted slab that is consistent with P- and S-wave tomography. This highlights that
1909 segmentation of the Neo-Tethyan and Indian Ocean plates across pre-existing structural fabric
1910 (Hall, 2012) is not required to account for the subduction history recorded on the Sumatra-Java
1911 Sundaland margin. Although Hall and Spakman (2015) invoke a leaky transform in the Neo-Tethys
1912 at ~90°E (Fig. 4c) to explain a possible ~90-45 Ma subduction hiatus, the mantle discontinuity
1913 linked to this interpretation is much further east at 110°E. There is a clearer discontinuity in slab
1914 structure east of ~120°E (Fig. 24), which represents the complex subduction history of New Guinea
1915 that is possibly linked to the evolution of the Philippine Sea Plate and the Pacific, rather than
1916 Sundaland.

1917 The relatively small slabs predicted at ~600 to 1000 km depth beneath northern Borneo in
1918 our models roughly correspond to the interpreted Proto South China Sea slab (Zahirovic et al.,
1919 2014) imaged in seismic tomography at shallower depths in the mantle transition zone (~410 to
1920 660 km). This suggests that Proto South China Sea subduction along northern Borneo may have
1921 started later than 45 Ma, which would be consistent with a shallower slab, and perhaps linked to a
1922 ~32 Ma onset in seafloor spreading of the South China Sea (Briais et al., 1993). However, a major
1923 phase of volcanism along northern Borneo from ~50 Ma (Soeria-Atmadja et al., 1999) might
1924 instead indicate earlier subduction initiation. In this case, stagnation of the Proto South China Sea
1925 slab in the mantle transition zone could play an important role in the depth mismatch between our
1926 numerical experiments and the seismic tomographic constraints. Recent backward-advection
1927 modelling by Yang et al. (2016) suggests that the large volume of subducted slab beneath

1928 Sundaland stagnated in the mantle transition zone before ~30 Ma, and entered the lower mantle as a
1929 slab avalanche in the Miocene from ~20 Ma. This work highlights the time-varying slab sinking
1930 rates in the region, but more importantly, demonstrates that a slab avalanche resulted in dynamic
1931 subsidence of Sundaland and flooding (Yang et al., 2016) that was asynchronous with global
1932 eustasy (Haq et al., 1987). In addition, the slab avalanche was likely responsible for Miocene basin
1933 inversions (Doust and Sumner, 2007) by propagating stresses acting on the lithosphere. Since Proto
1934 South China Sea subduction ceased at ~15 Ma, recorded by cessation of seafloor spreading in the
1935 South China Sea (Briais et al., 1993), it is therefore likely that the Proto South China Sea slab is in
1936 the upper mantle or transition zone when considering the role of slab stagnation in this region. This
1937 interpretation is in contrast with that of Hall and Spakman (2015) who argued for a lower mantle
1938 (~1200 km deep) position of the Proto South China Sea slab.

1939 Further east on New Guinea, the complexity of the surface geology has led to competing
1940 plate tectonic reconstruction scenarios (van Ufford and Cloos, 2005), some of which are discussed
1941 in this study. Our plate reconstructions and numerical experiments of mantle flow require Sepik
1942 oceanic gateway subduction in the Late Cretaceous, likely from ~70 Ma, which accounts for the
1943 present-day slab at mid-mantle depths at ~30°S beneath Lake Eyre in northern South Australia,
1944 consistent with recent interpretations (Schellart and Spakman, 2015). However, the slab our mantle
1945 flow model predicts is smaller, which raises the possibility that the Sepik oceanic basin was larger
1946 than modelled in our plate reconstructions. The refinement to the plate reconstructions and
1947 inclusion of south-dipping Maramuni Arc subduction along New Guinea from ~20 to 6 Ma, with
1948 coeval north-dipping subduction along the Halmahera Arc, improves the fit between predicted slab
1949 distributions and the mantle structure inferred from seismic tomography. We interpret the presently-
1950 inactive Trobriand Trough as the Maramuni Arc subduction zone (active ~18 to 8 Ma). The
1951 Maramuni subduction may have caused the dynamic subsidence and progressive flooding inferred
1952 for the northern Australian shelf since the Oligocene (DiCaprio et al., 2009; DiCaprio et al., 2011;
1953 Sandiford, 2007; Spasojevic and Gurnis, 2012). Although our results reproduce the Sepik and

1954 Maramuni slabs, more work is required to account for a consistently-imaged near-equatorial slab at
1955 ~1500 km depths that is not reproduced by either of the plate reconstruction scenarios presented in
1956 this study. Further work using numerical techniques is required to improve the understanding of the
1957 complex tectonic linkage between Southeast Asia and the Pacific through New Guinea.

1958

1959 **6.3 Relevance to global plate reconstructions and geodynamics**

1960

1961 Our coupled plate kinematic and numerical geodynamic approach has wider implications for
1962 understanding the long-term evolution of the plate-mantle system. One important outcome is that
1963 numerical models testing alternative plate reconstruction scenarios that are compared to mantle
1964 structure from seismic tomography should consider the regional and global plate tectonic evolution.
1965 The evolution of Neo-Tethyan intra-oceanic subduction along the Kohistan-Ladakh and Woyla arc
1966 systems also has wider geodynamic implications. Although we implemented subduction initiation at
1967 the passive margin of the back-arc systems, a more complicated geodynamic mechanism may be
1968 required, such as the inversion of a mid-oceanic ridge to become a subduction zone in order to
1969 accommodate convergence and explain ophiolite obduction (Hébert et al., 2012; Shemenda, 1993).
1970 Due to the paucity of data constraining the nature and location of subduction initiation of the Woyla
1971 back-arc basin, a south-dipping subduction zone as proposed by Morley (2012a) will also require
1972 testing in future work. However, India's Late Cretaceous northward acceleration from two coeval
1973 and coupled north-dipping subduction zones (Jagoutz et al., 2015) may also require two north-
1974 dipping subduction zones in the Woyla segment of the Neo-Tethyan active margin, which
1975 highlights the prevalence of intra-oceanic subduction in the Neo-Tethys.

1976 **7 Conclusions**

1977

1978 This study shows the power of considering the coupled plate-mantle system to study the
1979 geodynamics of the Tethyan tectonic domain that is dominated by long-term Eurasian, Indo-
1980 Australian and Pacific convergence following Pangea breakup. The reconstructions, used as
1981 boundary conditions in mantle flow simulations, consider intra-oceanic subduction along the entire
1982 south Eurasian active margin from ~160 Ma in the Neo-Tethys. We suggest that the Neo-Tethyan
1983 ridge was likely consumed along the Kohistan-Ladakh intra-oceanic arc from ~105 Ma, followed
1984 by northward subduction of the Indian Plate that significantly modified India's plate motion
1985 direction. For Sundaland, a tectonic scenario with Woyla Arc accretion at ~75-70 Ma, followed by
1986 a ~10 Myr subduction hiatus, and renewed subduction along the south Sundaland margin by
1987 ~60 Ma places the Sunda slab at the same depth as in P- and S-wave seismic tomography. In
1988 addition, our results suggest that a slab beneath northern Borneo, which is likely stagnant in the
1989 mantle transition zone, could be a remnant of the Proto South China Sea. Further east along New
1990 Guinea, the plate reconstructions coupled to geodynamic experiments are consistent with north-
1991 dipping subduction along the Halmahera Arc coeval with the ~20 Ma onset of south-dipping
1992 Maramuni subduction along New Guinea. The Late Cretaceous (~71 Ma) onset of Sepik oceanic
1993 basin subduction, followed by the docking of the Sepik composite terrane to southern New Guinea
1994 by ~30 Ma, produces a mid-mantle slab imaged in tomography beneath Lake Eyre in Australia, as
1995 discussed in Schellart and Spakman (2015), due to the combination of southward mantle flow and
1996 Australia's northward advance towards the Southeast Asian slab burial grounds.

1997 We present testable and reproducible plate reconstructions with regional refinements and
1998 improvements to the understanding of post-Jurassic eastern Tethyan geodynamics. The
1999 reconstructions may form the basis of future work to better understand the tectonics of the Tethyan
2000 domain, and could also be used to study oceanic circulation, long-term climate change and
2001 biogeographic dispersal pathways. In addition, our work highlights the need for testing competing
2002 plate reconstruction scenarios using numerical modelling approaches in a global and geodynamic
2003 framework.

2004

2005

2006 **Acknowledgements**

2007 N.F. and R.D.M. were supported by ARC grants DP130101946 and Statoil ASA through
2008 ARCIH130200012, S.Z. by ARC grant IH130200012, M.S. by ARC grant FT130101564, K.J.M.
2009 by ARC grant DP130101946. M.G. was supported by Statoil ASA and by the NSF through EAR-
2010 1161046 and EAR-1247022. This research was undertaken with the assistance of resources from
2011 the National Computational Infrastructure (NCI), which is supported by the Australian Government.
2012 We are grateful to John Cannon, Michael Chin, Robin Watson, Mark Turner, James Boyden and
2013 James Clark for their help in developing the open-source community plate reconstruction software
2014 GPLates, as well as relevant workflows. We thank Michael G. Tetley for providing technical support
2015 and workflow enhancement that improved the management of seafloor isochrons and other GPLates-
2016 related geometries, and Tobias Pfaffelmoser for help with implementing the GPLates 3D
2017 functionality. We are also grateful to Luke Mahoney for helpful discussions that improved the
2018 manuscript. We thank the Editor, Robert Holm and Bernhard Steinberger for constructive reviews.
2019 This work was conducted within the industry linkage and collaborative framework of the Basin
2020 GENeSIS Industrial Transformation Research Hub.

2021

2022

2023 **References**

2024

- 2025 Abrajevitch, A., van der Voo, R., Bazhenov, M.L., Levashova, N.M. and McCausland, P.J.A.,
2026 2008. The role of the Kazakhstan orocline in the late Paleozoic amalgamation of Eurasia.
2027 Tectonophysics, 455(1): 61-76.
- 2028 Acharyya, S.K., 1998. Break-up of the greater Indo-Australian continent and accretion of blocks
2029 framing south and east Asia. Journal of Geodynamics, 26(1): 149-170.
- 2030 Aitchison, J.C., Ali, J.R. and Davis, A.M., 2007. When and where did India and Asia collide?
2031 Journal of Geophysical Research, 112(B05423): 1-19.
- 2032 Aitchison, J.C., Davis, A.M., Liu, J., Luo, H., Malpas, J.G., McDermid, I.R.C., Wu, H., Ziabrev,
2033 S.V. and Zhou, M., 2000. Remnants of a Cretaceous intra-oceanic subduction system within

the Yarlung-Zangbo suture (southern Tibet). *Earth and Planetary Science Letters*, 183(1-2): 231-244.

Alisic, L., Gurnis, M., Stadler, G., Burstedde, C. and Ghattas, O., 2012. Multi - scale dynamics and rheology of mantle flow with plates. *Journal of Geophysical Research: Solid Earth* 117(B10).

Alisic, L., Gurnis, M., Stadler, G., Burstedde, C., Wilcox, L.C. and Ghattas, O., 2010. Slab stress and strain rate as constraints on global mantle flow. *Geophysical Research Letters*, 37(22).

Amante, C., Eakins, B.W. and Boulder, C., 2009. ETOPO1 1 arc-minute global relief model: Procedures, data sources and analysis. NOAA Technical Memorandum.

Audley-Charles, M.G., 1966. Mesozoic palaeogeography of Australasia. *Palaeogeography, Palaeoclimatology, Palaeoecology*, 2: 1-25.

Audley-Charles, M.G., 1988. Evolution of the southern margin of Tethys (North Australian region) from early Permian to late Cretaceous. *Geological Society, London, Special Publications*, 37(1): 79-100.

Audley-Charles, M.G., Ballantyne, P.D. and Hall, R., 1988. Mesozoic-Cenozoic Rift-Drift Sequence of Asian Fragments from Gondwanaland. *Tectonophysics*, 155(1-4): 317-330.

Baldwin, S.L., Fitzgerald, P.G. and Webb, E.W., 2012. Tectonics of the New Guinea Region. *Annu. Rev. Earth Planet. Sci.*, 40: 495-520.

Balmino, G., Vales, N., Bonvalot, S. and Briais, A., 2012. Spherical harmonic modelling to ultra-high degree of Bouguer and isostatic anomalies. *Journal of Geodesy*, 86(7): 499-520.

Barber, A.J. and Crow, M.J., 2003. An evaluation of plate tectonic models for the development of Sumatra. *Gondwana Research*, 6(1): 1-28.

Baumann, T.S. and Kaus, B.J.P., 2015. Geodynamic inversion to constrain the non-linear rheology of the lithosphere. *Geophysical Journal International*, 202(2): 1289-1316.

Baxter, A.T., Aitchison, J.C., Zyabrev, S.V. and Ali, J.R., 2011. Upper Jurassic radiolarians from the Naga ophiolite, Nagaland, northeast India. *Gondwana Research*, 20(2): 638-644.

Becker, T., Schaeffer, A., Lebedev, S. and Conrad, C., 2015. Toward a generalized plate motion reference frame. *Geophysical Research Letters*, 42(9): 3188-3196.

Becker, T.W., 2006. On the effect of temperature and strain-rate dependent viscosity on global mantle flow, net rotation, and plate-driving forces. *Geophysical Journal International*, 167(2): 943-957.

Becker, T.W. and Faccenna, C., 2011. Mantle conveyor beneath the Tethyan collisional belt. *Earth and Planetary Science Letters*, 310(3-4): 453-461.

Bergman, S.C., Coffield, D.Q., Talbot, J.P. and Garrard, R.A., 1996. Tertiary tectonic and magmatic evolution of western Sulawesi and the Makassar Strait, Indonesia: evidence for a Miocene continent-continent collision. *Geological Society, London, Special Publications*, 106(1): 391-429.

Besse, J. and Courtillot, V., 1988. Paleogeographic maps of the continents bordering the Indian Ocean since the Early Jurassic. *Journal of Geophysical Research: Solid Earth* (1978–2012), 93(B10): 11791-11808.

Bijwaard, H. and Spakman, W., 2000. Non-linear global P-wave tomography by iterated linearized inversion. *Geophysical Journal International*, 141(1): 71-82.

Bijwaard, H., Spakman, W. and Engdahl, E., 1998. Closing the gap between regional and global travel time tomography. *Journal of Geophysical Research*, 103(B12): 30055.

Bird, P., 2003. An updated digital model of plate boundaries. *Geochemistry, Geophysics, Geosystems*, 4(3): 1-52.

Bouilhol, P., Jagoutz, O., Hanchar, J.M. and Dudas, F.O., 2013. Dating the India–Eurasia collision through arc magmatic records. *Earth and Planetary Science Letters*, 366: 163-175.

Bouilhol, P., Schaltegger, U., Chiaradia, M., Ovtcharova, M., Stracke, A., Burg, J.-P. and Dawood, H., 2011. Timing of juvenile arc crust formation and evolution in the Sapat Complex (Kohistan–Pakistan). *Chemical Geology*, 280(3): 243-256.

2085 Bower, D., Gurnis, M. and Seton, M., 2013. Lower mantle structure from paleogeographically
2086 constrained dynamic Earth models. *Geochemistry, Geophysics, Geosystems*, 14(1): 44-63.

2087 Bower, D.J., Gurnis, M. and Flament, N., 2015. Assimilating lithosphere and slab history in 4-D
2088 dynamic Earth models. *Physics of the Earth and Planetary Interiors*, 238: 8-22.

2089 Boyden, J., Müller, R., Gurnis, M., Torsvik, T., Clark, J., Turner, M., Ivey-Law, H., Watson, R. and
2090 Cannon, J., 2011. Next-generation plate-tectonic reconstructions using GPlates. In: G.
2091 Keller and C. Baru (Editors), *Geoinformatics: Cyberinfrastructure for the Solid Earth*
2092 *Sciences*. Cambridge University Press, Cambridge, UK, pp. 95-114.

2093 Briais, A., Patriat, P. and Tapponnier, P., 1993. Updated interpretation of magnetic anomalies and
2094 seafloor spreading stages in the South China Sea: implications for the Tertiary tectonics of
2095 Southeast Asia. *Journal of Geophysical Research*, 98(B4): 6299-6328.

2096 Brown, G.F., 1951. *Geologic reconnaissance of the mineral deposits of Thailand*. US Government
2097 Printing Office.

2098 Bunge, H.-P., Hagelberg, C. and Travis, B., 2003. Mantle circulation models with variational data
2099 assimilation: inferring past mantle flow and structure from plate motion histories and
2100 seismic tomography. *Geophysical Journal International*, 152(2): 280-301.

2101 Burg, J.P., 2011. The Asia–Kohistan–India Collision: Review and Discussion. In: D. Brown and P.
2102 Ryan (Editors), *Arc-Continent Collision*. *Frontiers in Earth Sciences*. Springer-Verlag
2103 Berlin, pp. 279-309.

2104 Burg, J.P., Jagoutz, O., Dawood, H. and Hussain, S.S., 2006. Precollision tilt of crustal blocks in
2105 rifted island arcs: structural evidence from the Kohistan Arc. *Tectonics*, 25(5).

2106 Burke, K. and Dewey, J., 1973. Plume-generated triple junctions: key indicators in applying plate
2107 tectonics to old rocks. *The Journal of Geology*: 406-433.

2108 Burrett, C., Duhid, N., Berry, R. and Varne, R., 1991. Asian and south-western Pacific continental
2109 terranes derived from Gondwana, and their biogeographic significance. *Australian*
2110 *Systematic Botany*, 4(1): 13-24.

2111 Butterworth, N., Talsma, A., Müller, R., Seton, M., Bunge, H.-P., Schuberth, B., Shephard, G. and
2112 Heine, C., 2014. Geological, tomographic, kinematic and geodynamic constraints on the
2113 dynamics of sinking slabs. *Journal of Geodynamics*, 73: 1-13.

2114 Cameron, N.R., Clarke, M.C.G., Aldiss, D.T., Aspden, J.A. and Djunuddin, A., 1980. The
2115 geological evolution of northern Sumatra.

2116 Cande, S.C. and Patriat, P., 2015. The anticorrelated velocities of Africa and India in the Late
2117 Cretaceous and early Cenozoic. *Geophysical Journal International*, 200(1): 227-243.

2118 Cande, S.C., Patriat, P. and Dymant, J., 2010. Motion between the Indian, Antarctic and African
2119 plates in the early Cenozoic. *Geophysical Journal International*(183): 127-149.

2120 Cande, S.C. and Stegman, D.R., 2011. Indian and African plate motions driven by the push force of
2121 the Reunion plume head. *Nature*, 475(7354): 47-52.

2122 Capitanio, F.A., Morra, G., Goes, S., Weinberg, R.F. and Moresi, L., 2010. India–Asia convergence
2123 driven by the subduction of the Greater Indian continent. *Nature Geoscience*, 3(2): 136-139.

2124 Carey, S.W., 1955. The orocline concept in geotectonics-Part I, *Papers and proceedings of the*
2125 *Royal Society of Tasmania*, pp. 255-288.

2126 Carlson, R. and Mortera-Gutiérrez, C., 1990. Subduction hinge migration along the Izu-Bonin-
2127 Mariana arc. *Tectonophysics*, 181(1-4): 331-344.

2128 Charlton, T.R., 2001. Permo-Triassic evolution of Gondwanan eastern Indonesia, and the final
2129 Mesozoic separation of SE Asia from Australia. *Journal of Asian Earth Sciences*, 19(5):
2130 595-617.

2131 Chatterjee, S., Goswami, A. and Scotese, C.R., 2013. The longest voyage: tectonic, magmatic, and
2132 paleoclimatic evolution of the Indian plate during its northward flight from Gondwana to
2133 Asia. *Gondwana Research*, 23(1): 238-267.

2134 Chung, S.L., Chu, M.F., Zhang, Y., Xie, Y., Lo, C.H., Lee, T.Y., Lan, C.Y., Li, X., Zhang, Q. and
2135 Wang, Y., 2005. Tibetan tectonic evolution inferred from spatial and temporal variations in
2136 post-collisional magmatism. *Earth-Science Reviews*, 68(3-4): 173-196.

- 2137 Clements, B., Burgess, P.M., Hall, R. and Cottam, M.A., 2011. Subsidence and uplift by slab-
2138 related mantle dynamics: a driving mechanism for the Late Cretaceous and Cenozoic
2139 evolution of continental SE Asia? Geological Society, London, Special Publications, 355(1):
2140 37-51.
- 2141 Clements, B. and Hall, R., 2007. Cretaceous to Late Miocene stratigraphic and tectonic evolution of
2142 West Java. Indonesian Petroleum Association Proceedings, 31(IPA07-G-037): 1-18.
- 2143 Clements, B. and Hall, R., 2011. A record of continental collision and regional sediment flux for the
2144 Cretaceous and Palaeogene core of SE Asia: implications for early Cenozoic
2145 palaeogeography. *Journal of the Geological Society*, 168: 1187-1200.
- 2146 Clift, P.D., Hannigan, R., Blusztajn, J. and Draut, A.E., 2002. Geochemical evolution of the Dras–
2147 Kohistan Arc during collision with Eurasia: evidence from the Ladakh Himalaya, India.
2148 *Island Arc*, 11(4): 255-273.
- 2149 Conrad, C.P. and Gurnis, M., 2003. Seismic tomography, surface uplift, and the breakup of
2150 Gondwanaland: Integrating mantle convection backwards in time. *Geochemistry*,
2151 *Geophysics, Geosystems*, 4(3).
- 2152 Conrad, C.P. and Lithgow - Bertelloni, C., 2004. The temporal evolution of plate driving forces:
2153 Importance of “slab suction” versus “slab pull” during the Cenozoic. *Journal of*
2154 *Geophysical Research: Solid Earth*, 109(B10).
- 2155 Crowhurst, P.V., Hill, K.C., Foster, D.A. and Bennett, A., 1996. Thermochronological and
2156 geochemical constraints on the tectonic evolution of northern Papua New Guinea.
2157 *Geological Society Special Publications*, 106(Tectonic Evolution of Southeast Asia): 525-
2158 537.
- 2159 Cullen, A.B., 2010. Transverse segmentation of the Baram-Balabac Basin, NW Borneo: refining the
2160 model of Borneo's tectonic evolution. *Petroleum Geoscience*, 16(1): 3-29.
- 2161 Daly, M.C., Cooper, M.A., Wilson, I., Smith, D.G. and Hooper, B.G.D., 1991. Cenozoic plate
2162 tectonics and basin evolution in Indonesia. *Marine and Petroleum Geology*, 8(1): 2-21.
- 2163 Davies, H.L., 2012. The geology of New Guinea-the cordilleran margin of the Australian continent.
2164 *Episodes*, 35(1): 87-102.
- 2165 de Bruyn, M., Stelbrink, B., Morley, R.J., Hall, R., Carvalho, G.R., Cannon, C.H., van den Bergh,
2166 G., Meijaard, E., Metcalfe, I. and Boitani, L., 2014. Borneo and Indochina are major
2167 evolutionary hotspots for Southeast Asian biodiversity. *Systematic biology*, 63(6): 879-901.
- 2168 Debayle, E. and Ricard, Y., 2013. Seismic observations of large-scale deformation at the bottom of
2169 fast-moving plates. *Earth and Planetary Science Letters*, 376: 165-177.
- 2170 Debon, F., Le Fort, P., Dautel, D., Sonet, J. and Zimmermann, J.L., 1987. Granites of western
2171 Karakorum and northern Kohistan (Pakistan): a composite Mid-Cretaceous to upper
2172 Cenozoic magmatism. *Lithos*, 20(1): 19-40.
- 2173 Deng, J., Yang, X., Zhang, Z.-F. and Santosh, M., 2015. Early Cretaceous arc volcanic suite in
2174 Cebu Island, Central Philippines and its implications on paleo-Pacific plate subduction:
2175 Constraints from geochemistry, zircon U–Pb geochronology and Lu–Hf isotopes. *Lithos*,
2176 230: 166-179.
- 2177 Deschamps, A. and Lallemand, S., 2002. The West Philippine Basin: An Eocene to early Oligocene
2178 back arc basin opened between two opposed subduction zones. *Journal of Geophysical*
2179 *Research: Solid Earth* (1978–2012), 107(B12): EPM 1-1-EPM 1-24.
- 2180 DiCaprio, L., Gurnis, M. and Müller, R.D., 2009. Long-wavelength tilting of the Australian
2181 continent since the Late Cretaceous. *Earth and Planetary Science Letters*, 278(3-4): 175-185.
- 2182 DiCaprio, L., Gurnis, M., Müller, R.D. and Tan, E., 2011. Mantle dynamics of continentwide
2183 Cenozoic subsidence and tilting of Australia. *Lithosphere*: L140. 1v1.
- 2184 Doglioni, C., 1991. A proposal for the kinematic modelling of W - dipping subductions - possible
2185 applications to the Tyrrhenian - Apennines system. *Terra Nova*, 3(4): 423-434.
- 2186 Domeier, M. and Torsvik, T.H., 2014. Plate tectonics in the late Paleozoic. *Geoscience Frontiers*,
2187 5(3): 303-350.

- 2188 Doust, H. and Sumner, H.S., 2007. Petroleum systems in rift basins—a collective approach
2189 in Southeast Asian basins. *Petroleum Geoscience*, 13(2): 127-144.
- 2190 Dow, D.B., 1977. A geological synthesis of Papua New Guinea, 201. Bureau of Mineral Resources,
2191 Australian Government Publishing Service.
- 2192 Elburg, M., van Leeuwen, T. and Foden, J., 2003. Spatial and temporal isotopic domains of
2193 contrasting igneous suites in Western and Northern Sulawesi, Indonesia. *Chemical Geology*,
2194 199(3): 243-276.
- 2195 Eldredge, S., Bachtadse, V. and van der Voo, R., 1985. Paleomagnetism and the orocline
2196 hypothesis. *Tectonophysics*, 119(1): 153-179.
- 2197 Encarnación, J., 2004. Multiple ophiolite generation preserved in the northern Philippines and the
2198 growth of an island arc complex. *Tectonophysics*, 392(1): 103-130.
- 2199 Faccenna, C., Becker, T.W., Lallemand, S. and Steinberger, B., 2012. On the role of slab pull in the
2200 Cenozoic motion of the Pacific plate. *Geophysical Research Letters*, 39(3).
- 2201 Fairbridge, R.W., 1963. The Indian Ocean and the status of Gondwanaland. *Progress in*
2202 *Oceanography*, 3: 83-136.
- 2203 Findlay, R.H., 2003. Collision tectonics of northern Papua New Guinea: key field relationships
2204 demand a new model. *Geological Society of America Special Papers*, 372: 291-307.
- 2205 Fitch, T.J., 1972. Plate convergence, transcurrent faults, and internal deformation adjacent to
2206 southeast Asia and the western Pacific. *Journal of Geophysical Research*, 77(23): 4432-
2207 4460.
- 2208 Fjeldskaar, W., Lindholm, C., Dehls, J.F. and Fjeldskaar, I., 2000. Postglacial uplift, neotectonics
2209 and seismicity in Fennoscandia. *Quaternary Science Reviews*, 19(14-15): 1413-1422.
- 2210 Flament, N., Gurnis, M., Müller, R.D., Bower, D.J. and Husson, L., 2015. Influence of subduction
2211 history on South American topography. *Earth and Planetary Science Letters*, 430: 9-18.
- 2212 Flament, N., Gurnis, M., Williams, S., Seton, M., Skogseid, J., Heine, C. and Müller, R.D., 2014.
2213 Topographic asymmetry of the South Atlantic from global models of mantle flow and
2214 lithospheric stretching. *Earth and Planetary Science Letters*, 387: 107-119.
- 2215 Flower, M.F.J. and Dilek, Y., 2003. Arc-trench rollback and forearc accretion: 1. A collision-
2216 induced mantle flow model for Tethyan ophiolites. *Geological Society, London, Special*
2217 *Publications*, 218(1): 21-41.
- 2218 Forsyth, D. and Uyeda, S., 1975. On the relative importance of the driving forces of plate motion.
2219 *Geophysical Journal International*, 43(1): 163-200.
- 2220 Forte, A.M. and Mitrovica, J.X., 1996. New inferences of mantle viscosity from joint inversion of
2221 long - wavelength mantle convection and post - glacial rebound data. *Geophysical Research*
2222 *Letters*, 23(10): 1147-1150.
- 2223 Foulger, G.R., Panza, G.F., Artemieva, I.M., Bastow, I.D., Cammarano, F., Evans, J.R., Hamilton,
2224 W.B., Julian, B.R., Lustrino, M. and Thybo, H., 2013. Caveats on tomographic images.
2225 *Terra Nova*, 25(4): 259-281.
- 2226 Fuller, M., Ali, J.R., Moss, S.J., Frost, G.M., Richter, B. and Mahfi, A., 1999. Paleomagnetism of
2227 Borneo. *Journal of Asian Earth Sciences*, 17(1-2): 3-24.
- 2228 Fuller, M., Haston, R., Lin, J.-L., Richter, B., Schmidtke, E. and Almasco, J., 1991. Tertiary
2229 paleomagnetism of regions around the South China Sea. *Journal of Southeast Asian Earth*
2230 *Sciences*, 6(3): 161-184.
- 2231 Fyhn, M.B.W., Pedersen, S.A.S., Boldreel, L.O., Nielsen, L.H., Green, P.F., Dien, P.T., Huyen,
2232 L.T. and Frei, D., 2010. Palaeocene–early Eocene inversion of the Phuquoc–Kampot Som
2233 Basin: SE Asian deformation associated with the suturing of Luconia. *Journal of the*
2234 *Geological Society*, 167(2): 281-295.
- 2235 Gaina, C. and Müller, R.D., 2007. Cenozoic tectonic and depth/age evolution of the Indonesian
2236 gateway and associated back-arc basins. *Earth-Science Reviews*, 83(3-4): 177-203.
- 2237 Gasperini, P. and Sabadini, R., 1989. Lateral heterogeneities in mantle viscosity and post glacial
2238 rebound. *Geophysical Journal International*, 98(3): 413-428.

- 2239 Geary, E.E., Harrison, T.M. and Heizler, M., 1988. Diverse ages and origins of basement
2240 complexes, Luzon, Philippines. *Geology*, 16(4): 341-344.
- 2241 Geary, E.E. and Kay, R.W., 1989. Identification of an Early Cretaceous ophiolite in the Camarines
2242 Norte-Calaguas Islands basement complex, eastern Luzon, Philippines. *Tectonophysics*,
2243 168(1): 109-126.
- 2244 Gee, J.S. and Kent, D.V., 2007. Source of oceanic magnetic anomalies and the geomagnetic
2245 polarity time scale. *Treatise on Geophysics*, Vol. 5: Geomagnetism: 455-507.
- 2246 Ghose, R., Yoshioka, S. and Oike, K., 1990. Three-dimensional numerical simulation of the
2247 subduction dynamics in the Sunda arc region, Southeast Asia. *Tectonophysics*, 181(1): 223-
2248 255.
- 2249 Gibbons, A., Zahirovic, S., Müller, R.D., Whittaker, J. and Yatheesh, V., 2015. A tectonic model
2250 reconciling evidence for the collisions between India, Eurasia and intra-oceanic arcs of the
2251 central-eastern Tethys. *Gondwana Research FOCUS*, 28(2): 451-492.
- 2252 Gibbons, A.D., Barckhausen, U., van den Bogaard, P., Hoernle, K., Werner, R., Whittaker, J.M. and
2253 Müller, R.D., 2012. Constraining the Jurassic extent of Greater India: Tectonic evolution of
2254 the West Australian margin. *Geochemistry Geophysics Geosystems*, 13(5): 25.
- 2255 Gibbons, A.D., Whittaker, J.M. and Müller, R.D., 2013. The breakup of East Gondwana:
2256 Assimilating constraints from Cretaceous ocean basins around India into a best - fit tectonic
2257 model. *Journal of Geophysical Research: Solid Earth*, 13(5).
- 2258 Glišović, P. and Forte, A.M., 2014. Reconstructing the Cenozoic evolution of the mantle:
2259 Implications for mantle plume dynamics under the Pacific and Indian plates. *Earth and
2260 Planetary Science Letters*, 390: 146-156.
- 2261 Goldfarb, R.J., Taylor, R.D., Collins, G.S., Goryachev, N.A. and Orlandini, O.F., 2014.
2262 Phanerozoic continental growth and gold metallogeny of Asia. *Gondwana Research*, 25(1):
2263 48-102.
- 2264 Görür, N. and Sengör, A.M.C., 1992. Paleogeography and tectonic evolution of the eastern
2265 Tethysides: implications for the northwest Australian margin breakup history, *Proceedings
2266 of the Ocean Drilling Program, Scientific Results*, pp. 83-106.
- 2267 Gurlan, A.T., Meynadier, L. and Allègre, C.J., 2008. Tectonically driven changes in the Indian
2268 Ocean circulation over the last 25 Ma: Neodymium isotope evidence. *Earth and Planetary
2269 Science Letters*, 267(1): 353-364.
- 2270 Gradstein, F.M. and Ludden, J.N., 1992. Radiometric age determinations for basement from Sites
2271 765 and 766, Argo Abyssal Plain and northwestern Australian margin, *Proceedings of the
2272 ocean drilling program, Scientific Results*, pp. 557-559.
- 2273 Grand, S.P., 2002. Mantle shear-wave tomography and the fate of subducted slabs. *Philosophical
2274 Transactions of the Royal Society of London. Series A: Mathematical, Physical and
2275 Engineering Sciences*, 360(1800): 2475.
- 2276 Guillaume, B., Martinod, J., Husson, L., Roddaz, M. and Riquelme, R., 2009. Neogene uplift of
2277 central eastern Patagonia: Dynamic response to active spreading ridge subduction?
2278 *Tectonics*, 28(2).
- 2279 Guntoro, A., 1999. The formation of the Makassar Strait and the separation between SE Kalimantan
2280 and SW Sulawesi. *Journal of Asian Earth Sciences* 17: 79-98.
- 2281 Gurnis, M., Hall, C. and Lavier, L., 2004. Evolving force balance during incipient subduction.
2282 *Geochemistry, Geophysics, Geosystems*, 5: -.
- 2283 Gurnis, M., Turner, M., Zahirovic, S., DiCaprio, L., Spasojevic, S., Müller, R.D., Boyden, J., Seton,
2284 M., Manea, V.C. and Bower, D.J., 2012. Plate Tectonic Reconstructions with Continuously
2285 Closing Plates. *Computers & Geosciences*, 38(1): 35-42.
- 2286 Hafkenscheid, E., Wortel, M.J.R. and Spakman, W., 2006. Subduction history of the Tethyan
2287 region derived from seismic tomography and tectonic reconstructions. *Journal of
2288 Geophysical Research-Solid Earth*, 111(B8): B08401.
- 2289 Hager, B.H., 1984. Subducted slabs and the geoid: constraints on mantle rheology and flow. *Journal
2290 of Geophysical Research*, 89(B7): 6003-6015.

2291 Hager, B.H. and O'Connell, R.J., 1981. A simple global model of plate dynamics and mantle
2292 convection. *Journal of Geophysical Research: Solid Earth* (1978–2012), 86(B6): 4843-4867.

2293 Haile, N.S., 1979. Palaeomagnetic evidence for rotation and northward drift of Sumatra. *Journal of*
2294 *the Geological Society*, 136(5): 541-546.

2295 Haile, N.S., McElhinny, M.W. and McDougall, I., 1977. Palaeomagnetic data and radiometric ages
2296 from the Cretaceous of West Kalimantan (Borneo), and their significance in interpreting
2297 regional structure. *Journal of the Geological Society*, 133(2): 133-144.

2298 Halbouty, M.T., King, R.E., Klemme, H.D., Dott, S., R H and Meyerhoff, A.A., 1970. World's
2299 Giant Oil and Gas Fields, Geologic Factors Affecting Their Formation, and Basin
2300 Classification: Part II: Factors Affecting Formation of Giant Oil and Gas Fields, and Basin
2301 Classification, M 14: *Geology of Giant Petroleum Fields*, pp. 528-555.

2302 Hall, C.E., Gurnis, M., Sdrolias, M., Lavier, L.L. and Müller, R.D., 2003. Catastrophic initiation of
2303 subduction following forced convergence across fracture zones. *Earth and Planetary Science*
2304 *Letters*, 212(1): 15-30.

2305 Hall, R., 1996. Reconstructing Cenozoic SE Asia. *Geological Society, London, Special*
2306 *Publications*, 106(1): 153-184.

2307 Hall, R., 2002. Cenozoic geological and plate tectonic evolution of SE Asia and the SW Pacific:
2308 computer-based reconstructions, model and animations. *Journal of Asian Earth Sciences*,
2309 20(4): 353-431.

2310 Hall, R., 2011. Australia–SE Asia collision: plate tectonics and crustal flow. *Geological Society,*
2311 *London, Special Publications*, 355(1): 75-109.

2312 Hall, R., 2012. Late Jurassic–Cenozoic reconstructions of the Indonesian region and the Indian
2313 Ocean. *Tectonophysics*, 570-571: 1-41.

2314 Hall, R., Ali, J.R. and Anderson, C.D., 1995a. Cenozoic Motion of the Philippine Sea Plate -
2315 Paleomagnetic Evidence from Eastern Indonesia. *Tectonics*, 14(5): 1117-1132.

2316 Hall, R., Ali, J.R., Anderson, C.D. and Baker, S.J., 1995b. Origin and motion history of the
2317 Philippine Sea Plate. *Tectonophysics*, 251(1): 229-250.

2318 Hall, R. and Spakman, W., 2002. Subducted slabs beneath the eastern Indonesia-Tonga region:
2319 insights from tomography. *Earth and Planetary Science Letters*, 201(2): 321-336.

2320 Hall, R. and Spakman, W., 2003. Mantle structure and tectonic evolution of the region north and
2321 east of Australia. *Geological Society of America Special Papers*, 372: 361-381.

2322 Hall, R. and Spakman, W., 2015. Mantle structure and tectonic history of SE Asia. *Tectonophysics*,
2323 658: 14-45.

2324 Hamilton, W.B., 1979. *Tectonics of the Indonesian region*. US Govt. Print. Off.

2325 Haq, B.U., Hardenbol, J. and Vail, P.R., 1987. Chronology of fluctuating sea levels since the
2326 Triassic. *Science*, 235(4793): 1156-1167.

2327 Hearn, P.J., Hare, T., Schruben, P., Sherrill, D., LaMar, C. and Tsushima, P., 2003. Global GIS,
2328 Global Coverage DVD (USGS). American Geological Institute, Alexandria, Virginia, USA.

2329 Hébert, R., Bezard, R., Guilmette, C., Dostal, J., Wang, C.S. and Liu, Z.F., 2012. The Indus–
2330 Yarlung Zangbo ophiolites from Nanga Parbat to Namche Barwa syntaxes, southern Tibet:
2331 First synthesis of petrology, geochemistry, and geochronology with incidences on
2332 geodynamic reconstructions of Neo-Tethys. *Gondwana Research*, 22(2): 377-397.

2333 Heine, C. and Müller, R.D., 2005. Late Jurassic rifting along the Australian North West Shelf:
2334 margin geometry and spreading ridge configuration. *Australian Journal of Earth Sciences*,
2335 52(1): 27-39.

2336 Heine, C., Müller, R.D. and Gaina, C., 2004. Reconstructing the lost eastern Tethys ocean basin:
2337 convergence history of the SE Asian margin and marine gateways. *Continent-Ocean*
2338 *Interactions Within East Asian Marginal Seas*, *Geophys. Monogr. Ser.*, 149: 37-54.

2339 Hellinger, S.J., 1981. The uncertainties of finite rotations in plate tectonics. *Journal of Geophysical*
2340 *Research: Solid Earth* (1978–2012), 86(B10): 9312-9318.

2341 Herold, N., Buzan, J., Seton, M., Goldner, A., Green, J.A.M., Müller, R.D., Markwick, P. and
 2342 Huber, M., 2014. A suite of early Eocene (~ 55 Ma) climate model boundary conditions.
 2343 Geoscientific Model Development, 7(5): 2077-2090.
 2344 Hilde, T.W.C. and Chao-Shing, L., 1984. Origin and evolution of the West Philippine Basin: a new
 2345 interpretation. Tectonophysics, 102(1): 85-104.
 2346 Hill, K.C. and Hall, R., 2003. Mesozoic–Cenozoic evolution of Australia’s New Guinea margin in a
 2347 west Pacific context. Geological Society of Australia Special Publications, 22: 265-289.
 2348 Hill, K.C. and Raza, A., 1999. Arc - continent collision in Papua Guinea: Constraints from fission
 2349 track thermochronology. Tectonics, 18(6): 950-966.
 2350 Holm, R.J., Spandler, C. and Richards, S.W., 2014. Continental collision, orogenesis and arc
 2351 magmatism of the Miocene Maramuni arc, Papua New Guinea. Gondwana Research.
 2352 Hopper, J.R., Mutter, J.C., Larson, R.L. and Mutter, C.Z., 1992. Magmatism and rift margin
 2353 evolution: Evidence from northwest Australia. Geology, 20(9): 853-857.
 2354 Hu, X., Garzanti, E., Moore, T. and Raffi, I., 2015. Direct stratigraphic dating of India-Asia
 2355 collision onset at the Selandian (middle Paleocene, 59±1 Ma). Geology, 43(10): 859-862.
 2356 Huber, M. and Goldner, A., 2012. Eocene monsoons. Journal of Asian Earth Sciences, 44: 3-23.
 2357 Hutchison, C.S., 1975. Ophiolite in Southeast Asia. Geological Society of America Bulletin, 86(6):
 2358 797-806.
 2359 Hutchison, C.S., 1996. The ‘Rajang accretionary prism’ and ‘Lupar Line’ problem of Borneo.
 2360 Geological Society, London, Special Publications, 106(1): 247-261.
 2361 Hutchison, C.S., 2004. Marginal basin evolution: the southern South China Sea. Marine and
 2362 Petroleum Geology, 21(9): 1129-1148.
 2363 Hutchison, C.S., 2010. Oroclines and paleomagnetism in Borneo and South-East Asia.
 2364 Tectonophysics, 496(1): 53-67.
 2365 Hutchison, C.S., Bergman, S.C., Swauger, D.A. and Graves, J.E., 2000. A Miocene collisional belt
 2366 in north Borneo: uplift mechanism and isostatic adjustment quantified by thermochronology.
 2367 Journal of the Geological Society, 157(4): 783-793.
 2368 Jagoutz, O., Macdonald, F.A. and Royden, L., 2016. Low-latitude arc–continent collision as a
 2369 driver for global cooling. Proceedings of the National Academy of Sciences, 113(18): 4935-
 2370 4940.
 2371 Jagoutz, O., Royden, L., Holt, A.F. and Becker, T.W., 2015. Anomalously fast convergence of
 2372 India and Eurasia caused by double subduction. Nature Geoscience, 8(6): 475-478.
 2373 Jagoutz, O. and Schmidt, M.W., 2012. The formation and bulk composition of modern juvenile
 2374 continental crust: the Kohistan arc. Chemical Geology, 298: 79-96.
 2375 Jahn, B.-M., Chen, P.Y. and Yen, T.P., 1976. Rb-Sr ages of granitic rocks in southeastern China
 2376 and their tectonic significance. Geological Society of America Bulletin, 87(5): 763-776.
 2377 Jarvis, G.T. and Lowman, J.P., 2005. Sinking slabs below fossil subduction zones. Physics of The
 2378 Earth and Planetary Interiors, 152(1-2): 103-115.
 2379 Jarvis, G.T. and Lowman, J.P., 2007. Survival times of subducted slab remnants in numerical
 2380 models of mantle flow. Earth and Planetary Science Letters, 260(1-2): 23-36.
 2381 Ji, W.-Q., Wu, F.-Y., Chung, S.-L., Li, J.-X. and Liu, C.-Z., 2009. Zircon U–Pb geochronology and
 2382 Hf isotopic constraints on petrogenesis of the Gangdese batholith, southern Tibet. Chemical
 2383 Geology, 262(3): 229-245.
 2384 Jolivet, L., Faccenna, C., D’Agostino, N., Fournier, M. and Worrall, D., 1999. The kinematics of
 2385 back-arc basins, examples from the Tyrrhenian, Aegean and Japan Seas. Geological Society,
 2386 London, Special Publications, 164(1): 21-53.
 2387 Jolivet, L., Huchon, P. and Rangin, C., 1989. Tectonic setting of Western Pacific marginal basins.
 2388 Tectonophysics, 160(1): 23-47.
 2389 Katili, J.A., 1971. A review of the geotectonic theories and tectonic maps of Indonesia. Earth-
 2390 Science Reviews, 7(3): 143-163.
 2391 Katili, J.A., 1975. Volcanism and plate tectonics in the Indonesian island arcs. Tectonophysics,
 2392 26(3): 165-188.

2393 Kendrick, R.D., 2000. Structure, tectonics and thermochronology of the Irian Jaya Fold Belt, Irian
2394 Jaya, Indonesia, La Trobe University.

2395 Khan, S.D., Walker, D.J., Hall, S.A., Burke, K.C., Shah, M.T. and Stockli, L., 2009. Did the
2396 Kohistan-Ladakh island arc collide first with India? *Geological Society of America Bulletin*,
2397 121(3-4): 366.

2398 Klootwijk, C., Giddings, J., Pigram, C.J., Loxton, C., Davies, H., Rogerson, R. and Falvey, D.,
2399 2003. North Sepik region of Papua New Guinea: palaeomagnetic constraints on arc
2400 accretion and deformation. *Tectonophysics*, 362: 273-301.

2401 Kobayashi, K., 2004. Origin of the Palau and Yap trench-arc systems. *Geophysical Journal*
2402 *International*, 157(3): 1303-1315.

2403 Lambeck, K., Smither, C. and Johnston, P., 1998. Sea level change, glacial rebound and mantle
2404 viscosity for northern Europe. *Geophysical Journal International*, 134(1): 102-144.

2405 Le Pichon, X., 1968. Sea-floor spreading and continental drift. *Journal of Geophysical Research*,
2406 73(12): 3661-3697.

2407 Lee, C.-T.A., Shen, B., Slotnick, B.S., Liao, K., Dickens, G.R., Yokoyama, Y., Lenardic, A.,
2408 Dasgupta, R., Jellinek, M. and Lackey, J.S., 2013. Continental arc–island arc fluctuations,
2409 growth of crustal carbonates, and long-term climate change. *Geosphere*, 9(1): 21-36.

2410 Lee, T.Y. and Lawver, L.A., 1994. Cenozoic plate reconstruction of the South China Sea region.
2411 *Tectonophysics*, 235(1-2): 149-180.

2412 Lee, T.Y. and Lawver, L.A., 1995. Cenozoic plate reconstruction of Southeast Asia.
2413 *Tectonophysics*, 251(1-4): 85-138.

2414 Leith, C., 1926. The mineral resources of the Far East. *Foreign Affairs*, 4(3): 433-442.

2415 Leng, W. and Gurnis, M., 2015. Subduction initiation at relic arcs. *Geophysical Research Letters*,
2416 42.

2417 Li, C., van der Hilst, R.D., Engdahl, E.R. and Burdick, S., 2008. A new global model for P wave
2418 speed variations in Earth's mantle. *Geochemistry, Geophysics, Geosystems*, 9(5): 21.

2419 Li, X., 2000. Cretaceous magmatism and lithospheric extension in Southeast China. *Journal of*
2420 *Asian Earth Sciences*, 18(3): 293-305.

2421 Li, Z.-H., Xu, Z., Gerya, T. and Burg, J.-P., 2013. Collision of continental corner from 3-D
2422 numerical modeling. *Earth and Planetary Science Letters*, 380: 98-111.

2423 Lithgow - Bertelloni, C. and Richards, M.A., 1998. The dynamics of Cenozoic and Mesozoic plate
2424 motions. *Reviews of Geophysics*, 36(1): 27-78.

2425 Liu, L. and Gurnis, M., 2008. Simultaneous inversion of mantle properties and initial conditions
2426 using an adjoint of mantle convection. *Journal of Geophysical Research B*, 113(B08405):
2427 17.

2428 Lohman, D.J., de Bruyn, M., Page, T., von Rintelen, K., Hall, R., Ng, P.K., Shih, H.-T., Carvalho,
2429 G.R. and von Rintelen, T., 2011. Biogeography of the Indo-Australian archipelago. *Annual*
2430 *Review of Ecology, Evolution, and Systematics*, 42: 205-226.

2431 Mathews, D.C., 2014. The Absolute Motion of Trenches and Age of the Subducting Slab. Master's
2432 Thesis, Department of Earth Science. Rice University: 49.

2433 Mathews, D., 1990. Serendipity or economics? Tin and the theory of mineral discovery and
2434 development, 1800–1920. *Business History*, 32(3): 15-48.

2435 Mathews, K.J., Müller, R.D. and Sandwell, D.T., 2016. Oceanic microplate formation records the
2436 onset of India–Eurasia collision. *Earth and Planetary Science Letters*, 433: 204-214.

2437 Mathews, K.J., Müller, R.D., Wessel, P. and Whittaker, J.M., 2011. The tectonic fabric of the
2438 ocean basins. *Journal of Geophysical Research*, 116(B12): B12109.

2439 Mathews, K.J., Seton, M. and Müller, R.D., 2012. A global-scale plate reorganization event at
2440 105– 100 Ma. *Earth and Planetary Science Letters*, 355: 283-298.

2441 McCourt, W.J., Crow, M.J., Cobbing, E.J. and Amin, T.C., 1996. Mesozoic and Cenozoic plutonic
2442 evolution of SE Asia: evidence from Sumatra, Indonesia. Geological Society, London,
2443 Special Publications, 106(1): 321-335.

- 2444 McDermid, I.R.C., Aitchison, J.C., Davis, A.M., Harrison, T.M. and Grove, M., 2002. The Zedong
2445 terrane: a Late Jurassic intra-oceanic magmatic arc within the Yarlung–Tsangpo suture
2446 zone, southeastern Tibet. *Chemical Geology*, 187(3): 267-277.
- 2447 McElhinny, M.W., Embleton, B.J.J., Ma, X.H. and Zhang, Z.K., 1981. Fragmentation of Asia in the
2448 Permian. *Nature*, 293(5829): 212-214.
- 2449 McKenzie, D.P., 1969. Speculations on the consequences and causes of plate motions. *Geophysical*
2450 *Journal International*, 18(1): 1-32.
- 2451 McKenzie, D.P. and Parker, R.L., 1967. The North Pacific: an example of tectonics on a sphere.
2452 *Nature*, 216: 1276-1280.
- 2453 McNamara, A.K. and Zhong, S., 2005. Thermochemical structures beneath Africa and the Pacific
2454 Ocean. *Nature*, 437(7062): 1136-1139.
- 2455 Metcalfe, I., 1988. Origin and assembly of south-east Asian continental terranes. *Geological*
2456 *Society, London, Special Publications*, 37(1): 101-118.
- 2457 Metcalfe, I., 1994. Gondwanaland origin, dispersion, and accretion of East and Southeast Asian
2458 continental terranes. *Journal of South American Earth Sciences*, 7(3): 333-347.
- 2459 Metcalfe, I., 1999. Gondwana dispersion and Asian accretion: an overview. In: I. Metcalfe (Editor),
2460 *Gondwana dispersion and Asian Accretion*. A.A. Balkema, Rotterdam, pp. 9-28.
- 2461 Metcalfe, I., 2002. Permian tectonic framework and palaeogeography of SE Asia. *Journal of Asian*
2462 *Earth Sciences*, 20(6): 551-566.
- 2463 Metcalfe, I., 2006. Palaeozoic and Mesozoic tectonic evolution and palaeogeography of East Asian
2464 crustal fragments: The Korean Peninsula in context. *Gondwana Research*, 9(1-2): 24-46.
- 2465 Metcalfe, I., 2009. Late Palaeozoic and Mesozoic tectonic and palaeogeographical evolution of SE
2466 Asia. *Geological Society, London, Special Publications*, 315(1): 7-23.
- 2467 Metcalfe, I., 2011. Tectonic framework and Phanerozoic evolution of Sundaland. *Gondwana*
2468 *Research*, 19(1): 3-21.
- 2469 Metcalfe, I. and Irving, E., 1990. Allochthonous Terrane Processes in Southeast Asia [and
2470 Discussion]. *Philosophical Transactions of the Royal Society of London A: Mathematical,*
2471 *Physical and Engineering Sciences*, 331(1620): 625-640.
- 2472 Miller, M.S., Kennett, B.L.N. and Toy, V.G., 2006. Spatial and temporal evolution of the
2473 subducting Pacific plate structure along the western Pacific margin. *Journal of Geophysical*
2474 *Research: Solid Earth*, 111(B2).
- 2475 Milsom, J., 2000. Stratigraphic constraints on suture models for eastern Indonesia. *Journal of Asian*
2476 *Earth Sciences*, 18(6): 761-779.
- 2477 Mitchell, A., Chung, S.-L., Oo, T., Lin, T.-H. and Hung, C.-H., 2012. Zircon U–Pb ages in
2478 Myanmar: Magmatic–metamorphic events and the closure of a neo-Tethys ocean? *Journal*
2479 *of Asian Earth Sciences*, 56: 1-23.
- 2480 Monnier, C., Girardeau, J., Maury, R.C. and Cotten, J., 1995. Back-arc basin origin for the East
2481 Sulawesi ophiolite (eastern Indonesia). *Geology*, 23(9): 851-854.
- 2482 Monnier, C., Girardeau, J., Pubellier, M. and Permana, H., 2000. The central ophiolite belt of Irian
2483 Jaya (Indonesia): petrological and geochemical evidence for a back-arc basin origin.
2484 *Comptes Rendus de l'Academie des Sciences Series IIA Earth and Planetary Science*,
2485 331(11): 691-699.
- 2486 Monod, L. and Prendini, L., 2015. Evidence for Eurogondwana: the roles of dispersal, extinction
2487 and vicariance in the evolution and biogeography of Indo - Pacific Hormuridae (Scorpiones:
2488 Scorpionoidea). *Cladistics*, 31(1): 71-111.
- 2489 Montelli, R., Nolet, G., Dahlen, F.A. and Masters, G., 2006. A catalogue of deep mantle plumes:
2490 new results from finite-frequency tomography. *Geochemistry, Geophysics, Geosystems*,
2491 7(11): Q11007.
- 2492 Morley, C.K., 2012a. Late Cretaceous-early Palaeogene tectonic development of SE Asia. *Earth-*
2493 *Science Reviews*, 115(1-2): 37-75.

2494 Morley, R.J., 2012b. A review of the Cenozoic palaeoclimate history of Southeast Asia. Biotic
2495 evolution and environmental change in Southeast Asia. The Systematics Association
2496 Special, 82: 79-114.

2497 Morra, G., Seton, M., Quevedo, L. and Müller, R.D., 2013. Organization of the tectonic plates in
2498 the last 200 Myr. *Earth and Planetary Science Letters*, 373: 93-101.

2499 Mubroto, B., Briden, J.C., McClelland, E. and Hall, R., 1994. Palaeomagnetism of the Balantak
2500 ophiolite, Sulawesi. *Earth and Planetary Science Letters*, 125(1): 193-209.

2501 Müller, R.D., Royer, J.Y. and Lawver, L.A., 1993. Revised plate motions relative to the hotspots
2502 from combined Atlantic and Indian Ocean hotspot tracks. *Geology*, 21(3): 275.

2503 Müller, R.D., Sdrolias, M., Gaina, C., Steinberger, B. and Heine, C., 2008. Long-term sea-level
2504 fluctuations driven by ocean basin dynamics. *Science*, 319(5868): 1357.

2505 Müller, R.D., Seton, M., Zahirovic, S., Williams, S.E., Matthews, K.J., Wright, N.M., Shephard, G.,
2506 Maloney, K.T., Barnett-Moore, N., Hosseinpour, M., Bower, D.J. and Cannon, J., 2016.
2507 Ocean basin evolution and global-scale plate reorganization events since Pangea breakup.
2508 *Annual Review of Earth and Planetary Sciences*, 44.

2509 Norton, I.O., 1999. Global plate reconstruction model. ExxonMobil Exploration.

2510 Obayashi, M., Yoshimitsu, J., Nolet, G., Fukao, Y., Shiobara, H., Sugioka, H., Miyamachi, H. and
2511 Gao, Y., 2013. Finite frequency whole mantle P wave tomography: Improvement of
2512 subducted slab images. *Geophysical Research Letters*, 40(21): 5652-5657.

2513 Page, R.W., 1976. Geochronology of igneous and metamorphic rocks in the New Guinea
2514 Highlands. Australian Government Publ. Service.

2515 Parkinson, C.D., Miyazaki, K., Wakita, K., Barber, A.J. and Carswell, D.A., 1998. An overview
2516 and tectonic synthesis of the pre - Tertiary very - high - pressure metamorphic and
2517 associated rocks of Java, Sulawesi and Kalimantan, Indonesia. *Island Arc*, 7(1 - 2): 184-
2518 200.

2519 Patriat, P. and Achache, J., 1984. India-Eurasia collision chronology has implications for crustal
2520 shortening and driving mechanism of plates. *Nature*, 311: 615-621.

2521 Paulson, A., Zhong, S. and Wahr, J., 2007. Inference of mantle viscosity from GRACE and relative
2522 sea level data. *Geophysical Journal International*, 171(2): 497-508.

2523 Pedersen, R.B., Searle, M.P., Carter, A. and Bandopadhyay, P.C., 2010. U-Pb zircon age of the
2524 Andaman ophiolite: implications for the beginning of subduction beneath the Andaman-
2525 Sumatra arc. *Journal of the Geological Society*, 167(6): 1105-1112.

2526 Penrose, R., 1903. The tin deposits of the Malay Peninsula with special reference to those of the
2527 Kinta district. *The Journal of Geology*, 11(2): 135-154.

2528 Permana, H., 1998. Dynamique de la mise en place des ophiolites d'Irian Jaya (Indonesie), PhD
2529 thesis of the Universite de Nantes, 314 pp.

2530 Petterson, M.G., 2010. A review of the geology and tectonics of the Kohistan island arc, north
2531 Pakistan. *Geological Society, London, Special Publications*, 338(1): 287-327.

2532 Petterson, M.G. and Windley, B.F., 1985. Rb Sr dating of the Kohistan arc-batholith in the Trans-
2533 Himalaya of north Pakistan, and tectonic implications. *Earth and Planetary Science Letters*,
2534 74(1): 45-57.

2535 Pieters, P.E., Pigram, C.J., Trail, D.S., Dow, D.B., Ratman, N. and Sukanto, R., 1983. The
2536 stratigraphy of western Irian Jaya.

2537 Pigram, C.J. and Panggabean, H., 1984. Rifting of the northern margin of the Australian continent
2538 and the origin of some microcontinents in eastern Indonesia. *Tectonophysics*, 107(3): 331-
2539 353.

2540 Pigram, C.J. and Symonds, P.A., 1991. A review of the timing of the major tectonic events in the
2541 New Guinea Orogen. *Journal of Southeast Asian Earth Sciences*, 6(3): 307-318.

2542 Polvé, M., Maury, R.C., Bellon, H., Rangin, C., Priadi, B., Yuwono, S., Joron, J.L. and Atmadja,
2543 R.S., 1997. Magmatic evolution of Sulawesi (Indonesia): constraints on the Cenozoic
2544 geodynamic history of the Sundaland active margin. *Tectonophysics*, 272(1): 69-92.

2545 Pubellier, M., Ali, J. and Monnier, C., 2003. Cenozoic Plate interaction of the Australia and
2546 Philippine Sea Plates: "hit-and-run" tectonics. *Tectonophysics*, 363(3): 181-199.

2547 Pubellier, M., Monnier, C., Maury, R. and Tamayo, R., 2004. Plate kinematics, origin and tectonic
2548 emplacement of supra-subduction ophiolites in SE Asia. *Tectonophysics*, 392(1): 9-36.

2549 Pubellier, M. and Morley, C.K., 2014. The basins of Sundaland (SE Asia): Evolution and boundary
2550 conditions. *Marine and Petroleum Geology*, 58: 555-578.

2551 Pudsey, C.J., 1986. The Northern Suture, Pakistan: margin of a Cretaceous island arc. *Geological*
2552 *Magazine*, 123(04): 405-423.

2553 Pudsey, C.J., Schroeder, R. and Skelton, P.W., 1985. Cretaceous (Aptian/Albian) Age for Island-
2554 Arc Volcanics, Kohistan, N Pakistan. In: V. Gupta (Editor), *Geology of Western Himalayas*.
2555 Hindustan Publishing Corporation, pp. 150-168.

2556 Pusok, A.E. and Kaus, B.J.P., 2015. Development of topography in 3 - D continental - collision
2557 models. *Geochemistry, Geophysics, Geosystems*.

2558 Queano, K.L., Ali, J.R., Milsom, J., Aitchison, J.C. and Pubellier, M., 2007. North Luzon and the
2559 Philippine Sea Plate motion model: Insights following paleomagnetic, structural, and age-
2560 dating investigations. *Journal of Geophysical Research*, 112(B5): B05101.

2561 Rangin, C., Jolivet, L. and Pubellier, M., 1990. A simple model for the tectonic evolution of
2562 southeast Asia and Indonesia region for the past 43 my. *Bulletin de la Société géologique de*
2563 *France*, 6(6): 889-905.

2564 Ratnaswamy, V., Stadler, G. and Gurnis, M., 2015. Adjoint-based estimation of plate coupling in a
2565 non-linear mantle flow model: theory and examples. *Geophysical Journal International*,
2566 202(2): 768-786.

2567 Rehault, J.P., Moussat, E. and Fabbri, A., 1987. Structural evolution of the Tyrrhenian back-arc
2568 basin. *Marine Geology*, 74(1): 123-150.

2569 Rehman, H.U.R., Seno, T., Yamamoto, H. and Khan, T., 2011. Timing of collision of the Kohistan-
2570 Ladakh Arc with India and Asia: Debate. *Island Arc*, 20(3): 308-328.

2571 Replumaz, A., Karason, H., van der Hilst, R.D., Besse, J. and Tapponnier, P., 2004. 4-D evolution
2572 of SE Asia's mantle from geological reconstructions and seismic tomography. *Earth and*
2573 *Planetary Science Letters*, 221(1-4): 103-115.

2574 Richter, C. and Ali, J.R., 2015. Philippine Sea Plate motion history: Eocene-Recent record from
2575 ODP Site 1201, central West Philippine Basin. *Earth and Planetary Science Letters*, 410:
2576 165-173.

2577 Rickwood, F.K., 1954. The geology of the western highlands of New Guinea. *Journal of the*
2578 *Geological Society of Australia*, 2(1): 63-82.

2579 Rock, N.M.S., Aldiss, D.T., Aspden, J.A., Clarke, M.C.G., Djunuddin, A., Miswar, W.K.,
2580 Thompson, S.J. and Whandoyo, R., 1983. The Geology of the Lubuksikaping Quadrangle,
2581 Sumatra. *Geol. Survey of Indonesia, Bandung*.

2582 Rohrman, M., 2015. Delineating the Exmouth mantle plume (NW Australia) from denudation and
2583 magmatic addition estimates. *Lithosphere*, 7(4): L445. 1.

2584 Rolland, J., Condamine, F.L., Beeravolu, C.R., Jiguet, F. and Morlon, H., 2015. Dispersal is a major
2585 driver of the latitudinal diversity gradient of Carnivora. *Global Ecology and Biogeography*,
2586 24(9): 1059-1071.

2587 Romanowicz, B., 2008. Using seismic waves to image Earth's internal structure. *Nature*, 451(7176):
2588 266-268.

2589 Rosenbaum, G., 2014. Geodynamics of oroclinal bending: Insights from the Mediterranean. *Journal*
2590 *of Geodynamics*, 82: 5-15.

2591 Royer, J.Y. and Chang, T., 1991. Evidence for relative motions between the Indian and Australian
2592 plates during the last 20 my from plate tectonic reconstructions: implications for the
2593 deformation of the Indo-Australian plate. *Journal of Geophysical Research*, 96(B7): 11779-
2594 11,802.

2595 Ryan, W.B., Carbotte, S.M., Coplan, J.O., O'Hara, S., Melkonian, A., Arko, R., Weissel, R.A.,
 2596 Ferrini, V., Goodwillie, A. and Nitsche, F., 2009. Global Multi - Resolution Topography
 2597 synthesis. *Geochemistry, Geophysics, Geosystems*, 10(3).
 2598 Sandiford, M., 2007. The tilting continent: a new constraint on the dynamic topographic field from
 2599 Australia. *Earth and Planetary Science Letters*, 261(1): 152-163.
 2600 Schaltegger, U., Frank, M. and Burg, J.-P., 2003. A 120 million years record of magmatism and
 2601 crustal melting in the Kohistan Batholith, EGS-AGU-EUG Joint Assembly, pp. 6816.
 2602 Schärer, U., Hamet, J. and Allègre, C.J., 1984. The Transhimalaya (Gangdese) plutonism in the
 2603 Ladakh region: a U Pb and Rb Sr study. *Earth and Planetary Science Letters*, 67(3): 327-
 2604 339.
 2605 Schellart, W. and Lister, G., 2005. The role of the East Asian active margin in widespread
 2606 extensional and strike-slip deformation in East Asia. *Journal of the Geological Society*,
 2607 162(6): 959-972.
 2608 Schellart, W.P. and Spakman, W., 2015. Australian plate motion and topography linked to fossil
 2609 New Guinea slab below Lake Eyre. *Earth and Planetary Science Letters*, 421: 107-116.
 2610 Scotese, C., Boucot, A. and McKerrow, W., 1999. Gondwanan palaeogeography and pal
 2611 oclimatology. *Journal of African Earth Sciences*, 28(1): 99-114.
 2612 Scotese, C.R., Gahagan, L.M. and Larson, R.L., 1988. Plate tectonic reconstructions of the
 2613 Cretaceous and Cenozoic ocean basins. *Tectonophysics*, 155(1): 27-48.
 2614 Sdrolias, M. and Müller, R.D., 2006. Controls on back - arc basin formation. *Geochemistry*,
 2615 *Geophysics, Geosystems*, 7(4).
 2616 Sdrolias, M., Roest, W.R. and Müller, R.D., 2004. An expression of Philippine Sea plate rotation:
 2617 the Parece Vela and Shikoku basins. *Tectonophysics*, 394(1): 69-86.
 2618 Searle, M.P., Whitehouse, M.J., Robb, L.J., Ghani, A.A., Hutchison, C.S., Sone, M., Ng, S.W.P.,
 2619 Roselee, M.H., Chung, S.-L. and Oliver, G.J.H., 2012. Tectonic evolution of the Sibumasu-
 2620 Indochina terrane collision zone in Thailand and Malaysia: constraints from new U-Pb
 2621 zircon chronology of SE Asian tin granitoids. *Journal of the Geological Society*, 169: 489.
 2622 Şengör, A.M.C., Altın, D., Cin, A., Ustaömer, T. and Hsü, K.J., 1988. Origin and assembly of the
 2623 Tethyside orogenic collage at the expense of Gondwana Land. *Geological Society, London*,
 2624 *Special Publications*, 37(1): 119-181.
 2625 Şengör, A.M.C. and Natal'in, B.A., 1996. Paleotectonics of Asia: Fragments of a synthesis. In: A.
 2626 Yin and T.M. Harrison (Editors), *The Tectonic Evolution of Asia*. Cambridge Univ. Press
 2627 New York, pp. 486-640.
 2628 Seton, M., Gaina, C., Müller, R.D. and Heine, C., 2009. Mid-Cretaceous seafloor spreading pulse:
 2629 Fact or fiction? *Geology*, 37(8): 687-690.
 2630 Seton, M., Müller, R.D., Zahirovic, S., Gaina, C., Torsvik, T.H., Shephard, G., Talsma, A., Gurnis,
 2631 M., Turner, M., Maus, S. and Chandler, M., 2012. Global continental and ocean basin
 2632 reconstructions since 200 Ma. *Earth-Science Reviews*, 113(3-4): 212-270.
 2633 Seton, M., Whittaker, J.M., Wessel, P., Müller, R.D., DeMets, C., Merkouriev, S., Cande, S., Gaina,
 2634 C., Eagles, G. and Granot, R., 2014. Community infrastructure and repository for marine
 2635 magnetic identifications. *Geochemistry, Geophysics, Geosystems*, 15(4): 1629-1641.
 2636 Sevastjanova, I., Hall, R., Rittner, M., Paw, S.M.T.L., Naing, T.T., Alderton, D.H. and Comfort, G.,
 2637 2015. Myanmar and Asia united, Australia left behind long ago. *Gondwana Research*.
 2638 Shemenda, A.I., 1993. Subduction of the lithosphere and back arc dynamics: Insights from physical
 2639 modeling. *Journal of Geophysical Research*, 98(B9): 16167-16185.
 2640 Shi, G., Cui, W., Cao, S., Jiang, N., Jian, P., Liu, D., Miao, L. and Chu, B., 2008. Ion microprobe
 2641 zircon U-Pb age and geochemistry of the Myanmar jadeite. *Journal of the Geological*
 2642 *Society*, 165(1): 221-234.
 2643 Shi, G., Lei, W., He, H., Ng, Y.N., Liu, Y., Liu, Y., Yuan, Y., Kang, Z. and Xie, G., 2014.
 2644 Superimposed tectono-metamorphic episodes of Jurassic and Eocene age in the jadeite
 2645 uplift, Myanmar, as revealed by 40 Ar/39 Ar dating. *Gondwana Research*, 26(2): 464-474.

2646 Shi, H. and Li, C.-F., 2012. Mesozoic and early Cenozoic tectonic convergence-to-rifting transition
2647 prior to opening of the South China Sea. *International Geology Review*, 54(15): 1801-1828.

2648 Simmons, N., Myers, S., Johannesson, G., Matzel, E. and Grand, S., 2015. Evidence for long -
2649 lived subduction of an ancient tectonic plate beneath the southern Indian Ocean.
2650 *Geophysical Research Letters*, 42(21): 9270-9278.

2651 Simmons, N.A., Forte, A.M., Boschi, L. and Grand, S.P., 2010. GyPSuM: A joint tomographic
2652 model of mantle density and seismic wave speeds. *Journal of Geophysical Research: Solid*
2653 *Earth* (1978–2012), 115(B12).

2654 Smyth, H.R., Hamilton, P.J., Hall, R. and Kinny, P.D., 2007. The deep crust beneath island arcs:
2655 Inherited zircons reveal a Gondwana continental fragment beneath East Java, Indonesia.
2656 *Earth and Planetary Science Letters*, 258(1-2): 269-282.

2657 Soeria-Atmadja, R., Noeradi, D. and Priadi, B., 1999. Cenozoic magmatism in Kalimantan and its
2658 related geodynamic evolution. *Journal of Asian Earth Sciences*, 17(1): 25-45.

2659 Spasojevic, S. and Gurnis, M., 2012. Sea level and vertical motion of continents from dynamic
2660 earth models since the Late Cretaceous. *AAPG bulletin*, 96(11): 2037-2064.

2661 Spasojevic, S., Liu, L. and Gurnis, M., 2009. Adjoint models of mantle convection with seismic,
2662 plate motion, and stratigraphic constraints: North America since the Late Cretaceous.
2663 *Geochemistry, Geophysics, Geosystems*, 10(5).

2664 Stampfli, G.M. and Borel, G.D., 2002. A plate tectonic model for the Paleozoic and Mesozoic
2665 constrained by dynamic plate boundaries and restored synthetic oceanic isochrons. *Earth*
2666 *and Planetary Science Letters*, 196(1-2): 17-33.

2667 Stauffer, P.H., 1983. Unraveling the mosaic of Paleozoic crustal blocks in Southeast Asia.
2668 *Geologische Rundschau*, 72(3): 1061-1080.

2669 Steinberger, B. and Calderwood, A.R., 2006. Models of large-scale viscous flow in the Earth's
2670 mantle with constraints from mineral physics and surface observations. *Geophysical Journal*
2671 *International*, 167(3): 1461-1481.

2672 Steinberger, B. and O'Connell, R.J., 1998. Advection of plumes in mantle flow: implications for
2673 hotspot motion, mantle viscosity and plume distribution. *Geophysical Journal International*,
2674 132(2): 412-434.

2675 Steinberger, B. and Torsvik, T.H., 2008. Absolute plate motions and true polar wander in the
2676 absence of hotspot tracks. *Nature*, 452(7187): 620-623.

2677 Steinberger, B., Torsvik, T.H. and Becker, T.W., 2012. Subduction to the lower mantle-a
2678 comparison between geodynamic and tomographic models. *Solid Earth*, 3(2): 415.

2679 Stern, R.J., Reagan, M., Ishizuka, O., Ohara, Y. and Whattam, S., 2012. To understand subduction
2680 initiation, study forearc crust: To understand forearc crust, study ophiolites. *Lithosphere*,
2681 4(6): 469-483.

2682 Sukamoto, R. and Westermann, G., 1992. The Jurassic of the Circum- Pacific. Indonesia and Papua
2683 New Guinea. Cambridge University Press.

2684 Tapponnier, P., Peltzer, G., Le Dain, A.Y., Armijo, R. and Cobbold, P., 1982. Propagating
2685 extrusion tectonics in Asia: New insights from simple experiments with plasticine. *Geology*,
2686 10(12): 611-616.

2687 Taylor, B. and Hayes, D.E., 1980. The tectonic evolution of the South China Basin. The tectonic
2688 and geologic evolution of Southeast Asian seas and islands: 89-104.

2689 Taylor, B. and Hayes, D.E., 1983. Origin and history of the South China Sea basin. The Tectonic
2690 and Geologic Evolution of Southeast Asian Seas and Islands: Part 2: 23-56.

2691 Torsvik, T.H., Müller, R.D., van der Voo, R., Steinberger, B. and Gaina, C., 2008. Global plate
2692 motion frames: toward a unified model. *Reviews of Geophysics*, 46(3).

2693 Tovaglieri, F. and George, A.D., 2014. Stratigraphic architecture of an Early–Middle Jurassic
2694 tidally influenced deltaic system (Plover Formation), Browse Basin, Australian North West
2695 Shelf. *Marine and Petroleum Geology*, 49: 59-83.

- 2696 Treloar, P.J., Petterson, M.G., Jan, M.Q. and Sullivan, M., 1996. A re-evaluation of the stratigraphy
2697 and evolution of the Kohistan arc sequence, Pakistan Himalaya: implications for magmatic
2698 and tectonic arc-building processes. *Journal of the Geological Society*, 153(5): 681-693.
- 2699 Turcotte, D.L. and Oxburgh, E.R., 1972. Mantle convection and the new global tectonics. *Annual*
2700 *Review of Fluid Mechanics*, 4(1): 33-66.
- 2701 Valenti, G.L., 1993. P'nyang Field: discovery and geology of a gas giant in the western Papuan Fold
2702 Belt, Western Province, Papua New Guinea, *Proceedings of the Second PNG Petroleum*
2703 *Convention*, pp. 413-430.
- 2704 van der Meer, D.G., Spakman, W., van Hinsbergen, D.J.J., Amaru, M.L. and Torsvik, T.H., 2010.
2705 Towards absolute plate motions constrained by lower-mantle slab remnants. *Nature*
2706 *Geoscience*, 3: 36-40.
- 2707 van der Meer, D.G., Zeebe, R.E., van Hinsbergen, D.J.J., Sluijs, A., Spakman, W. and Torsvik,
2708 T.H., 2014. Plate tectonic controls on atmospheric CO₂ levels since the Triassic.
2709 *Proceedings of the National Academy of Sciences*, 111(12): 4380-4385.
- 2710 van der Voo, R., Spakman, W. and Bijwaard, H., 1999a. Mesozoic subducted slabs under Siberia.
2711 *Nature*, 397(6716): 246-249.
- 2712 van der Voo, R., Spakman, W. and Bijwaard, H., 1999b. Tethyan subducted slabs under India.
2713 *Earth and Planetary Science Letters*, 171(1): 7-20.
- 2714 van Dongen, M., Weinberg, R.F., Tomkins, A.G., Armstrong, R.A. and Woodhead, J.D., 2010.
2715 Recycling of Proterozoic crust in Pleistocene juvenile magma and rapid formation of the Ok
2716 Tedi porphyry Cu–Au deposit, Papua New Guinea. *Lithos*, 114(3–4): 282-292.
- 2717 van Hinsbergen, D.J.J., Lippert, P.C., Dupont-Nivet, G., McQuarrie, N., Doubrovine, P.V.,
2718 Spakman, W. and Torsvik, T.H., 2012. Greater India Basin hypothesis and a two-stage
2719 Cenozoic collision between India and Asia. *Proceedings of the National Academy of*
2720 *Sciences*, 109(20): 7659-7664.
- 2721 van Hinsbergen, D.J.J., Steinberger, B., Doubrovine, P.V. and Gassmöller, R., 2011. Acceleration
2722 and deceleration of India-Asia convergence since the Cretaceous: roles of mantle plumes
2723 and continental collision. *Journal of Geophysical Research - Solid Earth*, 116(B06101).
- 2724 van Hunen, J. and Allen, M.B., 2011. Continental collision and slab break-off: a comparison of 3-D
2725 numerical models with observations. *Earth and Planetary Science Letters*, 302(1): 27-37.
- 2726 van Leeuwen, T.M., 1981. The geology of southwest Sulawesi with special reference to the Biru
2727 area. *The geology and tectonics of Eastern Indonesia*, 2: 277-304.
- 2728 van Ufford, A.Q. and Cloos, M., 2005. Cenozoic tectonics of New Guinea. *AAPG bulletin*, 89(1):
2729 119-140.
- 2730 Veevers, J.J., 2004. Gondwanaland from 650–500 Ma assembly through 320 Ma merger in Pangea
2731 to 185–100 Ma breakup: supercontinental tectonics via stratigraphy and radiometric dating.
2732 *Earth-Science Reviews*, 68(1-2): 1-132.
- 2733 Vérard, C., Flores, K. and Stampfli, G., 2012. Geodynamic reconstructions of the South America–
2734 Antarctica plate system. *Journal of Geodynamics*, 53: 43-60.
- 2735 von Rad, U. and Exon, N.F., 1983. Mesozoic-Cenozoic sedimentary and volcanic evolution of the
2736 starved passive continental margin off northwest Australia. In: J. Watkins and C. Drake
2737 (Editors), *Studies in Continental Margin Geology: AAPG Mem.*, pp. 252-281.
- 2738 von Rad, U., Exon, N.F. and Haq, B.U., 1992. 46. Rift-To-Drift History Of The Wombat Plateau,
2739 Northwest Australia: Triassic To Tertiary Leg 122 Results.
- 2740 Wajzer, M., Barber, A. and Hidayat, S., 1991. Accretion, collision and strike-slip faulting: the
2741 Woyla group as a key to the tectonic evolution of North Sumatra. *Journal of Southeast*
2742 *Asian Earth Sciences*, 6(3-4): 447-461.
- 2743 Wakita, K., 2000. Cretaceous accretionary–collision complexes in central Indonesia. *Journal of*
2744 *Asian Earth Sciences*, 18(6): 739-749.
- 2745 Wakita, K. and Metcalfe, I., 2005. Ocean plate stratigraphy in East and Southeast Asia. *Journal of*
2746 *Asian Earth Sciences*, 24(6): 679-702.

2747 Wakita, K., Miyazaki, K., Zulkarnain, I., Sopaheluwakan, J. and Sanyoto, P., 1998. Tectonic
2748 implications of new age data for the Meratus complex of south Kalimantan, Indonesia.
2749 Island Arc, 7(1 - 2): 202-222.

2750 Wang, P., 2004. Cenozoic Deformation and the History of Sea - Land Interactions in Asia.
2751 Continent-Ocean Interactions Within East Asian Marginal Seas: 1-22.

2752 Wen, D.-R., Chung, S.-L., Song, B., Iizuka, Y., Yang, H.-J., Ji, J., Liu, D. and Gallet, S., 2008a.
2753 Late Cretaceous Gangdese intrusions of adakitic geochemical characteristics, SE Tibet:
2754 petrogenesis and tectonic implications. Lithos, 105(1): 1-11.

2755 Wen, D.-R., Liu, D., Chung, S.-L., Chu, M.-F., Ji, J., Zhang, Q., Song, B., Lee, T.-Y., Yeh, M.-W.
2756 and Lo, C.-H., 2008b. Zircon SHRIMP U-Pb ages of the Gangdese Batholith and
2757 implications for Neotethyan subduction in southern Tibet. Chemical Geology, 252(3): 191-
2758 201.

2759 Wennekers, J.H.L., 1958. South Sumatra Basinal Area: Far East, SP 18: Habitat of Oil. AAPG
2760 Special Volumes, pp. 1347-1358.

2761 Wessel, P., Smith, W.H.F., Scharroo, R., Luis, J. and Wobbe, F., 2013. Generic Mapping Tools:
2762 Improved Version Released. Eos, Transactions American Geophysical Union, 94(45): 409-
2763 410.

2764 Whittaker, J.M., Müller, R.D., Sdrolias, M. and Heine, C., 2007. Sunda-Java trench kinematics, slab
2765 window formation and overriding plate deformation since the Cretaceous. Earth and
2766 Planetary Science Letters, 255(3): 445-457.

2767 Widiyantoro, S., Kennett, B. and Van der Hilst, R., 1998. Extending shear-wave tomography for the
2768 lower mantle using S and SKS arrival-time data. Earth, planets and space, 50(11-12): 999-
2769 1012.

2770 Widiyantoro, S. and van der Hilst, R.D., 1996. Structure and evolution of subducted lithosphere
2771 beneath the Sunda arc, Indonesia. Science Reports, 271(5255): 1566-1570.

2772 Williams, S.E., Whittaker, J.M. and Müller, R.D., 2011. Full - fit, palinspastic reconstruction of the
2773 conjugate Australian - Antarctic margins. Tectonics, 30(6): 21.

2774 Worthen, J., Stadler, G., Petra, N., Gurnis, M. and Ghattas, O., 2014. Towards adjoint-based
2775 inversion for rheological parameters in nonlinear viscous mantle flow. Physics of the Earth
2776 and Planetary Interiors, 234: 23-34.

2777 Worthing, M.A. and Crawford, A.J., 1996. The igneous geochemistry and tectonic setting of
2778 metabasites from the Emo Metamorphics, Papua New Guinea; a record of the evolution and
2779 destruction of a backarc basin. Mineralogy and Petrology, 58(1-2): 79-100.

2780 Wu, J., Suppe, J., Lu, R. and Kanda, R., 2016. Philippine Sea and East Asian plate tectonics since
2781 52 Ma constrained by new subducted slab reconstruction methods. Journal of Geophysical
2782 Research: Solid Earth.

2783 Xu, C., Boucot, A., Scotese, C. and Junxuan, F., 2012. Pangaean aggregation and disaggregation
2784 with evidence from global climate belts. Journal of Palaeogeography, 1: 5-13.

2785 Yang, S., Hu, S., Cai, D., Feng, X., Chen, L. and Gao, L., 2004. Present-day heat flow, thermal
2786 history and tectonic subsidence of the East China Sea Basin. Marine and petroleum geology,
2787 21(9): 1095-1105.

2788 Yang, T., Gurnis, M. and Zahirovic, S., 2016. Mantle - induced subsidence and compression in SE
2789 Asia since the early Miocene. Geophysical Research Letters.

2790 Yin, A. and Harrison, T.M., 2000. Geologic evolution of the Himalayan-Tibetan orogen. Annual
2791 Review of Earth and Planetary Sciences, 28(1): 211-280.

2792 Yirgu, G., Ebinger, C.J. and Maguire, P.K.H., 2006. The afar volcanic province within the East
2793 African Rift System: introduction. Geological Society, London, Special Publications,
2794 259(1): 1-6.

2795 Yoshida, M. and Hamano, Y., 2015. Pangea breakup and northward drift of the Indian subcontinent
2796 reproduced by a numerical model of mantle convection. Scientific reports, 5.

2797 Yumul, G.P., Dimalanta, C.B., Marquez, E.J. and Queaño, K.L., 2009. Onland signatures of the
2798 Palawan microcontinental block and Philippine mobile belt collision and crustal growth
2799 process: A review. *Journal of Asian Earth Sciences*, 34(5): 610-623.

2800 Yuwono, Y.S., Priyomarsono, S., Maury, R.C., Rampnoux, J.P., Soeria-Atmadja, R., Bellon, H. and
2801 Chotin, P., 1988. Petrology of the Cretaceous magmatic rocks from Meratus Range,
2802 southeast Kalimantan. *Journal of Southeast Asian Earth Sciences*, 2(1): 15-22.

2803 Zahirovic, S., Flament, N., Müller, R.D., Seton, M. and Gurnis, M., In Review. Large fluctuations
2804 of shallow seas in low-lying Southeast Asia driven by mantle flow. *Geochem. Geophys.*
2805 *Geosys.*

2806 Zahirovic, S., Müller, R.D., Seton, M. and Flament, N., 2015. Tectonic speed limits from plate
2807 kinematic reconstructions. *Earth and Planetary Science Letters*, 418: 40-52.

2808 Zahirovic, S., Müller, R.D., Seton, M., Flament, N., Gurnis, M. and Whittaker, J., 2012. Insights on
2809 the kinematics of the India-Eurasia collision from global geodynamic models. *Geochemistry*
2810 *Geophysics Geosystems*, 13(Q04W11).

2811 Zahirovic, S., Seton, M. and Müller, R., 2014. The Cretaceous and Cenozoic tectonic evolution of
2812 Southeast Asia. *Solid Earth (EGU)*, 5: 227-273.

2813 Zaman, H., Otofuji, Y.-i., Khan, S.R. and Ahmad, M.N., 2013. New paleomagnetic results from the
2814 northern margin of the Kohistan Island Arc. *Arabian Journal of Geosciences*, 6(4): 1041-
2815 1054.

2816 Zaman, H. and Torii, M., 1999. Palaeomagnetic study of Cretaceous red beds from the eastern
2817 Hindukush ranges, northern Pakistan: palaeoreconstruction of the Kohistan–Karakoram
2818 composite unit before the India–Asia collision. *Geophysical Journal International*, 136(3):
2819 719-738.

2820 Zaw, K., Meffre, S., Lai, C.-K., Burrett, C., Santosh, M., Graham, I., Manaka, T., Salam, A.,
2821 Kamvong, T. and Cromie, P., 2014. Tectonics and metallogeny of mainland Southeast
2822 Asia—A review and contribution. *Gondwana Research*, 26(1): 5-30.

2823 Zhang, K.-J., Zhang, Y.-X., Tang, X.-C. and Xia, B., 2012. Late Mesozoic tectonic evolution and
2824 growth of the Tibetan plateau prior to the Indo-Asian collision. *Earth-Science Reviews*,
2825 114(3): 236-249.

2826 Zhao, D., Maruyama, S. and Omori, S., 2007. Mantle dynamics of Western Pacific and East Asia:
2827 insight from seismic tomography and mineral physics. *Gondwana Research*, 11(1): 120-131.

2828 Zhong, S., Zuber, M.T., Moresi, L. and Gurnis, M., 2000. Role of temperature-dependent viscosity
2829 and surface plates in spherical shell models of mantle convection. *Journal of Geophysical*
2830 *Research*, 105(B5): 11063.

2831